THE EUROPEAN
PHYSICAL JOURNAL C

CrossMark

Measurement of the azimuthal anisotropy of charged particles produced in $\sqrt{s_{\mathrm{NN}}}$ = 5.02 TeV Pb+Pb collisions with the ATLAS detector

ATLAS Collaboration[⋆]

CERN, 1211 Geneva 23, Switzerland

Abstract Measurements of the azimuthal anisotropy in lead–lead collisions at $\sqrt{s_{\mathrm{NN}}}$ = 5.02 TeV are presented using a data sample corresponding to 0.49 nb^{-1} integrated luminosity collected by the ATLAS experiment at the LHC in 2015. The recorded minimum-bias sample is enhanced by triggers for "ultra-central" collisions, providing an opportunity to perform detailed study of flow harmonics in the regime where the initial state is dominated by fluctuations. The anisotropy of the charged-particle azimuthal angle distributions is characterized by the Fourier coefficients, v_2–v_7, which are measured using the two-particle correlation, scalar-product and event-plane methods. The goal of the paper is to provide measurements of the differential as well as integrated flow harmonics v_n over wide ranges of the transverse momentum, $0.5 < p_{\mathrm{T}} < 60$ GeV, the pseudorapidity, $|\eta| < 2.5$, and the collision centrality 0–80%. Results from different methods are compared and discussed in the context of previous and recent measurements in Pb+Pb collisions at $\sqrt{s_{\mathrm{NN}}}$ = 2.76 TeV and 5.02 TeV. In particular, the shape of the p_{T} dependence of elliptic or triangular flow harmonics is observed to be very similar at different centralities after scaling the v_n and p_{T} values by constant factors over the centrality interval 0–60% and the p_{T} range $0.5 < p_{\mathrm{T}} < 5$ GeV.

1 Introduction

One of the primary goals of ultra-relativistic heavy-ion collisions is the study of the hot and dense medium formed there, usually referred to as the quark-gluon plasma (QGP) [1–5]. The existence of the QGP phase of nuclear matter has been confirmed by a wealth of experimental data [5,6]. In particular, properties related to the collective expansion of the QGP (e.g. the equation of state [7] and shear viscosity [8]) are inferred from measurements of azimuthal anisotropies of produced particles. It is now understood that the azimuthal anisotropy results from large initial pressure gradients in the hot, dense matter created in the collisions [9,10]. These pressure gradients transform the initial spatial anisotropies of nuclear collisions into momentum anisotropies of the final-state particle production, which are experimentally characterized by Fourier (flow) harmonics of the azimuthal angle distributions of produced particles. The discovery of large flow harmonics at RHIC, and more recently at much higher collision energy at the LHC [11–14], has significantly deepened the understanding of the QGP, as explored theoretically by the QCD lattice [15]. In particular, the recent measurements of azimuthal anisotropy help to constrain the commonly used modelling of the dynamics of heavy-ion collisions based on relativistic viscous hydrodynamics. Typically, in the hydrodynamic models, a strongly interacting quark–gluon medium is formed shortly after the collision and its evolution is well described by relativistic fluid dynamics [8]. Detailed investigations, based on hydrodynamics, have shown that the produced medium has properties similar to those of an almost ideal fluid characterized by a very low ratio of viscosity to entropy density, η/s. Precise azimuthal anisotropy measurements over a wide range in kinematic variables and centrality are key elements to improving our understanding of the strongly coupled QGP because of their unique sensitivity to η/s.

The azimuthal angular distribution of single produced particles can be expanded in a Fourier series [16,17]:

$$\frac{\mathrm{d}N}{\mathrm{d}\phi} = \frac{N_0}{2\pi}\left(1 + \sum_{n=1} 2v_n \cos\left[n\left(\phi - \Phi_n\right)\right]\right), \qquad (1)$$

where N_0 is the total particle yield, ϕ is the azimuthal angle of the produced particles and the v_n and Φ_n are, respectively, the magnitude of the nth-order azimuthal anisotropy and the orientation of the nth-order symmetry plane. The v_n coefficients – also called *flow harmonics* – are typically mea-

sured as a function of particle pseudorapidity[1] (η), transverse momentum (p_T), and the degree of overlap between the colliding nuclei (centrality). Event-by-event fluctuations in the number and position of the interacting nucleons give rise to anisotropic flow fluctuations [18].

The first harmonic, v_1, is known as *directed flow* and refers to the sideward motion of participants in ultra-relativistic nuclear collisions, and it carries information from the early stage of the collision. The most extensive studies are related to the second flow harmonic, v_2, also known as *elliptic flow*. Elliptic flow is sensitive to the initial spatial asymmetry of the almond-shaped overlapping zone of the colliding nuclei. The higher-order coefficients, $n > 2$, are also important due to their sensitivity to initial-state geometric fluctuations and viscous effects [16–18].

During the first operational period at the LHC (Run 1) lead ions were collided at energy per colliding nucleon–nucleon pair $\sqrt{s_{NN}} = 2.76$ TeV, which is about 13 times larger than the highest collision energy attained at RHIC in Au+Au collisions. ATLAS and other LHC experiments collected large samples of heavy-ion data enabling extensive studies of the elliptic flow and higher-order Fourier coefficients. ATLAS measurements of flow harmonics were performed in broad regions of transverse momentum, pseudorapidity and event centrality, using the standard event-plane (EP) method [12], two-particle correlations (2PC) [13] and multi-particle cumulants [19]. Significant (non-zero) flow harmonics up to v_6 were measured in Pb+Pb collisions at $\sqrt{s_{NN}} = 2.76$ TeV, which provide important constraints on the bulk and shear viscosity of the QGP medium [20]. Additionally, by comparing RHIC (STAR [21] and PHENIX [22]) and LHC (ATLAS [12], ALICE [23] and CMS [24]) results, it was found that for similar centrality of Au+Au and Pb+Pb interactions, v_n as a function of p_T is approximately independent of collision energy. There is an initial rise of v_n with p_T up to about 3 GeV and then a drop-off at higher values of p_T, and only weak dependence for $p_T > 8-9$ GeV. As a function of centrality, there is similarly little variation with collision energy. The second harmonic, v_2, exhibits the most pronounced centrality variation, rising to a maximum for mid-central collisions, and then falling off for the most central collisions, reflecting variations in the shape of the initial collision geometry. The harmonic, v_3, referred as triangular flow, which has a value similar to v_2 in central collisions, shows a weaker dependence on centrality, as do the higher-order harmonics.

At the start of the second operational period of the LHC (Run 2), in November and December of 2015, lead–lead collisions with higher collision energy per nucleon pair of $\sqrt{s_{NN}} = 5.02$ TeV were collected by the LHC experiments. The goal of this paper is to present and discuss the first ATLAS measurements of v_n harmonics at this energy, using the two-particle correlation [17], scalar-product (SP) [25] and event-plane [16,17] methods. Comparing the 2PC and SP results can quantify the extent to which the two-particle correlations factorize into the product of the flow harmonics corresponding to single-particle angular distributions [26,27]. While the SP and EP methods are expected to yield similar values of the v_n, small variations due to their different sensitivity to initial-state geometric fluctuations can nevertheless occur [28]. To study the energy dependence, the 2PC and EP flow harmonics are compared with previous ATLAS measurements in 2.76 TeV Pb+Pb collisions [12,13]. The results presented in this paper, together with the results on azimuthal anisotropy from other LHC experiments [29,30], provide further opportunity to study the properties of the QGP, constrain hydrodynamic models, study transport coefficients and extract the temperature dependence of transport coefficients, including η/s.

The organization of this paper is as follows. Section 2 gives a brief overview of the ATLAS detector and the subsystems that are used in this analysis. Section 3 describes the datasets, triggers and the offline selection criteria used to select events and charged-particle tracks. Section 4 gives details of the scalar-product, event-plane and two-particle correlation methods, which are used to measure the v_n. Section 5 describes the systematic uncertainties associated with the measured v_n. Section 6 presents the main results of the analysis, which are the p_T, η and centrality dependence of the v_n and comparisons of results from the different methods. Section 7 gives a summary of the main results and observations.

2 Experimental set-up

The measurements were performed using the ATLAS detector [31] at the LHC. The principal components used in this analysis are the inner detector (ID), minimum-bias trigger scintillators (MBTS), calorimeter, zero-degree calorimeters (ZDC), and the trigger and data acquisition systems. The ID detects charged particles within the pseudorapidity range $|\eta| < 2.5$ using a combination of silicon pixel detectors, including the "insertable B-layer" [32,33] that was installed between Run 1 and Run 2, silicon microstrip detectors (SCT), and a straw-tube transition radiation tracker (TRT), all immersed in a 2 T axial magnetic field [34]. The MBTS system detects charged particles over $2.07 < |\eta| < 3.86$ using two scintillator-based hodoscopes on each side of

---

[1] ATLAS uses a right-handed coordinate system with its origin at the nominal interaction point (IP) in the centre of the detector and the z-axis along the beam pipe. The x-axis points from the IP to the centre of the LHC ring, and the y-axis points upward. Cylindrical coordinates (r, ϕ) are used in the transverse plane, ϕ being the azimuthal angle around the z-axis. The pseudorapidity is defined in terms of the polar angle θ as $\eta = -\ln \tan(\theta/2)$.

the detector, positioned at $z = \pm 3.6$ m. These hodoscopes were rebuilt between Run 1 and Run 2. The ATLAS calorimeter system consists of a liquid argon (LAr) electromagnetic (EM) calorimeter covering $|\eta| < 3.2$, a steel–scintillator sampling hadronic calorimeter covering $|\eta| < 1.7$, a LAr hadronic calorimeter covering $1.5 < |\eta| < 3.2$, and two LAr electromagnetic and hadronic forward calorimeters (FCal) covering $3.2 < |\eta| < 4.9$. The ZDC, situated at approximately ± 140 m from the nominal IP, detect neutral particles, mostly neutrons and photons, with $|\eta| > 8.3$. The ZDC use tungsten plates as absorbers, and quartz rods sandwiched between the tungsten plates as the active medium. The ATLAS trigger system [35] consists of a first-level (L1) trigger implemented using a combination of dedicated electronics and programmable logic, and a software-based high-level trigger.

3 Event and track selection

The Pb+Pb dataset used in this paper corresponds to an integrated luminosity of 0.49 nb^{-1}. Minimum-bias events were selected by two mutually exclusive triggers:

- Events with smaller impact parameter (semi-central and central collisions) were selected by a trigger that required the total transverse energy (E_T) deposited in the calorimeters at L1 to be above 50 GeV.
- Collisions with large impact parameter (peripheral events) were selected by a trigger that required the total transverse energy at L1 to be less than 50 GeV, one neutron on either side in the ZDC ($|\eta| > 8.3$), and at least one reconstructed track in the ID.

The minimum-bias triggers sampled a total luminosity of 22 μb^{-1}. To enhance the statistics of ultra-central collisions, additional data samples were recorded by two dedicated triggers – UCC-1 and UCC-2 – that selected events in which the total E_T in the FCal at L1 was more than 4.21 TeV and 4.54 TeV, respectively. The UCC-1 trigger sampled a luminosity of 45 μb^{-1} while the UCC-2 trigger sampled the entire luminosity of 0.49 nb^{-1}. The luminosities sampled by the different triggers are listed in Table 1.

Table 1 The luminosities sampled by the triggers used in the analysis

Trigger	Sampled luminosity
Minimum-bias	22 μb^{-1}
UCC-1	45 μb^{-1}
UCC-2	0.49 nb^{-1}

In the offline analysis the z coordinate of the primary vertex [36] is required to be within 10 cm of the nominal interaction point. The fraction of events containing more than one inelastic interaction (pile-up) is estimated to be at the level of 0.2%. The fraction varies with ΣE_T^{FCal}, and for ultra-central collisions it amounts to a few percent. Pile-up events were removed by exploiting the correlations between the transverse energy measured in the FCal and in the ZDC as well as the number of tracks associated with the primary vertex, N_{ch}^{rec}. As the pile-up is very small, in a typical pile-up event the track multiplicity associated with the primary vertex belongs to a single Pb+Pb collision, while the energy deposited in calorimeters contains contributions from multiple, mostly two, collisions. Therefore, events with small values of N_{ch}^{rec} and large ΣE_T^{FCal} that differ markedly from those of the majority of Pb+Pb collisions are removed from the analysis [19]. In addition, the anti-correlation between the ΣE_T^{FCal} and the number of neutrons detected in ZDC is also used to suppress pile-up events. Events with the number of neutrons (as recorded in the ZDC) much higher than the number expected from the bulk of events for a given value ΣE_T^{FCal} are rejected.

The heavy-ion collision geometry is defined by its impact parameter, b. As the actual event-by-event impact parameter is not accessible experimentally, the centrality classification is based on the transverse energy measured in the forward calorimeter, ΣE_T^{FCal}, which exhibits a strong monotonic correlation with b. A model based on the Monte Carlo (MC) Glauber approach [37,38] is used to obtain the mapping from the observed ΣE_T^{FCal} to the primary properties, such as the number of binary nucleon–nucleon interactions, N_{coll}, or the number of nucleons participating in the nuclear collision, N_{part}, for each centrality interval. The Glauber model also provides a correspondence between the ΣE_T^{FCal} distribution and the sampling fraction of the total inelastic Pb+Pb cross-section, allowing the setting of the centrality percentiles [12]. For this analysis a selection of the 80% most central collisions (i.e. centrality 0–80%) is used to avoid any diffractive, photonuclear, and other inelastic processes that contribute significantly to very peripheral collisions (centrality 80–100%). Additionally, the events selected by UCC-1 and UCC-2 are used only over the 0–1% and 0–0.1% centrality intervals, respectively. Figure 1 shows the distribution of ΣE_T^{FCal} in the data, and thresholds for the selection of several centrality intervals. The correspondence of centrality intervals to $\langle N_{part} \rangle$ values is provided in Table 2.

In order to study the performance of the ATLAS detector, a minimum-bias sample of 4M Pb+Pb MC events was generated using version 1.38b of HIJING [39]. The effect of flow was added after the generation using an "afterburner" [40] procedure in which the p_T, η and centrality dependence of the v_n, as measured in the $\sqrt{s_{NN}} = 2.76$ TeV Pb+Pb data [13], is implemented by artificially rearranging the ϕ posi-
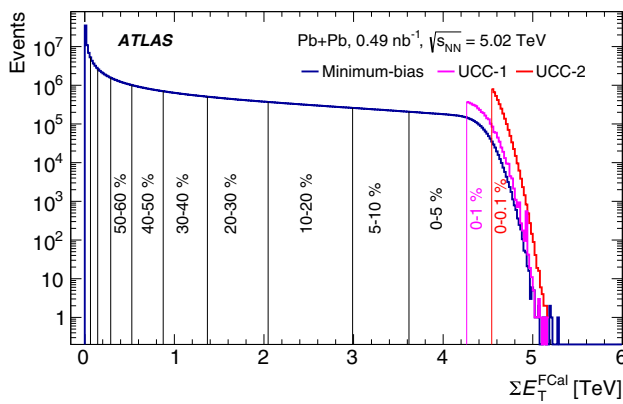
Fig. 1 The $\Sigma E_\mathrm{T}^\mathrm{FCal}$ distribution in $\sqrt{s_\mathrm{NN}}$ = 5.02 TeV Pb+Pb data for events selected by the minimum-bias trigger. The $\Sigma E_\mathrm{T}^\mathrm{FCal}$ thresholds for several centrality intervals are marked with vertical lines and labelled on the plot. Also shown are the number of events over the 0–1% and 0–0.1% centrality intervals selected by the ultra-central triggers

tions of the generated particles. The generated sample was passed through a full simulation of the ATLAS detector using GEANT4 [41], and the simulated events are reconstructed using the same algorithms as used for real data. Charged-particle tracks are reconstructed from the signals in the ID. A reconstruction procedure developed for tracking in dense environments in pp collisions, and optimized for heavy-ion collisions, was used for this purpose [42]. In the analysis the set of reconstructed tracks is filtered using several selection criteria. The tracks are required to have $p_\mathrm{T} > 0.5$ GeV, $|\eta| < 2.5$, at least two pixel hits, with the additional requirement of a hit in the first pixel layer when one is expected, at least eight SCT hits, and at most one missing hit in the SCT. A hit is expected if the extrapolated track crosses an active region of a pixel module that has not been disabled, and a hit is said to be missing when it is expected but not found. In addition, the transverse (d_0) and longitudinal ($z_0 \sin\theta$) impact parameters of the track relative to the vertex are required to be less than 1 mm. The track-fit quality parameter $\chi^2/$ndof is required to be less than 6.

The MC sample is used to determine the track-reconstruction efficiency as a function of p_T, η and centrality, $\epsilon(p_\mathrm{T}, \eta, \mathrm{centrality})$. The efficiency is defined as the fraction of primary [36] charged particles matched to reconstructed tracks. The matching criterion is that the weighted fraction of hits in a reconstructed track originating from a given gen-

erated particle is above 30%. Different weights are assigned to pixel, SCT and TRT signals to be more robust against fake tracks, which are defined below. At mid-rapidity ($|\eta| < 1$) and for events with centrality < 5%, the reconstruction efficiency is $\sim 60\%$ at low p_T and increases to $\sim 75\%$ at higher p_T. For $|\eta| > 1$ the efficiency decreases to about 40–60% depending on the p_T and centrality. The reconstruction efficiency depends weakly on the centrality for low-p_T tracks, for which it is smaller in the most central events by about 5% as compared to mid-central and peripheral collisions. For tracks with $p_\mathrm{T} > 1$ GeV the dependence on centrality is less than 1%.

The fraction of tracks that are not matched to primary, generated MC particles or are produced from random combinations of hits in the ID, both referred to as "fake tracks", is found to depend significantly on η. For $|\eta| < 1$, it is $\sim 10\%$ for low-p_T tracks in the most central 5% Pb+Pb events, and about 5% for more peripheral collisions. In the forward part of the detector, especially for $1 < |\eta| < 2$ where detector services reside, the fake rate can reach 18% for low p_T tracks in the most central collisions. The fake rate drops rapidly for higher p_T and also decreases gradually towards more peripheral collisions. For $p_\mathrm{T} > 10$ GeV and 0–5% centrality it rises to about 5%.

4 Analysis procedure

Three analysis techniques are used to determine the flow harmonics: the two-particle correlation method, which uses only the information from the tracking detectors, and the scalar-product and event-plane methods, which also use information from the FCal.

In all approaches the differential flow harmonics are first obtained in narrow intervals of p_T, η and centrality. Integrated quantities are obtained by taking into account the track reconstruction efficiency, ϵ, and fake rate, f. A p_T-, η- and centrality-dependent weight factor $w = (1 - f)/\epsilon$ is applied to each track in the 2PC measurement and to scale each bin of the differential v_n distributions in the SP and EP methods.

All analysis methods utilize the minimum-bias sample of 22 μb^{-1}. In addition, the SP and EP analyses use the ultra-central samples of 45 μb^{-1} and 0.49 nb^{-1}.

Table 2 The correspondence between centrality intervals used in the analysis and $\langle N_\mathrm{part}\rangle$ values

Centrality (%)	$\langle N_\mathrm{part}\rangle$	Centrality (%)	$\langle N_\mathrm{part}\rangle$	Centrality (%)	$\langle N_\mathrm{part}\rangle$
0–0.1	406.6 ± 1.3	10–20	264.1 ± 2.9	50–60	53.9 ± 2.0
0–1	402.9 ± 1.5	20–30	189.2 ± 2.8	60–70	30.6 ± 1.5
0–5	384.5 ± 1.9	30–40	131.4 ± 2.6	70–80	15.4 ± 1.0
5–10	333.1 ± 2.7	40–50	87.0 ± 2.4		

4.1 Two-particle correlation analysis

The 2PC method has been used extensively by ATLAS for correlation measurements [13,43–48]. In the 2PC method, the distribution of particle pairs in relative azimuthal angle $\Delta\phi = \phi^a - \phi^b$ and pseudorapidity separation $\Delta\eta = \eta^a - \eta^b$ is measured. Here the labels a and b denote the two particles used to make the pair. They are conventionally called the "trigger" and "associated" particles, respectively. In this analysis, the two particles are charged particles reconstructed by the ATLAS tracking system, over the full azimuth and $|\eta| < 2.5$, resulting in a pair-acceptance coverage of ± 5.0 units in $\Delta\eta$.

In order to account for the detector acceptance effects, the correlation is constructed from the ratio of the distribution in which the trigger and associated particles are taken from the same event to the distribution in which the trigger and associated particles are taken from two different events. These two distributions are referred to as the "same-event" (S) or "foreground" distribution and the "mixed-event" or "background" (B) distribution, respectively, and the ratio is written as:

$$C(\Delta\eta, \Delta\phi) = \frac{S(\Delta\phi, \Delta\eta)}{B(\Delta\phi, \Delta\eta)}.$$

The same-event distribution includes both the physical correlations and correlations arising from detector acceptance effects. On the other hand, the mixed-event distribution reflects only the effects of detector inefficiencies and non-uniformity, but contains no physical correlations. To ensure that the acceptance effects in the B distribution match closely those in the S distribution, the B distribution is constructed from particles from two different events that have similar multiplicity and z-vertex. Furthermore, in order to account for the effects of tracking efficiency $\epsilon(p_T, \eta)$, and fakes $f(p_T, \eta)$, each pair is weighted by

$$w_{a,b} = \frac{(1 - f(p_T^a, \eta^a))(1 - f(p_T^b, \eta^b))}{\epsilon(p_T^a, \eta^a)\epsilon(p_T^b, \eta^b)}$$

for S and B. In the ratio C, the acceptance effects largely cancel out and only the physical correlations remain [49]. Typically, the two-particle correlations are used only to study the shape of the correlations in $\Delta\phi$, and are conveniently normalized. In this paper, the normalization of $C(\Delta\eta, \Delta\phi)$ is chosen such that the $\Delta\phi$-averaged value of $C(\Delta\eta, \Delta\phi)$ is unity for $|\Delta\eta| > 2$.

Figure 2 shows $C(\Delta\eta, \Delta\phi)$ for several centrality intervals for $2 < p_T^{a,b} < 3$ GeV. In all cases a peak is seen in the correlation at $(\Delta\eta, \Delta\phi) \sim (0, 0)$. This "near-side" peak arises from a range of sources including resonance decays, Hanbury Brown and Twiss (HBT) correlations [50] and jet fragmentation [51]. The long-range (large $|\Delta\eta|$) correlations are the result of the global anisotropy of the event and are the focus of the study in this paper.

To investigate the $\Delta\phi$ dependence of the long-range ($|\Delta\eta| > 2$) correlation in more detail, the projection on to the $\Delta\phi$ axis is constructed as follows:

$$C(\Delta\phi) = \frac{\int_2^5 d|\Delta\eta| \, S(\Delta\phi, |\Delta\eta|)}{\int_2^5 d|\Delta\eta| \, B(\Delta\phi, |\Delta\eta|)} \equiv \frac{S(\Delta\phi)}{B(\Delta\phi)}.$$

The $|\Delta\eta| > 2$ requirement is imposed to reject the near-side jet peak and focus on the long-range features of the correlation functions.

In a similar fashion to the single-particle distribution (Eq. (1)), the 2PC can be expanded as a Fourier series:

$$C(\Delta\phi) = C_0 \left(1 + \Sigma_{n=1}^{\infty} v_{n,n}(p_T^a, p_T^b) \cos(n\Delta\phi) \right), \quad (2)$$

where the $v_{n,n}$ are the Fourier coefficients of the 2PC, and C_0 is its average value. If the two-particle distribution is simply the product of two single-particle distributions, then it can
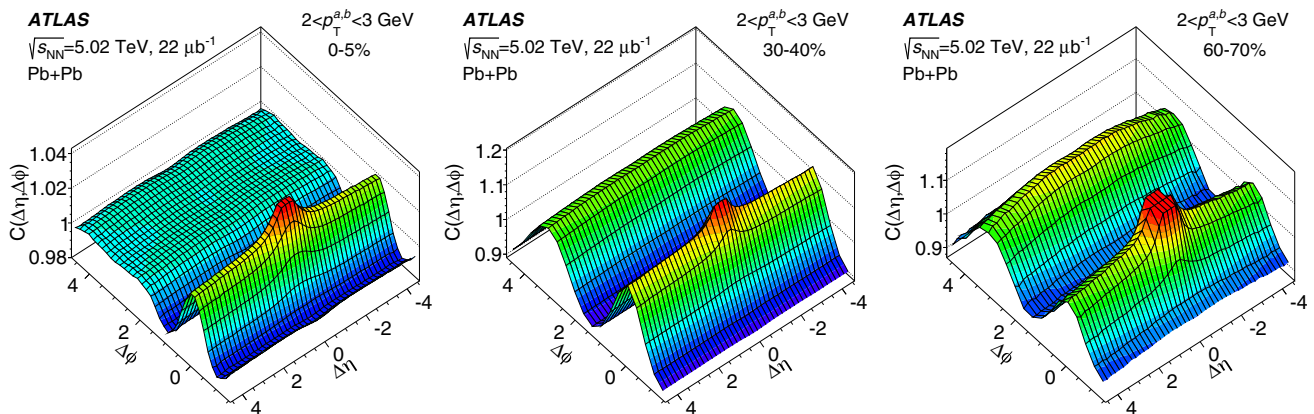
Fig. 2 Two-particle correlation functions $C(\Delta\eta, \Delta\phi)$ in 5.02 TeV Pb+Pb collisions for $2 < p_T^{a,b} < 3$ GeV. The left, middle and right panels correspond to the 0–5%, 30–40% and 60–70% central-ity classes, respectively. The distributions are truncated to suppress the peak at $\Delta\eta = \Delta\phi = 0$ to show the long-range correlations in greater detail

be shown that the Fourier coefficients of the 2PC factorize as [49]:

$$v_{n,n}(p_T^a, p_T^b) = v_n(p_T^a)v_n(p_T^b). \tag{3}$$

In Ref. [13] it was demonstrated that the factorization of $v_{n,n}$, given by Eq. (3), is valid in central and mid-central Pb+Pb collisions at $\sqrt{s_{NN}}$ = 2.76 GeV as long as one of the correlated particles is from a low p_T range. A breakdown of the factorization is expected when the anisotropy does not arise from flow, e.g. in peripheral collisions at high p_T. The factorization is also expected to break when the η separation between the particles is small, and short-range correlations dominate [13]. However, the $|\Delta\eta| > 2$ requirement removes most such short-range correlations. In the phase-space region where Eq. (3) holds, the $v_n(p_T^b)$ can be evaluated from the measured $v_{n,n}$ as:

$$v_n(p_T^b) = \frac{v_{n,n}(p_T^a, p_T^b)}{v_n(p_T^a)} = \frac{v_{n,n}(p_T^a, p_T^b)}{\sqrt{v_{n,n}(p_T^a, p_T^a)}}, \tag{4}$$

where $v_{n,n}(p_T^a, p_T^a) = v_n^2(p_T^a)$ is used in the denominator. In this analysis, for most of the 2PC results the $v_n(p_T^b)$ will be evaluated using Eq. (4) with $0.5 < p_T^a < 5.0$ GeV. The lower cut-off of 0.5 GeV on p_T^a is the lower limit of p_T measurements in this paper. The upper cut-off on p_T^a is chosen to exclude high-p_T particles, which predominantly come from jets and are not expected to obey Eq. (4).

Figure 3 shows one-dimensional 2PCs as a function of $\Delta\phi$ for $2 < p_T^{a,b} < 3$ GeV and for several different centrality intervals. The correlations are normalized to have a mean value (C_0 in Eq. (2)) of 1.0. The continuous line in Fig. 3 is a Fourier fit to the correlation (Eq. (2)) that includes harmonics up to $n = 6$. The contribution of the individual $v_{n,n}$ are also shown. The modulation in the correlation about its mean
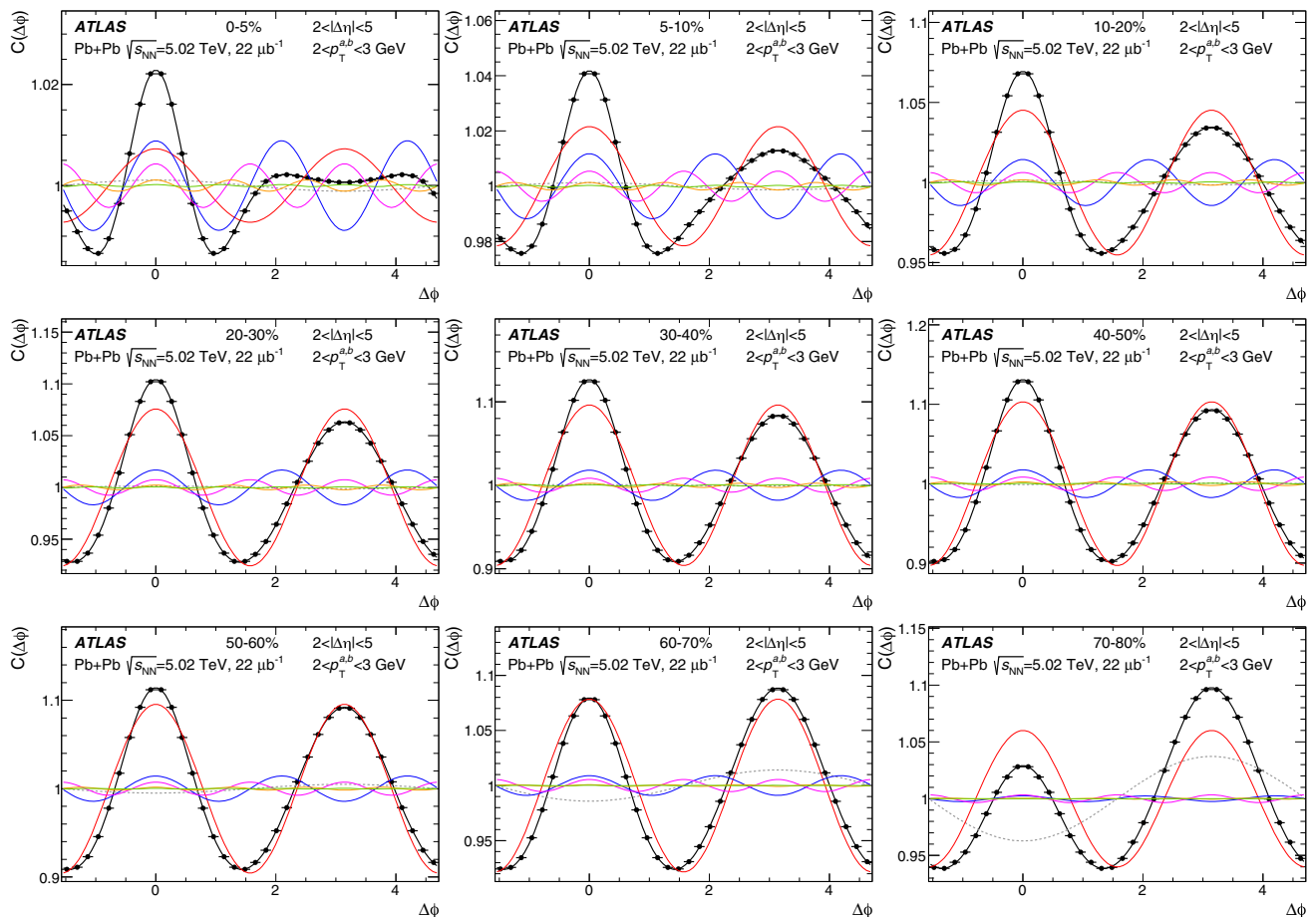

Fig. 3 One-dimensional two-particle correlation functions $C(\Delta\phi)$ in 5.02 TeV Pb+Pb collisions for $2 < p_T^{a,b} < 3$ GeV (points). The solid-black line indicates a fit to Eq. (2) containing harmonics $v_{n,n}$ up to $n = 6$. The dashed grey line shows the contribution of the $v_{1,1}$. The contributions of the $v_{2,2}$–$v_{6,6}$ are indicated by thecoloured lines ($v_{2,2}$-red, $v_{3,3}$-blue, $v_{4,4}$-magenta, $v_{5,5}$-orange, $v_{6,6}$-green), and can be identified by the number of peaks that they have. Each panel corresponds to a different centrality class. The y-axis range for the different panels is different

value is smallest in the most central events (top left panel) and increases towards mid-central events, reaching a maximum in the 40–50% centrality interval and then decreases. In central collisions, the $v_{2,2}-v_{4,4}$ are of comparable magnitude. But for other centralities, where the average collision geometry is elongated, the $v_{2,2}$ is significantly larger than the other $v_{n,n}$ for $n \geq 3$. In the central events the "away-side" peak at $\Delta\phi \sim \pi$ is also much broader because all the significant harmonics are of similar magnitude, while in mid-central events the near-side and away-side peaks are quite symmetric as the $v_{2,2}$ dominates. In central and mid-central events, the near-side peak is larger than the away-side peak. However, for the 60–70% and more peripheral centralities, the away-side peak becomes larger due to the presence of a large negative $v_{1,1}$ component. This negative $v_{1,1}$ component in the peripheral 2PCs arises largely from dijets: while the near-side jet peak is rejected by the $|\Delta\eta| > 2$ requirement, the "away-side jet" correlation that arises from back-to-back jets and contributes at $\Delta\phi = \pi$, cannot be rejected entirely as its position varies in $|\Delta\eta|$ from event to event. In the peripheral multiplicity intervals, the away-side jet significantly affects the 2PC. It produces a large negative $v_{1,1}$ and also affects the other harmonics by adding alternately positive and negative contributions to $v_{n,n}$ harmonics of even and odd order, respectively. In peripheral events the $v_{n,n}$ are strongly biased by dijets especially at higher p_{T}. The presence of the jets also results in the breakdown of the factorization relation (Eq. (3)).

4.2 Scalar product and event plane analysis

The SP method was introduced by the STAR Collaboration [25] and is further discussed in Ref. [17]. The SP method is very similar to the Event Plane method (EP) widely used in earlier analyses [12,13]. It is superior to the EP as $v_n\{\mathrm{SP}\}$

is an estimator of $\sqrt{\langle v_n^2 \rangle}$, independent of the detector resolution and acceptance, whereas $v_n\{\mathrm{EP}\}$ produces a detector-dependent estimate of v_n that lies between $\langle v_n \rangle$ and $\sqrt{\langle v_n^2 \rangle}$ [28].

Both the SP and EP method use flow vectors Q_n and $q_{n,j}$ defined as:

$$Q_n = |Q_n|\mathrm{e}^{in\Psi_n} = \frac{1}{M}\sum_{j=1,M} q_{n,j} = \frac{1}{M}\sum_{j=1,M} w_j \mathrm{e}^{in\phi_j},$$

(5)

where the sum runs over M particles in a single event. The ϕ_j is the particle azimuthal angle and n is the harmonic order. In this analysis the flow vectors are established separately for the two sides of the FCal and are denoted $Q_n^{N|P}$, where the N and P correspond to $\eta < 0$ and $\eta > 0$ sides, respectively. The sum in Eq. (5) in this case runs over the calorimeter towers of approximate granularity $\Delta\eta \times \Delta\phi = 0.1 \times 0.1$ and the weights w_i are the transverse energies E_{T} measured in the FCal towers. The flow vectors are also calculated using charged-particle tracks. In this case the sum in Eq. (5) is over tracks and w_j is obtained as the MC tracking weight $((1 - f)/\epsilon)$ multiplied by a factor that depends on azimuthal angle to correct for non-uniformity in the azimuthal-angle distribution of reconstructed tracks. This latter factor is obtained run-by-run from the data as the average track multiplicity in one η slice of 0.1 divided by the multiplicity in the narrow $\Delta\eta \times \Delta\phi = 0.1 \times 0.1$ interval.

The main idea of the SP method is to correlate single-track unit flow vectors with the flow vector of all particles measured in the FCal region ($3.2 < |\eta| < 4.9$). Therefore, the SP method differs from the two-particle correlation method, in which each single track is correlated with all tracks of $|\Delta\eta| > 2$ in the event. The values of v_n in this analysis are obtained as:
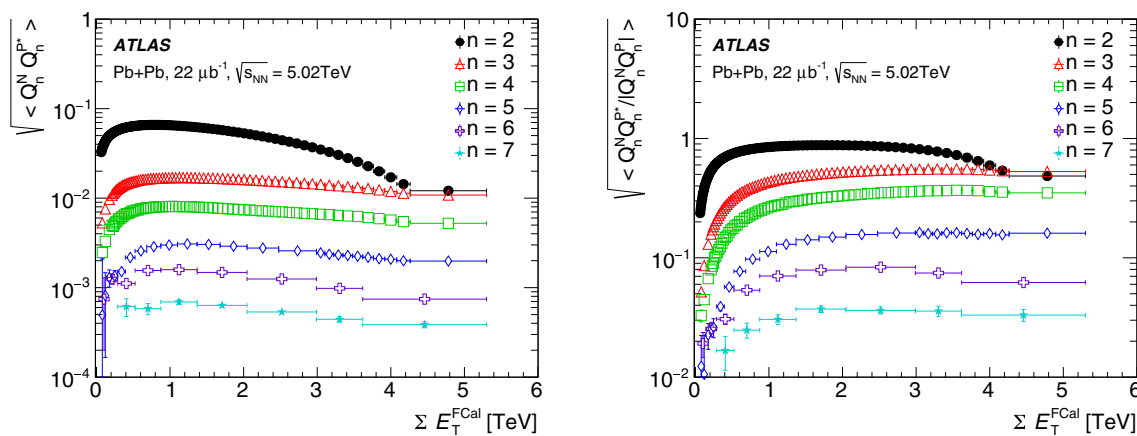

Fig. 4 The dependence of the correction factor in the SP method, $\sqrt{\langle Q_n^N Q_n^{P*} \rangle}$ (left panel), and EP method, $\sqrt{\left\langle \frac{Q_n^N Q_n^{P*}}{|Q_n^N||Q_n^P|} \right\rangle}$ (right panel), for all measured harmonics as a function of $\Sigma E_{\mathrm{T}}^{\mathrm{FCal}}$ binned according to the centrality bins definition

$$v_n\{SP\} = Re\,\frac{\langle q_{n,j} Q_n^{N|P*}\rangle}{\sqrt{\langle Q_n^N Q_n^{P*}\rangle}}$$
$$= \frac{\langle |q_{n,j}||Q_n^{N|P}|\cos[n(\phi_j - \Psi_n^{N|P})]\rangle}{\sqrt{\langle |Q_n^N||Q_n^P|\cos[n(\Psi_n^N - \Psi_n^P)]\rangle}}, \qquad (6)$$

where $q_{n,j}$ is the flow vector obtained for a small (η, p_T) interval (typically 0.1 in η and 0.1 GeV in p_T below 5 GeV and 1 GeV at higher p_T) using tracks, $Q_n^{N|P}$ is the flow vector obtained using either the N or P side of the FCal, chosen so that the η gap between the $q_{n,j}$ and Q_n is maximized, the * denotes complex conjugation, the Ψ_n are estimates of the nth-order reaction-plane angles (Eq. (1)) and the angular brackets indicate an average over all events. In the last line of Eq. (6) it is assumed that the sine terms disappear, as required from symmetry. The correction factor, $1/\sqrt{\langle Q_n^N Q_n^{P*}\rangle}$, (Eq. (6)) depends on the harmonic order and ΣE_T^{FCal} as shown in the left panel of Fig. 4. The event-plane angles, Ψ_n, and the Q_n vectors, both measured in the FCal, may be biased due to non-uniform detector response. As Ψ_n varies randomly from event to event, its distribution should be uniform, and the components of the Q_n vector,

$Q_{n,x} = |Q_n,|\cos(\Psi_n)$ and $Q_{n,y} = |Q_n|\sin(\Psi_n)$, should be zero when averaged over many events. This is achieved by the following procedure. In its first step, non-zero offsets of the mean of raw flow vector coordinates are removed for each run: $Q_{n,i} = Q_{n,i}^{raw} - \langle Q_{n,i}^{raw}\rangle$ where $i = x, y$ and $\langle Q_n^{raw}\rangle$ is the mean calculated for each run. However, even after this correction, residual higher-order non-uniformities persist, indicated by non-zero values of $\langle Q_{n,x} Q_{n,y}\rangle$. These are removed by rotating the Q_n vector so that the corrected Q_n vector has no skew ($\langle Q_{n,x}^2\rangle = \langle Q_{n,y}^2\rangle$; $\langle Q_{n,x} Q_{n,y}\rangle = 0$) and the distributions of the resulting EP angles, Ψ_n, are uniform [52].

In the Event Plane analysis the reference Q_n vectors are normalized to unity, $Q_n^{N|P} \to Q_n^{N|P}/|Q_n^{N|P}|$, before using them in Eq. (6). So the v_n estimate is obtained as:

$$v_n\{EP\} = Re\,\frac{\left\langle q_{n,j}\frac{Q_n^{N|P*}}{|Q_n^{N|P}|}\right\rangle}{\sqrt{\left\langle\frac{Q_n^N}{|Q_n^N|}\frac{Q_n^{P*}}{|Q_n^P|}\right\rangle}} = \frac{\langle\cos[n(\phi_j - \Psi_n^{N|P})]\rangle}{\sqrt{\langle\cos[n(\Psi_n^N - \Psi_n^P)]\rangle}}. \qquad (7)$$

The denominator of Eq. (7), shown in the right panel of Fig. 4, can be thought of as a resolution. It is distinct for each harmonic and depends on ΣE_T^{FCal}.

Table 3 The systematic uncertainties associated with the 2PC v_n measurements for selected intervals of p_T and for 5–10% and 40–50% centrality bins. The contributions are expressed in %. The total systematic uncertainty is obtained by adding the contribution of the individual sources in quadrature

Systematic sources	nth harmonic	5–10%		40–50%	
		0.8–1.0 GeV	6–8 GeV	0.8–1.0 GeV	6–8 GeV
Track selection	v_2	0.5	0.5	0.5	< 0.5
	v_3	1	1	0.5	0.5
	v_4	0.5	< 0.5	< 0.5	1
	v_5	2	< 0.5	0.5	5
	v_6	2	2	2	2
Tracking efficiency	v_2	0.1	0.1	0.1	0.1
	v_3	0.1	0.1	0.1	0.1
	v_4	0.1	0.1	0.1	0.1
	v_5	0.1	0.1	0.1	0.3
	v_6	1	0.1	1	0.1
Centrality determination	v_2	1	1	0.5	0.5
	v_3	0.5	0.5	0.5	3
	v_4	0.5	0.5	0.5	3
	v_5	0.5	0.5	0.5	3
	v_6	0.5	0.5	0.5	3
MC corrections	v_2	2	< 0.5	< 0.5	< 0.5
	v_3	2	< 0.5	< 0.5	< 0.5
	v_4	1	< 0.5	< 0.5	< 0.5
	v_5	1	< 0.5	1	1
	v_6	3	< 0.5	2	< 0.5
Event-mixing	v_2	1	1	1	1
	v_3	1	3	1	3
	v_4	2	6	1	6
	v_5	3	10	3	10
	v_6	5	15	5	15

Table 4 The systematic uncertainties associated with the SP and EP (in parentheses) v_n measurements for v_n in 5–10% and 40–50% centrality bins. The contributions are expressed in %. The total systematic uncertainty is obtained by adding the contribution of the individual sources in quadrature

| Systematic sources	nth harmonic	5–10%		40–50%	
		0.8–1 GeV	9–10 GeV	0.8–1 GeV	9–10 GeV
Track selection	v_2	0.5 (1)	0.5 (<0.5)	<0.5 (<0.5)	<0.5 (<0.5)
	v_3	1 (1)	1 (<0.5)	0.5 (0.5)	0.5 (0.5)
	v_4	0.5 (0.5)	<0.5 (0.5)	<0.5 (<0.5)	1 (1)
	v_5	2 (1)	0.5 (<0.5)	0.6 (0.5)	5 (4)
	v_6	2 (2)		2 (2)	
	v_7	6 (6)		4 (5)	
Tracking efficiency	v_2	0.1 (0.1)		0.1 (0.1)	
	v_3	0.1 (0.1)		0.1 (0.1)	
	v_4	0.1 (0.1)		0.1 (0.1)	
	v_5	0.1 (0.1)		0.1 (0.1)	
	v_6	1 (1)	0.1 (0.1)	1 (1)	0.1 (0.1)
	v_7	1.5 (1.5)		1.5 (1.5)	
Centrality determination	v_2	0.5 (0.5)	0.5 (0.5)	<0.5 (<0.5)	<0.5 (<0.5)
	v_3	<0.5 (<0.5)	<0.5 (<0.5)	<0.5 (<0.5)	0.5 (1)
	v_4	<0.5 (<0.5)	<0.5 (<0.5)	0.5 (0.5)	<0.5 (<0.5)
	v_5	<0.5 (<0.5)	<0.5 (0.5)	1 (1)	1 (1)
	v_6	2 (2)		2 (3)	2 (3)
	v_7	2 (3)		5 (5)	
Residual sine term	v_2	0.5 (0.5)	0.5 (0.5)	0.5 (0.5)	0.5 (0.5)
	v_3	1 (1)	1 (1)	0.5 (1)	0.5 (0.5)
	v_4	1 (0.5)	1 (1)	1 (0.5)	1 (1)
	v_5	1 (0.5)	1 (1)	1 (1)	0.5 (0.5)
	v_6	22 (26)	2 (1)	19 (11)	1 (3)
	v_7	20 (20)		17 (4)	
MC corrections	v_2	2 (2)	<0.5 (<0.5)	<0.5 (<0.5)	<0.5 (<0.5)
	v_3	2 (2)	<0.5 (<0.5)	<0.5 (<0.5)	<0.5 (<0.5)
	v_4	1 (1)	<0.5 (<0.5)	<0.5 (<0.5)	<0.5 (<0.5)
	v_5	1 (1)	<0.5 (0.5)	1 (1)	1 (0.5)
	v_6	3 (3)	<0.5 (0.5)	2 (2)	0.5 (0.5)
	v_7	–	–	–	–
FCal response	v_2	<0.5 (1)	0.5 (1)	<0.5 (0.5)	1 (1)
	v_3	0.5 (0.5)	0.5 (1)	<0.5 (<0.5)	2 (3)
	v_4	1 (2)	<0.5 (<0.5)	1 (1)	2 (2)
	v_5	1 (1)	3 (1)	4 (8)	9 (16)
	v_6	3 (5)		16 (14)	
	v_7	27 (34)		20 (9)	
Detector non-uniformity	v_2	<0.5 (<0.5)	<0.5 (<0.5)	<0.5 (<0.5)	<0.5 (<0.5)
	v_3	0.5 (<0.5)	<0.5 (<0.5)	<0.5 (<0.5)	<0.5 (<0.5)
	v_4	<0.5 (1)	<0.5 (0.5)	0.5 (0.5)	<0.5 (0.5)
	v_5	2 (2)	1 (0.5)	1 (0.5)	1 (0.5)
	v_6	8 (10)		0.5 (2)	
	v_7	2 (3)		18 (14)	
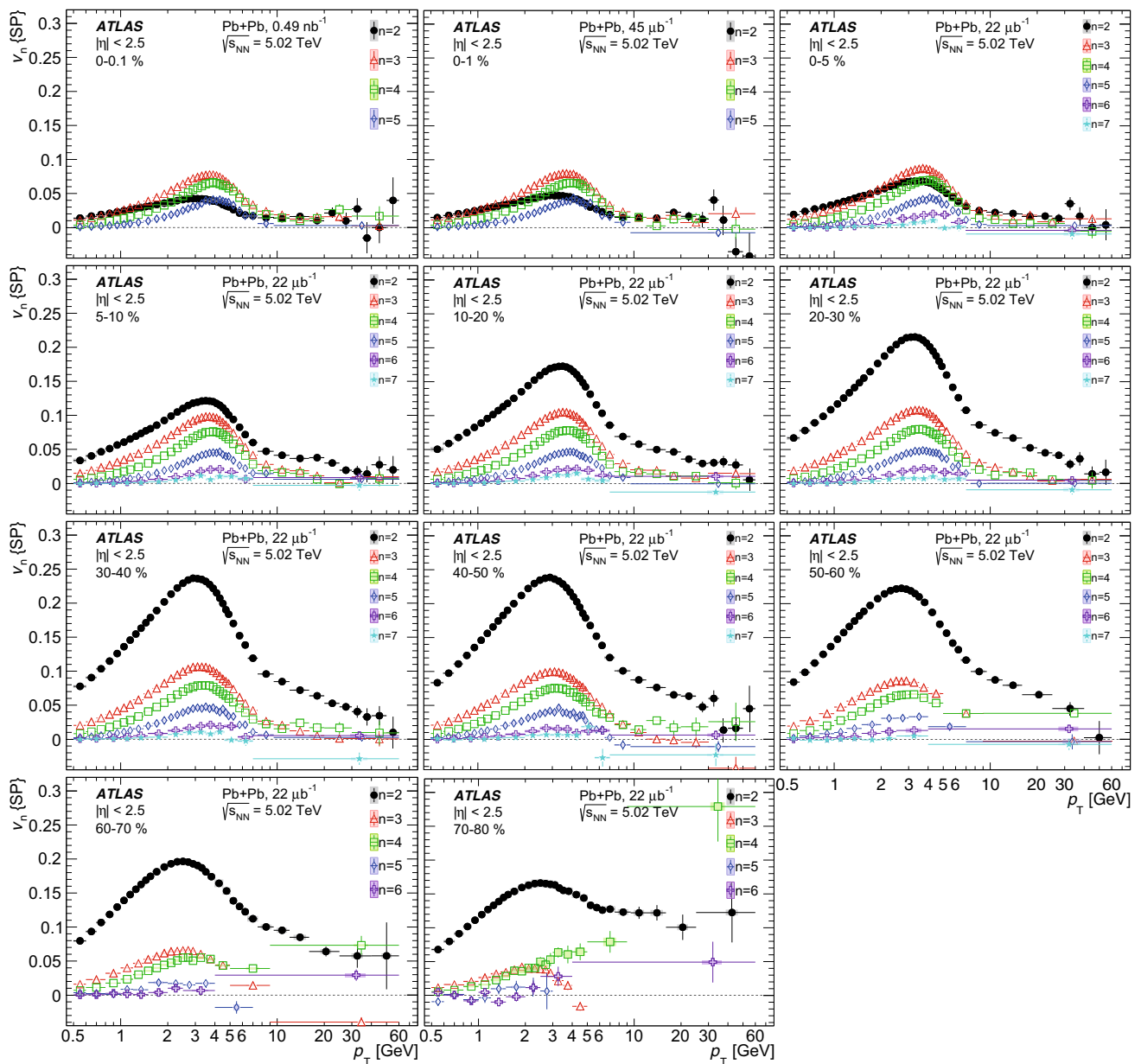
Fig. 5 The v_n obtained with the SP method as a function of transverse momentum p_T, integrated over $|\eta| < 2.5$ in 11 centrality intervals, from the most central at the top left panel to the most peripheral at the bottom right panel. Results are averaged over the intervals indicated by horizontal error bars. The vertical error bars indicate statistical uncertainties; the shaded boxes indicate systematic uncertainties

In this analysis the EP method is used only for the purpose of a direct comparison with the results obtained in Run 1 [13], in which only the EP method was used.

The analysis is performed in intervals of centrality. The v_n values are obtained in narrow bins of p_T and η, which are summed, taking into account tracking efficiency and fake rate, to obtain the integrated results.

A detailed study based on a HIJING [39] Monte Carlo sample showed a difference for the most central events between the v_n obtained with generated particles and the v_n

obtained with reconstructed tracks (the "MC closure test"). The discrepancies are due to the presence of fake tracks, which at low p_T distort the v_n measurements, and a tracking inefficiency in the event-plane direction due to increased detector occupancy resulting from the flow phenomenon itself, which lowers the measured v_n values. The study based on the d_0 distribution also showed that the fake-track rates are overestimated in MC simulation as compared to the data. This disagreement was removed by weighting MC tracks so that the d_0-distribution tails ($2 < |d_0| < 10$ mm) match
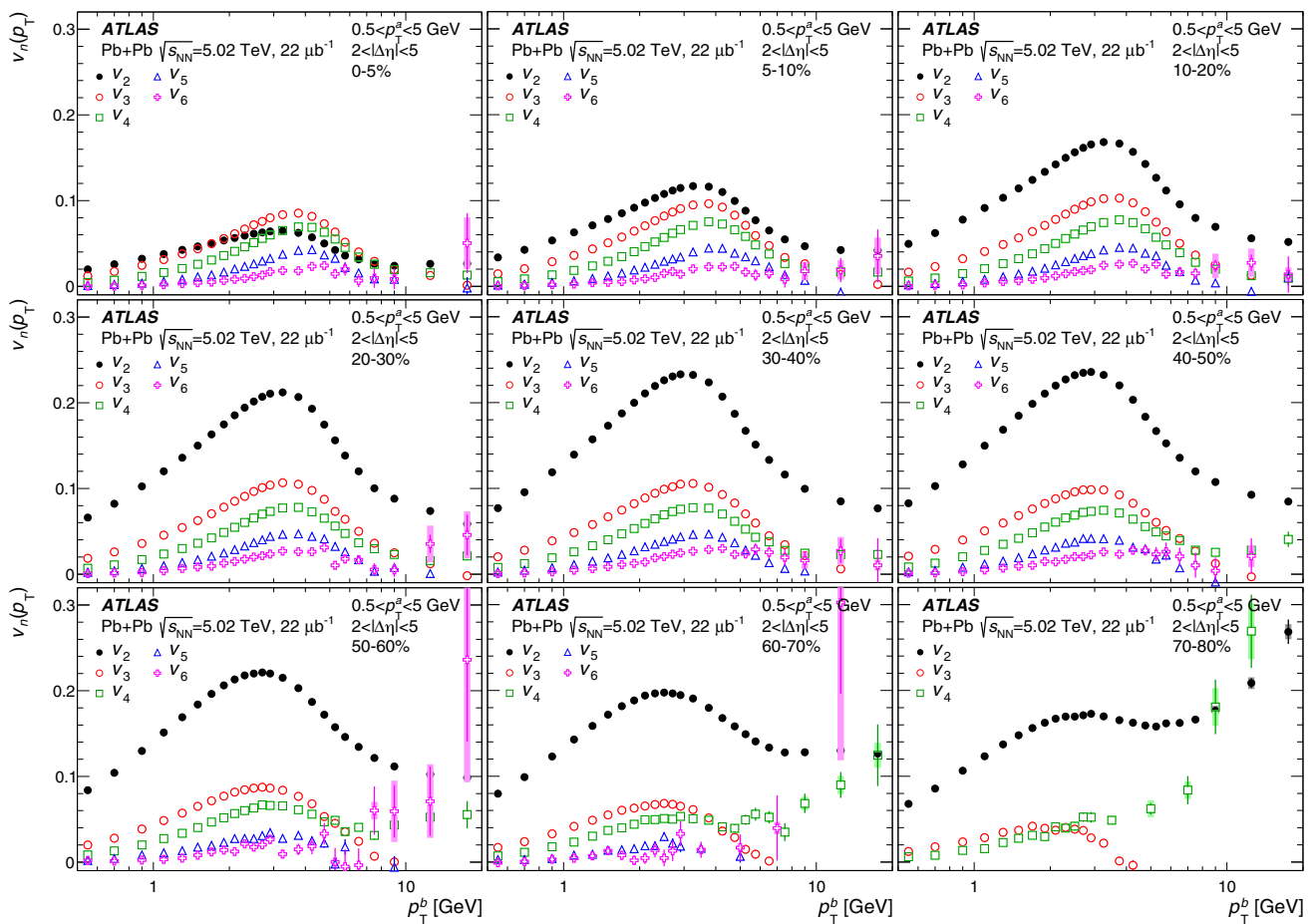
Fig. 6 The v_n values obtained with the 2PC method as a function of p_T^b for $0.5 < p_T^a < 5$ GeV. Each panel represents a different centrality interval. The vertical error bars indicate statistical uncertainties. The shaded bands indicate systematic uncertainties

those in data, following the procedure described in Ref. [53]. It was observed that the contribution of fakes to the "MC non-closure" is significant only for events with centrality $< 30\%$ and at low p_T, which is the region where the fake rate is the largest. In this modified MC sample, the relative differences between values of the v_n measured with generated particles and reconstructed tracks are used as corrections to account for both effects; the fakes and the Ψ_n-dependent inefficiency. Corrections are at most 5–10%. For example, for v_2 in the 0–5% centrality interval, the correction is as large as 7% at low p_T and becomes negligible above $p_T > 2$ GeV. Corrections of a similar magnitude are obtained for higher-order harmonics.

5 Systematic uncertainties

The systematic uncertainties of the measured v_n are evaluated by varying several aspects of the analysis. As the EP and SP results are subject to the same uncertainty sources, the uncertainty values are of the similar magnitude and are

not discussed separately. Similarly, some of the uncertainty sources are common to the SP/EP and the 2PC methods and are discussed together. The uncertainties for two representative p_T intervals are summarized in the Tables 3 and 4 for the 2PC and SP/EP methods, respectively. In the discussion below, other p_T ranges are referred to if uncertainties are significantly higher than in the p_T ranges shown in the tables. The following sources of uncertainty are considered:

- **Track selection:** The tracking selection requirements control the relative contribution of genuine charged particles and fake tracks entering the analysis. The stability of the results to the track selection is evaluated by varying the requirements imposed on the reconstructed tracks. Two sets of variations are used. In the first case the required number of pixel and SCT hits on the reconstructed track are relaxed to one and six, respectively. Additionally, the requirements on the transverse and longitudinal impact parameters of the track are relaxed to 1.5 mm. In the second case, the track selection is based on requirements used for the baseline measurement, but

Fig. 7 Comparison of the v_n obtained with EP and SP methods as a function of p_T in three centrality bins: 0–5%, 20–30% and 40–50%. The right bottom panel shows the v_n as a function of N_{part}, integrated over $0.5 < p_T < 60$ GeV. The correspondence of N_{part} to centrality intervals is provided in Table 2. In the inset the v_6 and v_7 integrated over $0.5 < p_T < 60$ GeV are shown with adjusted scale. For the $v_n(p_T)$ comparisons, the results are averaged over the intervals indicated by horizontal error bars. The vertical error bars indicate the quadrature sum of statistical and systematical uncertainties
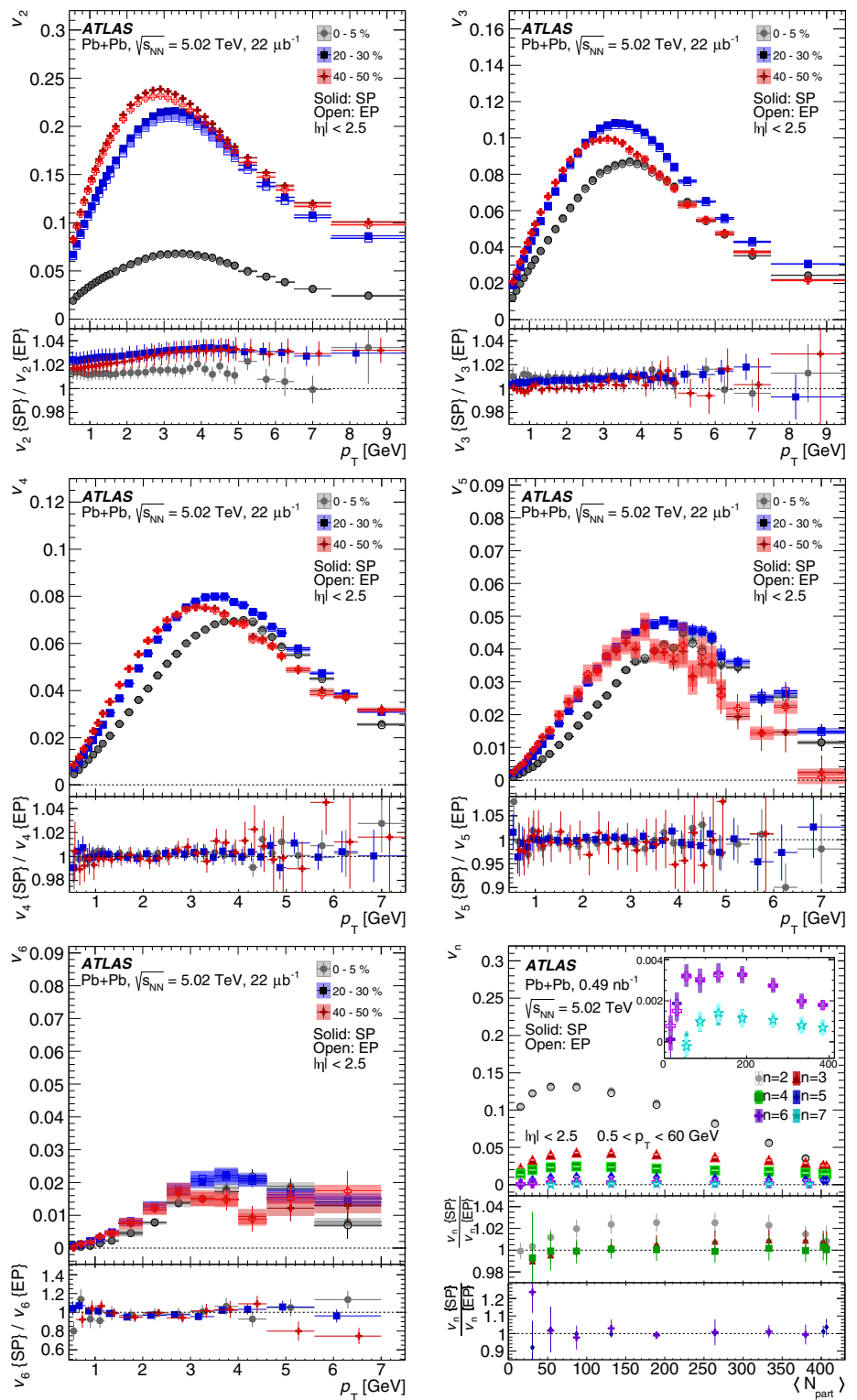

the transverse and longitudinal impact parameters of the track are restricted to 0.5 mm. For each variation, the entire analysis is repeated including the evaluation of the corresponding efficiencies and fake rates. The fake rate is largest at the lowest p_T (0.5 GeV) and for the most central events, and consequently the variation in the v_n

values obtained from this procedure is largest, typically 10%, in this region of phase space.

- **Tracking efficiency:** As mentioned above, the tracks are weighted by a factor $(1 - f)/\epsilon(p_T, \eta)$ when calculating the v_n to account for the effects of the tracking efficiency. Uncertainties in the efficiency, resulting e.g.

Fig. 8 Comparison of the v_n obtained with 2PC and SP methods as a function of p_T. Each panel shows the comparison for a different order harmonic. The comparisons are shown for three different centrality intervals: 0–5%, 20–30% and 40–50%. The vertical error bars indicate statistical uncertainties only
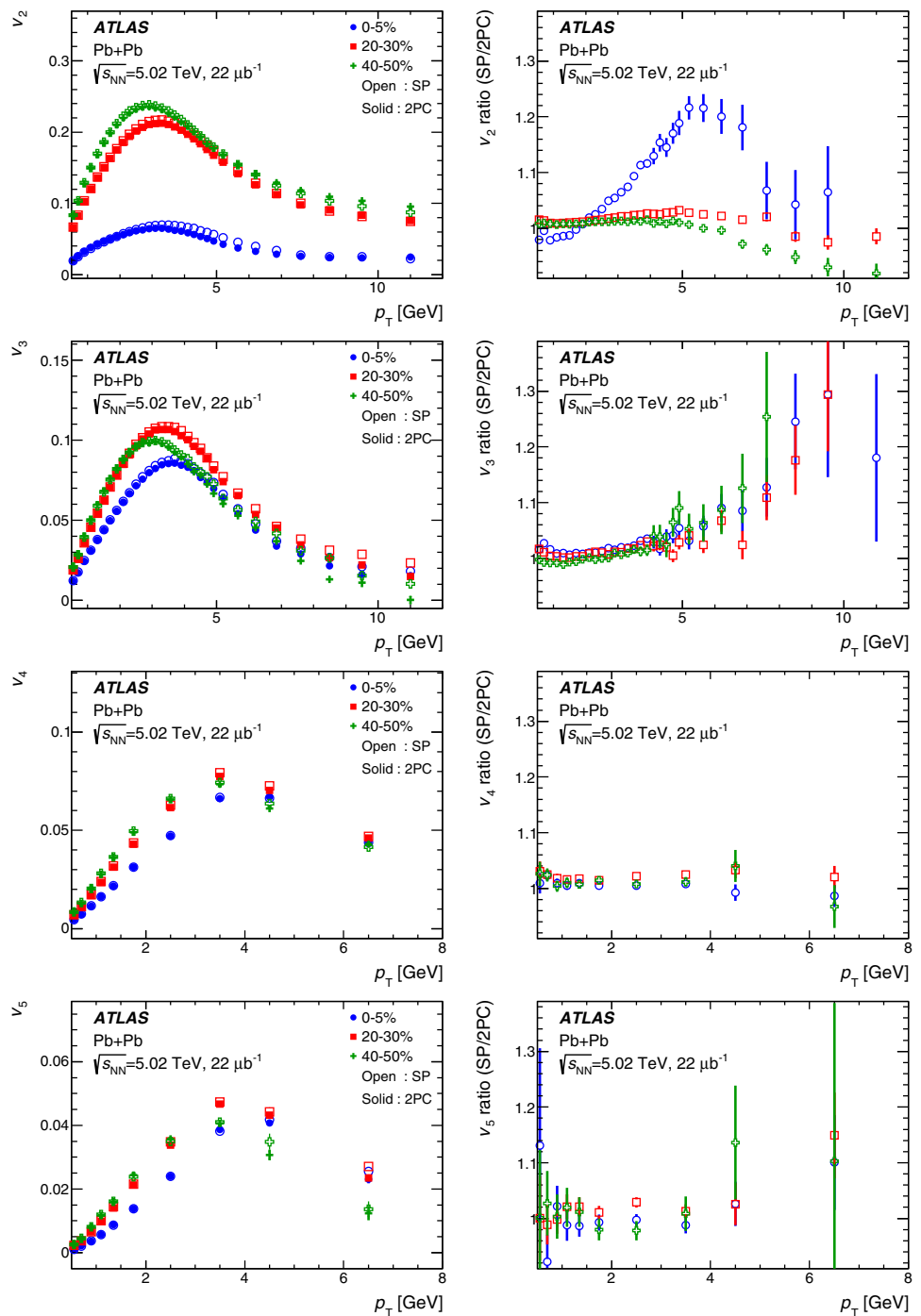
from an uncertainty in the amount of detector material, need to be propagated into the measured v_n [54]. This uncertainty is evaluated by varying the efficiency up and down within its uncertainties in a p_T-dependent manner and re-evaluating the v_n. This contribution to the overall uncertainty is very small and amounts to less than 1% on average. This is because the change of efficiency largely cancels out in the differential $v_n(p_T)$ measurement, and for v_n integrated over p_T the low-p_T particles dominate

the measurement. It does not change significantly with centrality nor with the order of harmonics.

- **Centrality determination:** An uncertainty in the flow harmonics comes from the uncertainty in the fraction of the total inelastic cross-section accepted by the trigger and the event selection criteria, which was estimated to be at a level of 1%. The v_n uncertainty is evaluated by repeating the analysis with the modified centrality selections on the ΣE_T^{FCal} distribution shown in Fig. 1, that

give the $\pm 1\%$ uncertainty in the sampled fraction of the cross-section [12]. The changes in the v_n are largest in the peripheral-centrality intervals, for which the bin definitions are significantly changed when remapping the centralities. For v_2, a change of $\sim 0.8\%$ (2PC) and $\sim 1\%$ (SP) is also observed in the most central events. This is because the v_2 changes rapidly with centrality in central events, so slight variations in the centrality definition result in significant change in v_2. For v_3 this uncertainty varies from less than 0.5% over the 0–50% centrality range to $\sim 5\%$ in the 70–80% centrality interval. For the higher-order harmonics, $n > 3$, the uncertainty is less than 0.5% over the 0–50% centrality range and increases to about 2% for more peripheral bins. The variation in the v_n when using these alternative centrality definitions is taken as a systematic uncertainty. To limit the statistical instability of v_6 and v_7 in uncertainty estimation, the variations for this measurement were determined over a wide range of $p_T = 0.5$–60 GeV.

- **MC corrections:** To assess the uncertainty related to the MC corrections the closure test is repeated with the two selections of tracks described in the "track selection" paragraph. Differences between the correction factors obtained with loose, nominal and tight tracking selections are compared. The difference between them is largest at low p_T and central events and amounts typically to a few percent. It is negligibly small above 2 GeV. The larger of the two differences (between the nominal and loose tracking selections) is used as an uncertainty estimate.

- **Residual sine term:** The ability of the detector to measure small v_n signals can be quantified by comparing the value of the v_n calculated as the real part of the flow vector product (SP) in Eq. (6) with its imaginary part. The ratio $Im(SP)/v_n$ is taken as a contribution to the systematic uncertainty. The contribution from this source is $\sim 1\%$ in most of the phase space, while for the higher harmonics ($n = 6, 7$) it can reach 20% in the most central collisions. This uncertainty is only relevant for the v_n values measured by the EP and SP methods.

- **Variation of FCal acceptance in the $Q_n^{N|P}$ estimation:** In order to quantify an uncertainty arising from the FCal acceptance in the $Q_n^{N|P}$ estimation, v_n harmonics are compared for two distinct FCal regions $3.2 < |\eta| < 4$ and $4 < |\eta| < 4.8$ used for the determination of the reference flow vector, Q_n. The differences between the v_n values are treated as the systematic uncertainty, which, similarly to the η symmetry (next paragraph), quantifies the ability of the detector to measure small signals. Accordingly, this contribution is small ($\sim 1\%$) for v_2 and v_3 and starts growing for higher-order harmonics, reaching about 27% for v_7. This uncertainty is only relevant to the v_n values measured by the EP and SP methods.

- **Detector non-uniformity:** Due to the symmetry of the Pb+Pb collision system the $v_n(\eta)$ are expected to be on average symmetric in rapidity. Any difference between the event-averaged v_n at $\pm \eta$ arises from residual detector non-uniformity. The difference between the v_n values measured in opposite hemispheres is treated as the systematic uncertainty quantifying non-perfect detector performance. This uncertainty is in general very low (less than 1%) except for high-order harmonics: v_5 and v_6 at high p_T and v_7 at all p_T. This uncertainty only contributes to the v_n values measured by the EP and SP methods. For the 2PC method, the residual non-uniformity is estimated by varying the event-mixing procedure.

- **Event-mixing:** As explained in Sect. 4.1, the 2PC analysis uses the event-mixing technique to estimate and correct for the detector-acceptance effects. Potential systematic uncertainties in the v_n due to the residual pair-acceptance effects, which were not removed by the mixed events, are evaluated by varying the multiplicity and z-vertex matching criteria used to make the mixed-event distributions, following Ref. [13]. The resulting uncertainty for v_2–v_5 is between 1–3%, and for v_6 is between 4–8% for most of the centrality and p_T ranges measured in this paper. However, the uncertainties for v_4–v_6 are significantly larger for $p_T < .7$ GeV, where the v_n signals are quite small and very susceptible to acceptance effects, and for v_6 are correlated with statistical uncertainties. The uncertainties are also significantly larger for $p_T > 10$ GeV, where they are difficult to determine due to large statistical uncertainties in the measurements.

6 Results

6.1 The p_T dependence of v_n

Figures 5 and 6 show the v_n obtained from the SP and 2PC methods, respectively, as a function of p_T for several centrality intervals. For the SP method the v_2–v_5 harmonics are also shown for the 0–0.1% and 0–1% ultra-central collisions. The SP results are integrated over the pseudorapidity $|\eta| < 2.5$ and the 2PC results are obtained with $0.5 < p_T^a < 5$ GeV and for $2 < |\Delta\eta| < 5$. The v_n values show a similar p_T dependence across all centralities: a nearly linear rise to about 2 GeV, followed by a gradual increase to reach a maximum around 2–4 GeV and a gradual fall at higher p_T. However, significant v_n values persist at high $p_T (\sim 20$ GeV). The v_2 is positive even at the highest measured p_T of 60 GeV (Fig. 5). This indicates the parton energy loss in the created medium [30]. Such elliptic flow is expected due to path-length dependence of the energy loss of high-p_T partons traversing the hot and dense medium. In peripheral events, at the highest p_T, the 2PC and SP v_2 values again show an
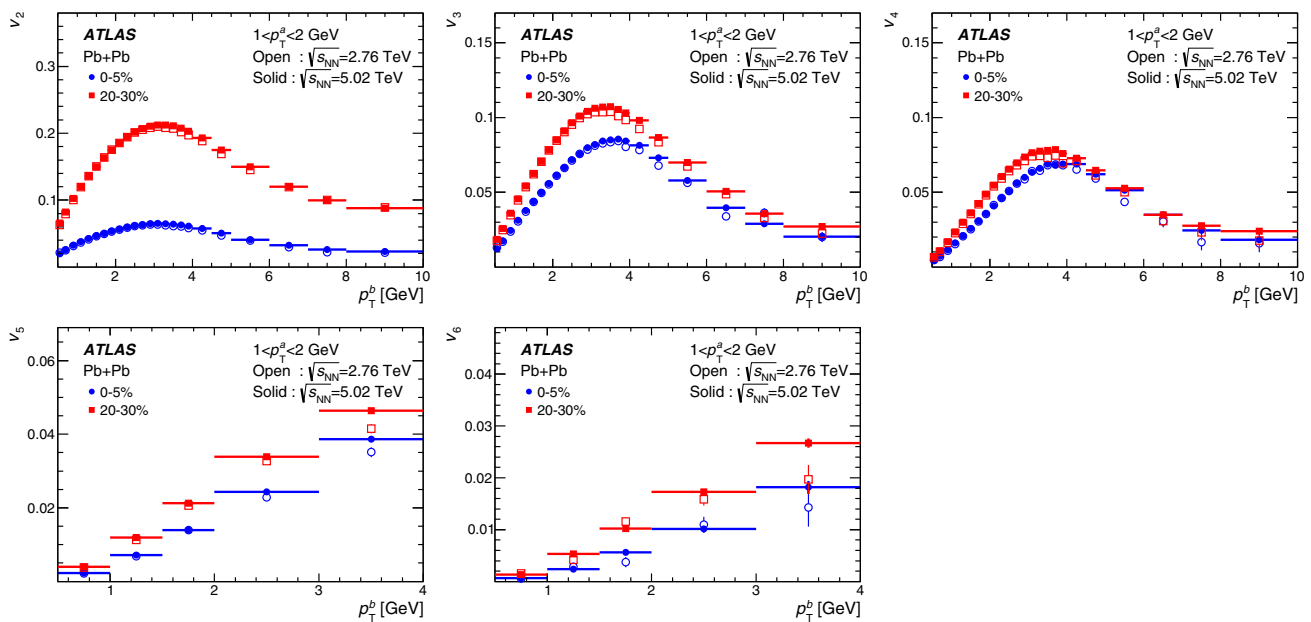
Fig. 9 Comparisons of the 2PC v_n harmonics measured at $\sqrt{s_{NN}} = 2.76$ TeV (Run 1) and at $\sqrt{s_{NN}} = 5.02$ TeV (Run 2). The results are plotted as a function of p_T^b for $1 < p_T^a < 2$ GeV for two centralities: 0–5% and 20–30%. Each panel corresponds to a different harmonic. Results are averaged over the intervals indicated by horizontal error bars. The vertical error bars indicate statistical uncertainties

increasing trend due to the increasing influence of the away-side jet. The increased v_2 in peripheral collisions at high-p_T is accompanied by reduced values of v_3 and increased values of v_4, which is characteristic of a large away-side peak, as described in Sect. 4.1. This is most clearly seen in the 70–80% centrality interval.

The v_2 varies significantly with centrality, reflecting a change in the shape of the average initial collision geometry, from nearly circular in ultra-central collisions to an almond shape in peripheral events. The higher harmonics do not show similar behaviour, as neither higher-order eccentricities nor the fluctuations vary so significantly with the centrality. The v_2 is dominant at all centralities, except for the most central collisions interval where, at intermediate p_T, v_3 and v_4 become larger than v_2, indicating that the dominant source of observed flow comes from the initial geometry fluctuations. This change in the v_n ordering is even more pronounced in the 1% and 0.1% ultra-central collisions measured using the SP method, which shows that, in the p_T region around the v_n peak, $v_3 > v_4 > v_2 \approx v_5$. The v_4, similarly to v_2, exhibits an increase beyond $p_T \sim 10$ GeV, which can be attributed to the presence of the events with dijets in the data. In the SP measurement the v_7 results are also presented. The characteristics of v_7 are similar to the other high-order harmonics, but the values are smaller and significant, given the uncertainties, only in central and mid-central collisions and for the p_T range of 2–6 GeV.

6.1.1 The scalar product and event plane methods comparison

Figure 7 compares the v_n values measured with the EP and SP methods as a function of p_T and N_{part} for the integrated p_T range of $0.5 < p_T < 60$ GeV. A small difference is seen between the v_2 values measured with the two methods. The difference is largest in mid-central events: about 3% in the 20–30% and 40–50% centrality intervals, about 1% in the 0–5% most central collisions and negligible in peripheral collisions. This difference is expected according to Ref. [28] as the SP method measures $\sqrt{\langle v_n^2 \rangle}$ while the EP method measures values between $\langle v_n \rangle$ and $\sqrt{\langle v_n^2 \rangle}$, with the former value attained in the limit of a small correction factor (the inverse of the denominator in Eq. (7)) and approaching the latter when the correction factor is large. In the most central and peripheral events, where the correction is large for the second-order harmonic, the EP v_2 values are closer to the SP ones, while for the mid-central events where the correction is small, the EP v_2 values are systematically lower than the SP v_2 values. Higher-order EP and SP v_n harmonics are consistent with each other.

6.1.2 The scalar product and two-particle correlation methods comparison

A comparison of the SP and 2PC results is presented in Fig. 8. In general, results from the two methods are quite consistent.

Fig. 10 Comparison of the v_n obtained with EP method using Run 1 and Run 2 data as a function of p_T. The results are shown in three centrality intervals: 0–5%, 20–30% and 40–50%. Results are averaged over the intervals indicated by horizontal error bars. The vertical error bars indicate statistical uncertainties. The shaded areas indicate systematic uncertainties
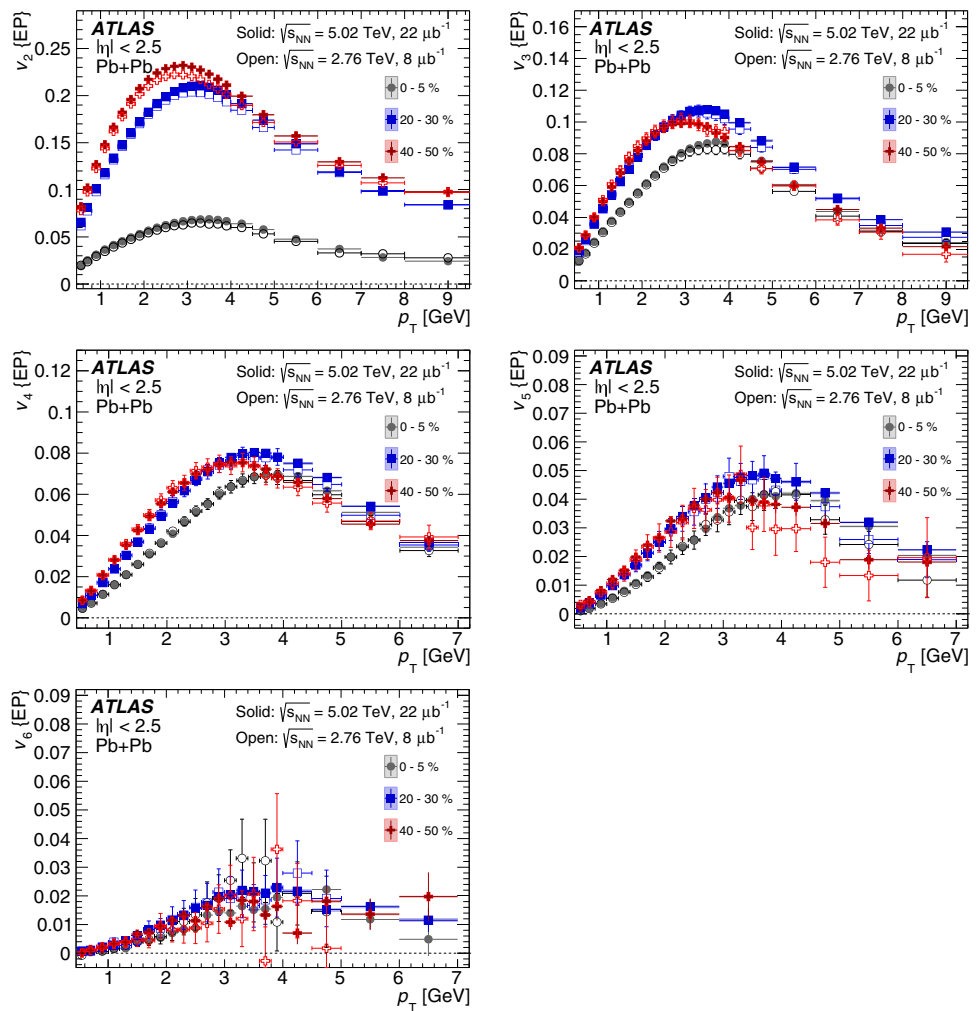
There is a significant difference in v_2 from the two methods in the phase-space region $p_T < 5$ GeV, 0–5% centrality. This difference decreases considerably for 20–30% mid-central events, where the v_2 values match within 2–5% up to $p_T \sim 10$ GeV. For v_3–v_5, where there are enough events for a clear comparison, the v_n values match within $\sim$4% for $p_T < 4$ GeV for the three centrality intervals shown in Fig. 8. In principle, both the SP and 2PC methods measure $\sqrt{\langle v_n^2 \rangle}$ and the flow harmonics measured by the two methods should be identical. However, a breakdown of factorization (Eq. (3)) results in systematic differences in the flow harmonics measurement. Such factorization breakdown has been observed to be significant for v_2 in central events [55], and in general for all v_n at higher p_T, and is the leading source of disagreement between the 2PC and SP results. Furthermore, in the 2PC method the $\Delta\eta$ gap between the reference and associated particles is chosen to be $|\Delta\eta| > 2$, while in the SP method, where the reference flow is measured in the FCal, the minimum gap between the tracks and the FCal is 3.2 units in η. The presence of longitudinal-flow fluctuations, in which the event-plane angle can change with η, can result in different v_n values depending on the η range where the

reference flow is measured [27,56]. This effect is also found to be larger in central events and relatively smaller in mid-central events [56]. These effects can further contribute to the observed difference between the SP and 2PC v_n values.

6.1.3 Comparison to Pb+Pb results at $\sqrt{s_{NN}}$ = 2.76 TeV

Figure 9 shows a comparison of the v_n measured in the present analysis at $\sqrt{s_{NN}} = 5.02$ TeV with the corresponding measurements at $\sqrt{s_{NN}} = 2.76$ TeV for harmonics v_2 to v_6 obtained using the 2PC method [13]. The comparisons are shown for two centralities: a central interval of 0–5% and a mid-central interval of 20–30%. Figure 10 shows a similar comparison of results obtained using the EP method for 0–5%, 20–30% and 40–50% centrality bins. The v_n at the two energies are quite similar and almost consistent throughout within systematic and statistical uncertainties, even though the MC non-closure correction was applied only in the $\sqrt{s_{NN}} = 5.02$ TeV measurement. These results are consistent with the recent ALICE measurements comparing the measurement of v_n at the two collision energies [29].
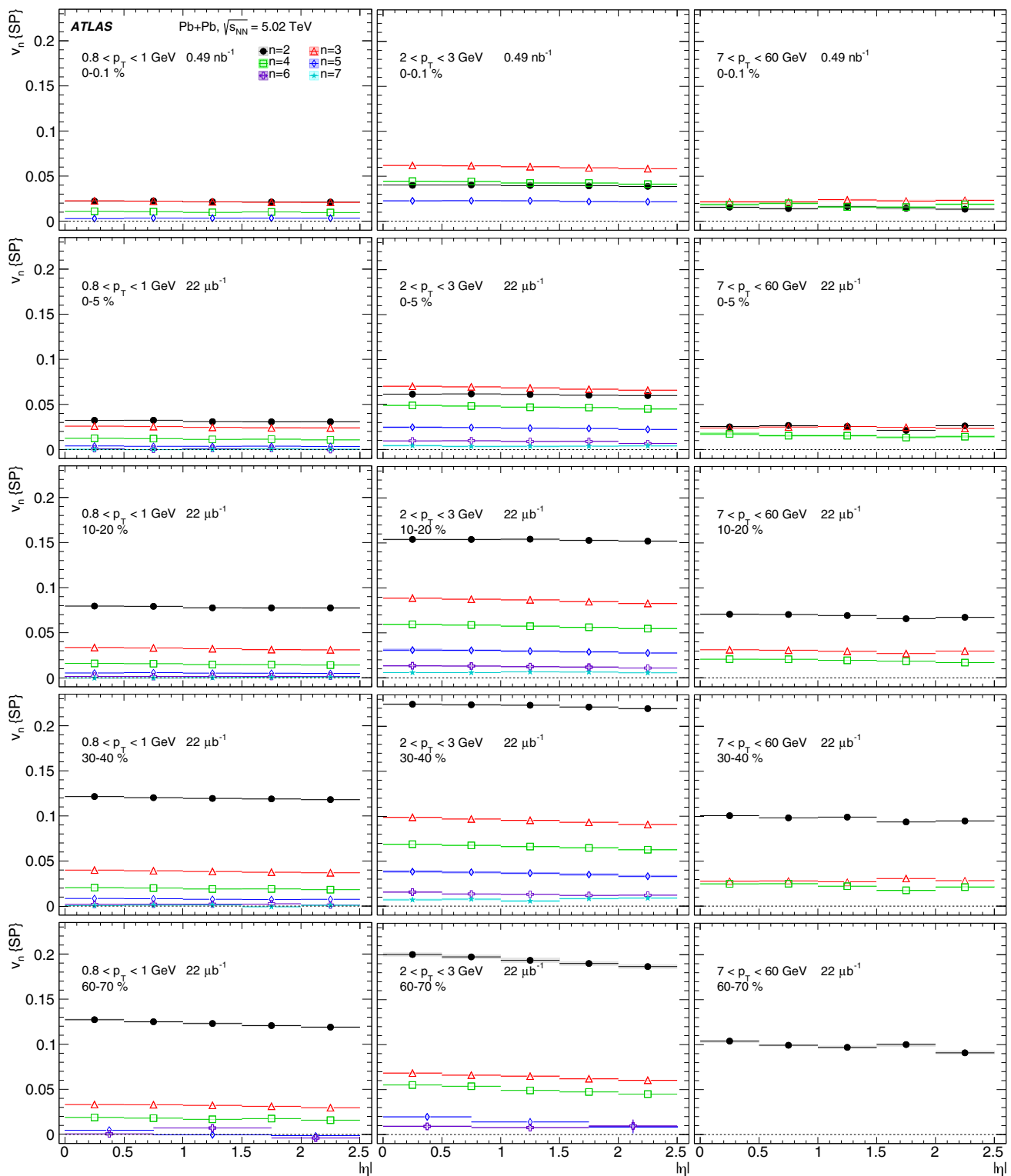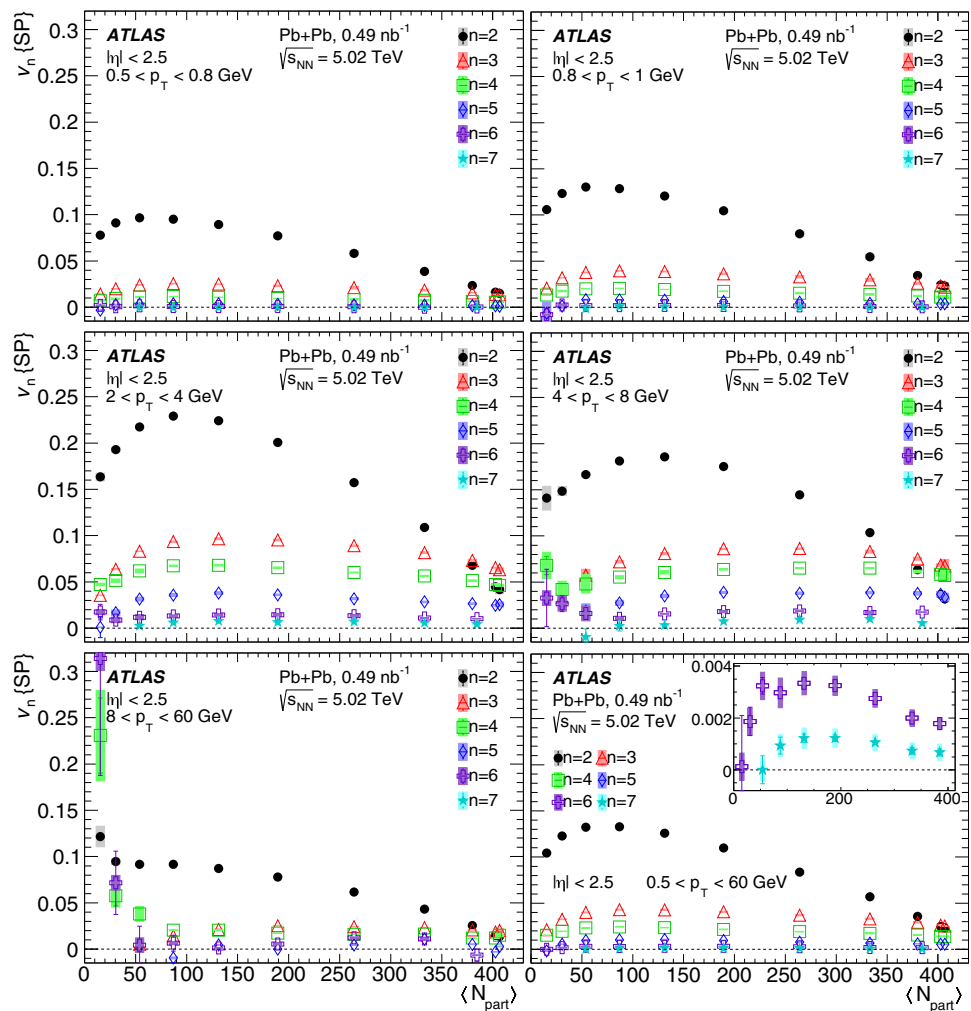
Fig. 11 The v_n as a function of pseudorapidity obtained with the SP method, for transverse momentum ranges: $0.8 < p_T < 1$ GeV (left column), $2 < p_T < 3$ GeV (middle column) and $7 < p_T < 60$ GeV (right column) and for centrality intervals: 0–0.1% (top row), 0–5%, 10–20%, 30–40% and 60–70% (bottom row). The vertical error bars indicate statistical uncertainties. The shaded boxes indicate systematic uncertainties

Fig. 12 Integrated $v_n\{SP\}$ vs. N_{part} for six p_T ranges shown in the panels from lowest p_T range at the top left to the highest at the bottom middle, measured using the scalar-product method. In the inset in the bottom-right panel the v_6 and v_7 integrated over $0.5 < p_T < 60$ GeV are shown with adjusted scale. The correspondence of N_{part} to centrality intervals is provided in Table 2. Results are averaged over the intervals indicated by horizontal error bars. The vertical error bars indicate statistical uncertainties. The shaded areas indicate systematic uncertainties


6.2 The η dependence of v_n

The pseudorapidity dependence of the v_2–v_7 obtained from the SP method is shown in Fig. 11 as a function of $|\eta|$. Benefiting from the symmetry of $v_n(\eta)$ with respect to $\eta = 0$, the v_n pseudorapidity dependence over the full range of pseudorapidity was folded into the η range 0–2.5. The η-dependence is shown for three ranges of transverse momenta $0.8 < p_T < 1$ GeV, $2 < p_T < 3$ GeV and $7 < p_T < 60$ GeV and for five centrality intervals 0–0.1%, 0–5%, 10–20%, 30–40% and 60–70%. The strong dependence of flow harmonics on p_T and centrality shown across different panels (all vertical axes in Fig. 11 have the same range) is discussed in the previous section. On the other hand, no strong pseudorapidity dependence of v_n harmonics is observed. The v_2 harmonic in central and mid-central collisions for $p_T < 3$ GeV drops only by about 2–4% over the pseudorapidity range $|\eta| = 0$–2.5. For peripheral collisions and for high $p_T > 7$ GeV a larger decrease of about 10% is observed. The v_3 harmonic in central and mid-central collisions over the p_T range from 2 to 3 GeV decreases by about 10% with a larger drop of ~15% for peripheral collisions. Similar pseudorapidity dependence

is measured for the v_4 harmonic in central and mid-central collisions over the p_T range from 2 to 3 GeV where it changes by about 10%, but a larger drop of 25% is observed in peripheral collisions. In other cases, v_n harmonics are almost consistent with a uniform distribution within the statistical and systematic uncertainties. As observed in the earlier measurement of v_n harmonics in 2.76 TeV Pb+Pb collisions [19], such a weak η dependence of v_2 may be partially attributed to a contribution of "non-flow" short-range two-particle correlations.

6.3 Centrality dependence of v_n

Figure 12 shows the N_{part} dependence of v_n integrated over $|\eta| < 2.5$ and for various ranges of p_T using the SP method. The elliptic flow is the dominant anisotropy, except at the largest N_{part} ($N_{part} \gtrsim 350$), which corresponds to the 0–5% most central collisions. For $p_T < 8$ GeV, a clear dependence on initial geometry can be observed as v_2 is highest in mid-central collisions, where this asymmetry is most significant. For $p_T > 8$ GeV, v_2 is still the dominant harmonic, and it is non-zero even in peripheral collisions as non-flow effects

Fig. 13 Left panels: the v_2 (p_T) (top) and v_3 (p_T) (bottom) for different centrality intervals. Right panels: the corresponding scaled-$v_n(p_T)$. The error bars indicate statistical and systematic uncertainties added in quadrature and are typically too small to be seen
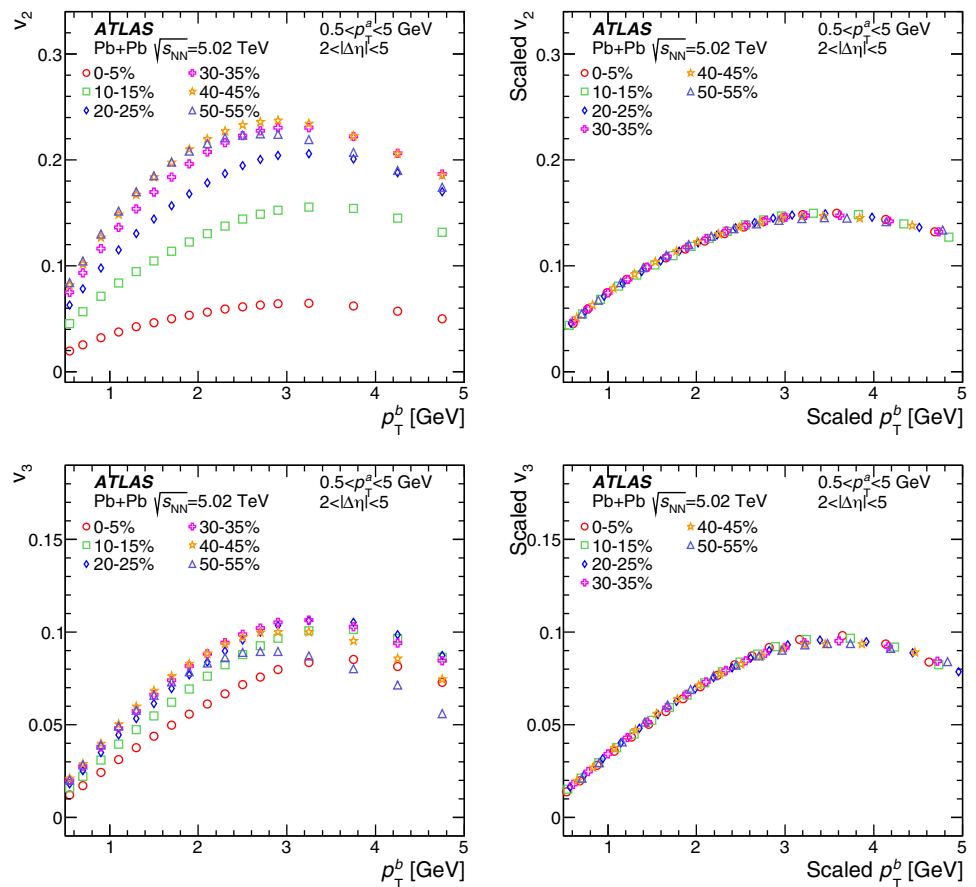
start to contribute in this region. A hierarchy $v_{n+1} < v_n$ is observed for $n = 2$–7 for all ranges of p_T and all centralities, except for the two bins 0–0.1% and 0–1% of the ultra-central collisions at intermediate p_T, which are characterised by the flow harmonics ordering $v_3 > v_4 > v_2 \approx v_5$.

6.4 $v_n(p_T)$ scaling

The left panels of Fig. 13 compare the p_T dependence of v_2 and v_3 for different centrality intervals obtained from the 2PC method. Two distinct features are observed to change in the shape of the $v_n(p_T)$ (for the same n) between the different centrality intervals:

1. Change in the v_n-scale: The overall magnitude of the v_n changes from one centrality to another. This effect is particularly large for v_2, and has to do with the changing of the average collision geometry from one centrality to another.
2. Change in the p_T scale: The p_T value at which the v_n reaches its maximum also changes systematically from one centrality to another.

In a recent ATLAS paper [45] it was observed that for a given order n, the $v_n(p_T)$ in p+Pb and Pb+Pb collisions have

a very similar p_T dependence. In fact, after a scaling along the p_T axis to account for the difference in $\langle p_T \rangle$ between p+Pb and Pb+Pb collisions, and an empirical scaling along the v_n (i.e. y-axis) to account for the difference in the collision geometry between the two systems, the scaled $v_n(p_T)$ in p+Pb and Pb+Pb collisions were found to be nearly identical. In this section, a check is done to see if such a scaling along the p_T and v_n axes can yield universal shapes for the v_n across the different centrality classes. Accordingly, the $v_n(p_T)$ are scaled along the x- and y-axes to match their shapes across the different centrality intervals. For the matching, the 0–60% centrality interval is chosen as the reference, and the $v_n(p_T)$ for the individual 5%-wide centralities are scaled to match best the $v_n(p_T)$ in the 0–60% centrality interval over the 0.5–5 GeV p_T range, with the scales along the x- and y-axes treated as fit parameters. The right panels of Fig. 13 show the scaled-v_n, for $n = 2$ and 3. Overall, the $v_n(p_T)$ shapes match well after the p_T and v_n scalings.

Figure 14 shows the x (or p_T) and y-scale factors obtained for v_2 and v_3 as a function of centrality. It is interesting to note that the p_T-scale factors are quite comparable between v_2 and v_3 across most of the centrality ranges. However, in the 0–10% most central events, some significant difference is observed between the two scale factors. This difference could be due to larger jet-bias and factorization-breaking effects in

Fig. 14 Left panel: the x-scale factors for the $v_2(p_T)$ and $v_3(p_T)$ (see text) as a function of the collision centrality. Also shown for comparison are the ALICE $1/\langle p_T \rangle$ for positively charged protons and pions (scaled by constant factors of 1.4 GeV and 0.57 GeV, respectively for plotting purposes). Right panel: the y-scale factors. The error bars on the scale factors and on the ALICE data indicate systematic and statistical uncertainties added in quadrature
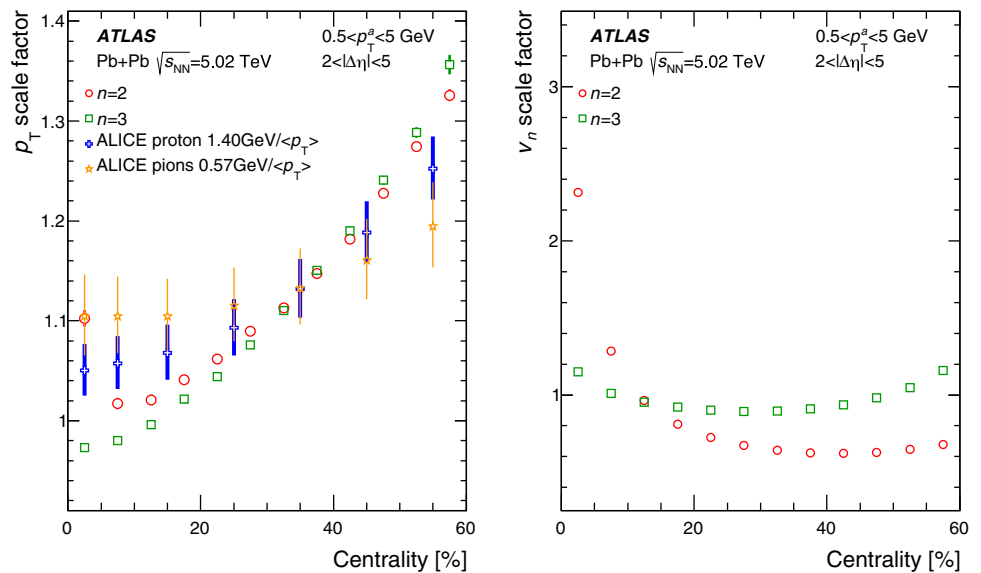
the v_2 as compared to v_3. The right panel of Fig. 14 shows the y-scale factors for v_2 and v_3 as well. Their centrality dependence is very different for the two harmonics. This is to be expected as the y-scale factors are mostly indicative of the changing collision geometry, which becomes more and more elliptic from central to mid-central events resulting in a large increase in v_2, while v_3, which is driven by fluctuations, changes only gradually.

In order to check if the change in $\langle p_T \rangle$ between the different centralities accounts for the change in the x-scale of the v_n, the $1/\langle p_T \rangle$ for protons and pions, as measured by the ALICE Collaboration [57], are also shown for comparison. While the centrality dependence of these $1/\langle p_T \rangle$ factors is qualitatively similar to the scale factors for the v_n, the relative variation in $1/\langle p_T \rangle$ is significantly smaller than the variation in the x-scale of the v_n, indicating that there are additional effects at play besides the change in the mean p_T. However, whatever the origin of these effects may be, they result in nearly identical scaling factors for v_2 and v_3.

7 Summary

This paper presents the first ATLAS measurements of azimuthal anisotropy of charged particles in Pb+Pb collisions at 5.02 TeV collected during LHC running in 2015. The measurements are based on the Pb+Pb sample of 0.49 nb^{-1} integrated luminosity and are performed with the two-particle correlation, scalar-product and event-plane methods. The azimuthal anisotropy is quantified by the flow harmonics v_2–v_6 and v_2–v_7 for measurements based on the 2PC and SP/EP methods, respectively. The flow harmonics are obtained in wide transverse momentum ($0.5 < p_T < 60$ GeV), pseudorapidity ($|\eta| < 2.5$) and centrality 0–80% ranges. All harmonics show a similar trend in the p_T dependence; first

increasing with p_T up to a maximum around 3–4 GeV and then decreasing for higher p_T. Significant values of the second-order harmonic v_2 persist up to 60 GeV. The v_2 results at high p_T provide a useful handle for the study of partonic energy loss in the dense medium, and so can improve our understanding of the QGP properties. The values of the flow harmonics decrease strongly with increasing harmonic order for all centralities, except for 0–5% central collisions where a different ordering is seen: $v_3 > v_4 > v_2 \approx v_5$ for p_T above 1 GeV, which is indicative of the presence of significant v_2 fluctuations in these ultra-central collisions. The elliptic flow signal is strongly dependent on event centrality and is largest in mid-central collisions of 30–50%. The higher-order harmonics show a weak centrality dependence, which is consistent with an anisotropy associated with fluctuations in the initial geometry. After scaling the p_T and magnitude of the differential elliptic and triangular, v_3, flow harmonics at different centralities to best match the reference v_2 and v_3 for the 0–60% centrality interval over the p_T range $0.5 < p_T < 5$ GeV, the shapes of the rescaled harmonics agree well, indicating similarity among p_T-shapes of flow harmonics evolving from different initial conditions. The v_n coefficients are shown to exhibit a weak η-dependence, irrespective of the harmonic order, centrality and p_T. A weaker pseudorapidity dependence of $v_n(\eta)$ in more central collisions is suggested by data. The results obtained using the EP and SP methods are consistent for harmonics of order $n \geq 3$. A small, systematic difference is observed for v_2, where the values obtained from the SP method are up to 3% larger than the values obtained using the EP method. The 2PC and SP methods give values for v_n that are quite consistent up to ~10 GeV. However, in the most central events the SP method gives systematically larger values for v_2 for $p_T > 2$ GeV. Comparisons with measurements in Pb+Pb collisions at $\sqrt{s_{NN}} = 2.76$ TeV show that the p_T depen-

dence of the v_n shows no change from $\sqrt{s_{NN}} = 2.76$ TeV to $\sqrt{s_{NN}} = 5.02$ TeV.

The set of results on flow harmonics presented in this paper provides a tool for studies of the underlying mechanism leading to the large azimuthal anisotropy observed in the Pb+Pb collision system, and can be used to constrain the theoretical modelling of the initial state of the QGP, its subsequent hydrodynamic evolution as well as partonic energy loss in the dense and hot medium.

References

1. PHOBOS Collaboration, B.B. Back et al., The PHOBOS perspective on discoveries at RHIC. Nucl. Phys. A **757**, 28 (2005). arXiv:nucl-ex/0410022 [nucl-ex]
2. STAR Collaboration, J. Adams et al., Experimental and theoretical challenges in the search for the quark gluon plasma: the STAR Collaboration's critical assessment of the evidence from RHIC collisions. Nucl. Phys. A **757**, 102 (2005). arXiv:nucl-ex/0501009 [nucl-ex]
3. BRAHMS Collaboration, I. Arsene et al., Quark-gluon plasma and color glass condensate at RHIC? The perspective from the BRAHMS experiment. Nucl. Phys. A **757**, 1 (2005). arXiv:nucl-ex/0410020 [nucl-ex]
4. PHENIX Collaboration, K. Adcox et al., Formation of dense partonic matter in relativistic nucleus–nucleus collisions at RHIC: experimental evaluation by the PHENIX Collaboration. Nucl. Phys. A **757**, 184 (2005). arXiv:nucl-ex/0410003 [nucl-ex]
5. J. Schukraft, QM2017: status and key open questions in ultra-relativistic heavy-ion physics. Nucl. Phys. A **967**, 1 (2017). arXiv:1705.02646 [hep-ex]
6. P. Foka, M.A. Janik, An overview of experimental results from ultra-relativistic heavy-ion collisions at the CERN LHC: bulk properties and dynamical evolution. Rev. Phys. **1**, 154 (2016). arXiv:1702.07233 [hep-ex]
7. S. Pratt, E. Sangaline, P. Sorensen, H. Wang, Constraining the equation of state of superhadronic matter from heavy-ion collisions. Phys. Rev. Lett. **114**, 202301 (2015)
8. S. Ryu et al., Importance of the bulk viscosity of QCD in ultrarelativistic heavy-ion collisions. Phys. Rev. Lett. **115**, 132301 (2015)
9. J.-Y. Ollitrault, Anisotropy as a signature of transverse collective flow. Phys. Rev. D **46**, 229 (1992)
10. S. Voloshin, Y. Zhang, Flow study in relativistic nuclear collisions by Fourier expansion of Azimuthal particle distributions. Z. Phys. C **70**, 665 (1996). arXiv:hep-ph/9407282 [hep-ph]
11. ALICE Collaboration, Elliptic flow of charged particles in Pb–Pb collisions at $\sqrt{s_{NN}}$ = 2.76 TeV. Phys. Rev. Lett. **105**, 252302 (2010)
12. ATLAS Collaboration, Measurement of the pseudorapidity and transverse momentum dependence of the elliptic flow of charged particles in lead–lead collisions at $\sqrt{s_{NN}}$ = 2.76 TeV with the ATLAS detector. Phys. Lett. B **707**, 330 (2012). arXiv:1108.6018 [hep-ex]
13. ATLAS Collaboration, Measurement of the azimuthal anisotropy for charged particle production in $\sqrt{s_{NN}}$ = 2.76 TeV lead–lead collisions with the ATLAS detector. Phys. Rev. C **86**, 014907 (2012). arXiv:1203.3087 [hep-ex]
14. CMS Collaboration, Measurement of the elliptic anisotropy of charged particles produced in PbPb collisions at $\sqrt{s_{NN}}$ = 2.76 TeV. Phys. Rev. C **87**, 014902 (2013). arXiv:1204.1409 [hep-ex]
15. F. Karsch, Properties of the quark gluon plasma: a lattice perspective. Nucl. Phys. A **783**, 13 (2007)
16. A.M. Poskanzer, S. Voloshin, Methods for analyzing anisotropic flow in relativistic nuclear collisions. Phys. Rev. C **58**, 1671 (1998). arXiv:nucl-ex/9805001 [nucl-ex]
17. S.A. Voloshin, A.M. Poskanzer, R. Snellings, Collective phenomena in non-central nuclear collisions. Landolt Bornstein **23**, 293 (2010). arXiv:0809.2949 [nucl-ex]
18. B. Schenke, P. Tribedy, R. Venugopalan, Fluctuating Glasma initial conditions and flow in heavy ion collisions. Phys. Rev. Lett. **108**, 252301 (2012). arXiv:1202.6646 [nucl-th]
19. ATLAS Collaboration, Measurement of flow harmonics with multi-particle cumulants in Pb+Pb collisions at $\sqrt{s_{NN}}$ = 2.76 TeV with the ATLAS detector. Eur. Phys. J. C **74**, 3157 (2014). arXiv:1408.4342 [hep-ex]
20. S. Ryu et al., Importance of the bulk viscosity of QCD in ultrarelativistic heavy-ion collisions. Phys. Rev. Lett. **115**, 132301 (2015). arXiv:1502.01675 [nucl-th]
21. STAR Collaboration, J. Adams et al., Azimuthal anisotropy in Au+Au collisions at $\sqrt{s_{NN}}$ = 200GeV. Phys. Rev. C **72**, 014904 (2005). arXiv:nucl-ex/0409033 [nucl-ex]
22. PHENIX Collaboration, A. Adare et al., azimuthal anisotropy of π^0 production in Au+Au collisions at $\sqrt{s_{NN}}$ = 200 GeV: path-

length dependence of jet quenching and the role of initial geometry. Phys. Rev. Lett. **105**, 142301 (2010). arXiv:1006.3740 [nucl-ex]

23. ALICE Collaboration, Elliptic flow of charged particles in Pb–Pb collisions at $\sqrt{s_{NN}}$ = 2.76 TeV. Phys. Rev. Lett. **105**, 252302 (2010). arXiv:1011.3914 [nucl-ex]

24. CMS Collaboration, Measurement of the elliptic anisotropy of charged particles produced in PbPb collisions at $\sqrt{s_{NN}}$ = 2.76 TeV. Phys. Rev. C **87**, 014902 (2013). arXiv:1204.1409 [nucl-ex]

25. STAR Collaboration, C. Adler et al., Elliptic flow from two and four particle correlations in Au+Au collisions at $\sqrt{s_{NN}}$ = 130 GeV. Phys. Rev. C **66**, 034904 (2002). arXiv:nucl-ex/0206001 [nucl-ex]

26. ATLAS Collaboration, Measurement of longitudinal flow decorrelations in Pb+Pb collisions at $\sqrt{s_{NN}}$ = 2.76 and 5.02 TeV with the ATLAS detector. Eur. Phys. J. C **78**, 142 (2018). arXiv:1709.02301 [hep-ex]

27. J. Jia, P. Huo, A method for studying the rapidity fluctuation and decorrelation of harmonic flow in heavy-ion collisions. Phys. Rev. C **90**, 034905 (2014). arXiv:1402.6680 [nucl-th]

28. M. Luzum, J.-Y. Ollitrault, Eliminating experimental bias in anisotropic-flow measurements of high-energy nuclear collisions. Phys. Rev. C **87**, 044907 (2013). arXiv:1209.2323 [nucl-ex]

29. ALICE Collaboration, Anisotropic flow of charged particles in Pb–Pb collisions at $\sqrt{s_{NN}}$ = 5.02 TeV. Phys. Rev. Lett. **116**, 132302 (2016). arXiv:1602.01119 [nucl-ex]

30. CMS Collaboration, Azimuthal anisotropy of charged particles with transverse momentum up to 100 GeV/c in PbPb collisions at $\sqrt{s_{NN}}$ = 5.02 TeV. Phys. Lett. B **776**, 195 (2018). arXiv:1702.00630 [hep-ex]

31. ATLAS Collaboration, The ATLAS experiment at the CERN large hadron collider. JINST **3**, S08003 (2008)

32. ATLAS Collaboration, ATLAS insertable B-layer technical design report. Technical report. CERN-LHCC-2010-013. ATLAS-TDR-19 (2010). http://cds.cern.ch/record/1291633

33. ATLAS Collaboration, ATLAS insertable B-layer technical design report addendum. Technical report. CERN-LHCC-2012-009. ATLAS-TDR-19-ADD-1. Addendum to CERN-LHCC-2010-013, ATLAS-TDR-019: CERN (2012). http://cds.cern.ch/record/1451888

34. ATLAS Collaboration, The ATLAS inner detector commissioning and calibration. Eur. Phys. J. C **70**, 787 (2010). arXiv:1004.5293 [hep-ex]

35. ATLAS Collaboration, Performance of the ATLAS trigger system in 2010. Eur. Phys. J. C **72**, 1849 (2012). arXiv:1110.1530 [hep-ex]

36. G. Aad et al., Measurement of charged-particle spectra in Pb+Pb collisions at $\sqrt{s_{NN}}$ = 2.76 TeV with the ATLAS detector at the LHC. JHEP **09**, 050 (2015). arXiv:1504.04337 [hep-ex]

37. M.L. Miller, K. Reygers, S.J. Sanders, P. Steinberg, Glauber modeling in high energy nuclear collisions. Ann. Rev. Nucl. Part. Sci. **57**, 205 (2007). arXiv:nucl-ex/0701025

38. C. Loizides, J. Nagle, P. Steinberg, Improved version of the PHOBOS Glauber Monte Carlo. SoftwareX **1–2**, 13 (2015). arXiv:1408.2549 [nucl-ex]

39. X.-N. Wang, M. Gyulassy, HIJING: a Monte Carlo model for multiple jet production in pp, pA, and AA collisions. Phys. Rev. D **44**, 3501 (1991)

40. J. Jia, S. Mohapatra, Disentangling flow and nonflow correlations via Bayesian unfolding of the event-by-event distributions of harmonic coefficients in ultrarelativistic heavy-ion collisions. Phys. Rev. C **88**, 014907 (2013). arXiv:1304.1471 [nucl-ex]

41. S. Agostinelli et al., GEANT4 Collaboration, GEANT4: a simulation toolkit. Nucl. Instrum. Methods A **506**, 250 (2003)

42. ATLAS Collaboration, The optimization of ATLAS track reconstruction in dense environments. Technical report. ATL-PHYS-PUB-2015-006 (2015). http://cdsweb.cern.ch/record/2002609

43. ATLAS Collaboration, Measurement of the distributions of event-by-event flow harmonics in lead–lead collisions at $\sqrt{s_{NN}}$ = 2.76 TeV with the ATLAS detector at the LHC. JHEP **11**, 183 (2013). arXiv:1305.2942 [hep-ex]

44. ATLAS Collaboration, Observation of associated near-side and away-side long-range correlations in $\sqrt{s_{NN}}$ = 5.02 TeV proton–lead collisions with the ATLAS detector. Phys. Rev. Lett. **110**, 182302 (2013). arXiv:1212.5198 [hep-ex]

45. ATLAS Collaboration, Measurement of long-range pseudorapidity correlations and azimuthal harmonics in $\sqrt{s_{NN}}$ = 5.02 TeV proton–lead collisions with the ATLAS detector. Phys. Rev. C **90**, 044906 (2014). arXiv:1409.1792 [hep-ex]

46. ATLAS Collaboration, Measurement of the correlation between flow harmonics of different order in lead–lead collisions at $\sqrt{s_{NN}}$ = 2.76 TeV with the ATLAS detector. Phys. Rev. C **92**, 034903 (2015). arXiv:1504.01289 [hep-ex]

47. ATLAS Collaboration, Observation of long-range elliptic azimuthal anisotropies in $\sqrt{s}$ = 13 and 2.76 TeV pp Collisions with the ATLAS detector. Phys. Rev. Lett. **116**, 172301 (2016). arXiv:1509.04776 [hep-ex]

48. ATLAS Collaboration, Measurements of long-range azimuthal anisotropies and associated Fourier coefficients for pp collisions at $\sqrt{s}$ = 5.02 and 13 TeV and p+Pb collisions at $\sqrt{s_{NN}}$ = 5.02 TeV with the ATLAS detector. Phys. Rev. C **96**, 024908 (2017). arXiv:1609.06213 [nucl-ex]

49. PHENIX Collaboration, A. Adare et al., Dihadron azimuthal correlations in Au+Au collisions at $\sqrt{s_{NN}}$ = 200-GeV. Phys. Rev. C **78**, 014901 (2008). arXiv:0801.4545 [nucl-ex]

50. M.A. Lisa, S. Pratt, R. Soltz, U. Wiedemann, Femtoscopy in relativistic heavy ion collisions. Ann. Rev. Nucl. Part. Sci. **55**, 357 (2005). arXiv:nucl-ex/0505014 [nucl-ex]

51. ATLAS Collaboration, Measurement of jet fragmentation in Pb+Pb and pp collisions at $\sqrt{s_{NN}}$ = 2.76 TeV with the ATLAS detector at the LHC. Eur. Phys. J. C **77**, 379 (2017). arXiv:1702.00674 [hep-ex]

52. Azimuthal femtoscopy in central p+Pb collisions at $\sqrt{s_{NN}}$ = 5.02 TeV with ATLAS. Technical report. ATLAS-CONF-2017-008, CERN (2017). https://cds.cern.ch/record/2244818

53. ATLAS Collaboration, Charged-particle multiplicities in pp interactions at $\sqrt{s}$ = 900 GeV measured with the ATLAS detector at the LHC. Phys. Lett. B **688**, 21 (2010). arXiv:1003.3124 [hep-ex]

54. ATLAS Collaboration, Charged-particle distributions in $\sqrt{s}$ = 13 TeV pp interactions measured with the ATLAS detector at the LHC. Phys. Lett. B **758**, 67 (2016). arXiv:1602.01633 [hep-ex]

55. CMS Collaboration, Studies of azimuthal dihadron correlations in ultra-central PbPb collisions at $\sqrt{s_{NN}}$ = 2.76 TeV. JHEP **02**, 088 (2014). arXiv:1312.1845 [hep-ex]

56. CMS Collaboration, Evidence for transverse-momentum- and pseudorapidity-dependent event-plane fluctuations in PbPb and pPb collisions. Phys. Rev. C **92**, 034911 (2015). arXiv:1503.01692 [hep-ex]

57. ALICE Collaboration, Centrality dependence of π, K, p production in Pb–Pb collisions at $\sqrt{s_{NN}}$ = 2.76 TeV. Phys. Rev. C **88**, 044910 (2013). arXiv:1303.0737 [hep-ex]

58. ATLAS Collaboration, ATLAS Computing Acknowledgements, ATL-GEN-PUB-2016-002 (2016). https://cds.cern.ch/record/2202407

ATLAS Collaboration

M. Aaboud[34d], G. Aad[99], B. Abbott[124], O. Abdinov[13,*], B. Abeloos[128], D. K. Abhayasinghe[91], S. H. Abidi[164], O. S. AbouZeid[39], N. L. Abraham[153], H. Abramowicz[158], H. Abreu[157], Y. Abulaiti[6], B. S. Acharya[64a,64b,n], S. Adachi[160], L. Adamczyk[81a], J. Adelman[119], M. Adersberger[112], A. Adiguzel[12c,ag], T. Adye[141], A. A. Affolder[143], Y. Afik[157], C. Agheorghiesei[27c], J. A. Aguilar-Saavedra[136a,136f], F. Ahmadov[77,ae], G. Aielli[71a,71b], S. Akatsuka[83], T. P. A. Åkesson[94], E. Akilli[52], A. V. Akimov[108], G. L. Alberghi[23a,23b], J. Albert[173], P. Albicocco[49], M. J. Alconada Verzini[86], S. Alderweireldt[117], M. Aleksa[35], I. N. Aleksandrov[77], C. Alexa[27b], T. Alexopoulos[10], M. Alhroob[124], B. Ali[138], G. Alimonti[66a], J. Alison[36], S. P. Alkire[145], C. Allaire[128], B. M. M. Allbrooke[153], B. W. Allen[127], P. P. Allport[21], A. Aloisio[67a,67b], A. Alonso[39], F. Alonso[86], C. Alpigiani[145], A. A. Alshehri[55], M. I. Alstaty[99], B. Alvarez Gonzalez[35], D. Álvarez Piqueras[171], M. G. Alviggi[67a,67b], B. T. Amadio[18], Y. Amaral Coutinho[78b], L. Ambroz[131], C. Amelung[26], D. Amidei[103], S. P. Amor Dos Santos[136a,136c], S. Amoroso[44], C. S. Amrouche[52], C. Anastopoulos[146], L. S. Ancu[52], N. Andari[142], T. Andeen[11], C. F. Anders[59b], J. K. Anders[20], K. J. Anderson[36], A. Andreazza[66a,66b], V. Andrei[59a], C. R. Anelli[173], S. Angelidakis[37], I. Angelozzi[118], A. Angerami[38], A. V. Anisenkov[120a,120b], A. Annovi[69a], C. Antel[59a], M. T. Anthony[146], M. Antonelli[49], D. J. A. Antrim[168], F. Anulli[70a], M. Aoki[79], J. A. Aparisi Pozo[171], L. Aperio Bella[35], G. Arabidze[104], J. P. Araque[136a], V. Araujo Ferraz[78b], R. Araujo Pereira[78b], A. T. H. Arce[47], R. E. Ardell[91], F. A. Arduh[86], J.-F. Arguin[107], S. Argyropoulos[75], A. J. Armbruster[35], L. J. Armitage[90], A. Armstrong[168], O. Arnaez[164], H. Arnold[118], M. Arratia[31], O. Arslan[24], A. Artamonov[109,*], G. Artoni[131], S. Artz[97], S. Asai[160], N. Asbah[44], A. Ashkenazi[158], E. M. Asimakopoulou[169], L. Asquith[153], K. Assamagan[29], R. Astalos[28a], R. J. Atkin[32a], M. Atkinson[170], N. B. Atlay[148], K. Augsten[138], G. Avolio[35], R. Avramidou[58a], M. K. Ayoub[15a], G. Azuelos[107,as], A. E. Baas[59a], M. J. Baca[21], H. Bachacou[142], K. Bachas[65a,65b], M. Backes[131], P. Bagnaia[70a,70b], M. Bahmani[82], H. Bahrasemani[149], A. J. Bailey[171], J. T. Baines[141], M. Bajic[39], C. Bakalis[10], O. K. Baker[180], P. J. Bakker[118], D. Bakshi Gupta[93], E. M. Baldin[120a,120b], P. Balek[177], F. Balli[142], W. K. Balunas[133], J. Balz[97], E. Banas[82], A. Bandyopadhyay[24], S. Banerjee[178,j], A. A. E. Bannoura[179], L. Barak[158], W. M. Barbe[37], E. L. Barberio[102], D. Barberis[53a,53b], M. Barbero[99], T. Barillari[113], M.-S. Barisits[35], J. Barkeloo[127], T. Barklow[150], N. Barlow[31], R. Barnea[157], S. L. Barnes[58c], B. M. Barnett[141], R. M. Barnett[18], Z. Barnovska-Blenessy[58a], A. Baroncelli[72a], G. Barone[26], A. J. Barr[131], L. Barranco Navarro[171], F. Barreiro[96], J. Barreiro Guimarães da Costa[15a], R. Bartoldus[150], A. E. Barton[87], P. Bartos[28a], A. Basalaev[134], A. Bassalat[128], R. L. Bates[55], S. J. Batista[164], S. Batlamous[34e], J. R. Batley[31], M. Battaglia[143], M. Bauce[70a,70b], F. Bauer[142], K. T. Bauer[168], H. S. Bawa[150,l], J. B. Beacham[122], T. Beau[132], P. H. Beauchemin[167], P. Bechtle[24], H. C. Beck[51], H. P. Beck[20,q], K. Becker[50], M. Becker[97], C. Becot[44], A. Beddall[12d], A. J. Beddall[12a], V. A. Bednyakov[77], M. Bedognetti[118], C. P. Bee[152], T. A. Beermann[35], M. Begalli[78b], M. Begel[29], A. Behera[152], J. K. Behr[44], A. S. Bell[92], G. Bella[158], L. Bellagamba[23b], A. Bellerive[33], M. Bellomo[157], P. Bellos[9], K. Belotskiy[110], N. L. Belyaev[110], O. Benary[158,*], D. Benchekroun[34a], M. Bender[112], N. Benekos[10], Y. Benhammou[158], E. Benhar Noccioli[180], J. Benitez[75], D. P. Benjamin[47], M. Benoit[52], J. R. Bensinger[26], S. Bentvelsen[118], L. Beresford[131], M. Beretta[49], D. Berge[44], E. Bergeaas Kuutmann[169], N. Berger[5], L. J. Bergsten[26], J. Beringer[18], S. Berlendis[7], N. R. Bernard[100], G. Bernardi[132], C. Bernius[150], F. U. Bernlochner[24], T. Berry[91], P. Berta[97], C. Bertella[15a], G. Bertoli[43a,43b], I. A. Bertram[87], G. J. Besjes[39], O. Bessidskaia Bylund[179], M. Bessner[44], N. Besson[142], A. Bethani[98], S. Bethke[113], A. Betti[24], A. J. Bevan[90], J. Beyer[113], R. M. Bianchi[135], O. Biebel[112], D. Biedermann[19], R. Bielski[35], K. Bierwagen[97], N. V. Biesuz[69a,69b], M. Biglietti[72a], T. R. V. Billoud[107], M. Bindi[51], A. Bingul[12d], C. Bini[70a,70b], S. Biondi[23a,23b], M. Birman[177], T. Bisanz[51], J. P. Biswal[158], C. Bittrich[46], D. M. Bjergaard[47], J. E. Black[150], K. M. Black[25], T. Blazek[28a], I. Bloch[44], C. Blocker[26], A. Blue[55], U. Blumenschein[90], Dr. Blunier[144a], G. J. Bobbink[118], V. S. Bobrovnikov[120a,120b], S. S. Bocchetta[94], A. Bocci[47], D. Boerner[179], D. Bogavac[112], A. G. Bogdanchikov[120a,120b], C. Bohm[43a], V. Boisvert[91], P. Bokan[169,51], T. Bold[81a], A. S. Boldyrev[111], A. E. Bolz[59b], M. Bomben[132], M. Bona[90], J. S. Bonilla[127], M. Boonekamp[142], A. Borisov[140], G. Borissov[87], J. Bortfeldt[35], D. Bortoletto[131], V. Bortolotto[61b,61c,71a,71b], D. Boscherini[23b], M. Bosman[14], J. D. Bossio Sola[30], K. Bouaouda[34a], J. Boudreau[135], E. V. Bouhova-Thacker[87], D. Boumediene[37], C. Bourdarios[128], S. K. Boutle[55], A. Boveia[122], J. Boyd[35], D. Boye[32b], I. R. Boyko[77], A. J. Bozson[91], J. Bracinik[21], N. Brahimi[99], A. Brandt[8], G. Brandt[179], O. Brandt[59a], F. Braren[44], U. Bratzler[161], B. Brau[100], J. E. Brau[127], W. D. Breaden Madden[55], K. Brendlinger[44], A. J. Brennan[102], L. Brenner[44], R. Brenner[169], S. Bressler[177], B. Brickwedde[97], D. L. Briglin[21], D. Britton[55], D. Britzger[59b], I. Brock[24], R. Brock[104], G. Brooijmans[38], T. Brooks[91], W. K. Brooks[144b], E. Brost[119], J. H Broughton[21], P. A. Bruckman de Renstrom[82], D. Bruncko[28b], A. Bruni[23b], G. Bruni[23b], L. S. Bruni[118], S. Bruno[71a,71b], B.H. Brunt[31], M. Bruschi[23b], N. Bruscino[135], P. Bryant[36], L. Bryngemark[44], T. Buanes[17], Q. Buat[35], P. Buchholz[148], A. G. Buckley[55], I. A. Budagov[77], F. Buehrer[50], M. K. Bugge[130], O. Bulekov[110], D. Bullock[8], T. J. Burch[119], S. Burdin[88], C. D. Burgard[118], A. M. Burger[5], B. Burghgrave[119], K. Burka[82], S. Burke[141], I. Burmeister[45], J. T. P. Burr[131],

D. Büscher[50], V. Büscher[97], E. Buschmann[51], P. Bussey[55], J. M. Butler[25], C. M. Buttar[55], J. M. Butterworth[92], P. Butti[35], W. Buttinger[35], A. Buzatu[155], A. R. Buzykaev[120a,120b], G. Cabras[23a,23b], S. Cabrera Urbán[171], D. Caforio[138], H. Cai[170], V. M. M. Cairo[2], O. Cakir[4a], N. Calace[52], P. Calafiura[18], A. Calandri[99], G. Calderini[132], P. Calfayan[63], G. Callea[40a,40b], L. P. Caloba[78b], S. Calvente Lopez[96], D. Calvet[37], S. Calvet[37], T. P. Calvet[152], R. Camacho Toro[132], S. Camarda[35], P. Camarri[71a,71b], D. Cameron[130], R. Caminal Armadans[100], C. Camincher[35], S. Campana[35], M. Campanelli[92], A. Camplani[39], A. Campoverde[148], V. Canale[67a,67b], M. Cano Bret[58c], J. Cantero[125], T. Cao[158], Y. Cao[170], M. D. M. Capeans Garrido[35], I. Caprini[27b], M. Caprini[27b], M. Capua[40b,40a], R. M. Carbone[38], R. Cardarelli[71a], F. C. Cardillo[146], I. Carli[139], T. Carli[35], G. Carlino[67a], B. T. Carlson[135], L. Carminati[66a,66b], R. M. D. Carney[43a,43b], S. Caron[117], E. Carquin[144b], S. Carrá[66a,66b], G. D. Carrillo-Montoya[35], D. Casadei[32b], M. P. Casado[14,f], A. F. Casha[164], D. W. Casper[168], R. Castelijn[118], F. L. Castillo[171], V. Castillo Gimenez[171], N. F. Castro[136a,136e], A. Catinaccio[35], J. R. Catmore[130], A. Cattai[35], J. Caudron[24], V. Cavaliere[29], E. Cavallaro[14], D. Cavalli[66a], M. Cavalli-Sforza[14], V. Cavasinni[69a,69b], E. Celebi[12b], F. Ceradini[72a,72b], L. Cerda Alberich[171], A. S. Cerqueira[78a], A. Cerri[153], L. Cerrito[71a,71b], F. Cerutti[18], A. Cervelli[23a,23b], S. A. Cetin[12b], A. Chafaq[34a], D. Chakraborty[119], S. K. Chan[57], W. S. Chan[118], Y. L. Chan[61a], J. D. Chapman[31], B. Chargeishvili[156b], D. G. Charlton[21], C. C. Chau[33], C. A. Chavez Barajas[153], S. Che[122], A. Chegwidden[104], S. Chekanov[6], S. V. Chekulaev[165a], G. A. Chelkov[77,ar], M. A. Chelstowska[35], C. Chen[58a], C. H. Chen[76], H. Chen[29], J. Chen[58a], J. Chen[38], S. Chen[133], S. J. Chen[15c], X. Chen[15b,aq], Y. Chen[80], Y.-H. Chen[44], H. C. Cheng[103], H. J. Cheng[15d], A. Cheplakov[77], E. Cheremushkina[140], R. Cherkaoui El Moursli[34e], E. Cheu[7], K. Cheung[62], L. Chevalier[142], V. Chiarella[49], G. Chiarelli[69a], G. Chiodini[65a], A. S. Chisholm[35], A. Chitan[27b], I. Chiu[160], Y. H. Chiu[173], M. V. Chizhov[77], K. Choi[63], A. R. Chomont[128], S. Chouridou[159], Y. S. Chow[118], V. Christodoulou[92], M. C. Chu[61a], J. Chudoba[137], A. J. Chuinard[101], J. J. Chwastowski[82], L. Chytka[126], D. Cinca[45], V. Cindro[89], I. A. Cioară[24], A. Ciocio[18], F. Cirotto[67a,67b], Z. H. Citron[177], M. Citterio[66a], A. Clark[52], M. R. Clark[38], P. J. Clark[48], C. Clement[43a,43b], Y. Coadou[99], M. Cobal[64a,64c], A. Coccaro[53a,53b], J. Cochran[76], A. E. C. Coimbra[177], L. Colasurdo[117], B. Cole[38], A. P. Colijn[118], J. Collot[56], P. Conde Muiño[136a,136b], E. Coniavitis[50], S. H. Connell[32b], I. A. Connelly[98], S. Constantinescu[27b], F. Conventi[67a,at], A. M. Cooper-Sarkar[131], F. Cormier[172], K. J. R. Cormier[164], M. Corradi[70a,70b], E. E. Corrigan[94], F. Corriveau[101,ac], A. Cortes-Gonzalez[35], M. J. Costa[171], D. Costanzo[146], G. Cottin[31], G. Cowan[91], B. E. Cox[98], J. Crane[98], K. Cranmer[121], S. J. Crawley[55], R. A. Creager[133], G. Cree[33], S. Crépé-Renaudin[56], F. Crescioli[132], M. Cristinziani[24], V. Croft[121], G. Crosetti[40b,40a], A. Cueto[96], T. Cuhadar Donszelmann[146], A. R. Cukierman[150], J. Cúth[97], S. Czekierda[82], P. Czodrowski[35], M. J. Da Cunha Sargedas De Sousa[58b,136b], C. Da Via[98], W. Dabrowski[81a], T. Dado[28a,x], S. Dahbi[34e], T. Dai[103], F. Dallaire[107], C. Dallapiccola[100], M. Dam[39], G. D'amen[23a,23b], J. Damp[97], J. R. Dandoy[133], M. F. Daneri[30], N. P. Dang[178,j], N. D. Dann[98], M. Danninger[172], V. Dao[35], G. Darbo[53b], S. Darmora[8], O. Dartsi[5], A. Dattagupta[127], T. Daubney[44], S. D'Auria[55], W. Davey[24], C. David[44], T. Davidek[139], D. R. Davis[47], E. Dawe[102], I. Dawson[146], K. De[8], R. De Asmundis[67a], A. De Benedetti[124], M. De Beurs[118], S. De Castro[23a,23b], S. De Cecco[70a,70b], N. De Groot[117], P. de Jong[118], H. De la Torre[104], F. De Lorenzi[76], A. De Maria[51,s], D. De Pedis[70a], A. De Salvo[70a], U. De Sanctis[71a,71b], A. De Santo[153], K. De Vasconcelos Corga[99], J. B. De Vivie De Regie[128], C. Debenedetti[143], D. V. Dedovich[77], N. Dehghanian[3], M. Del Gaudio[40b,40a], J. Del Peso[96], Y. Delabat Diaz[44], D. Delgove[128], F. Deliot[142], C. M. Delitzsch[7], M. Della Pietra[67a,67b], D. Della Volpe[52], A. Dell'Acqua[35], L. Dell'Asta[25], M. Delmastro[5], C. Delporte[128], P. A. Delsart[56], D. A. DeMarco[164], S. Demers[180], M. Demichev[77], S. P. Denisov[140], D. Denysiuk[118], L. D'Eramo[132], D. Derendarz[82], J. E. Derkaoui[34d], F. Derue[132], P. Dervan[88], K. Desch[24], C. Deterre[44], K. Dette[164], M. R. Devesa[30], P. O. Deviveiros[35], A. Dewhurst[141], S. Dhaliwal[26], F. A. Di Bello[52], A. Di Ciaccio[71a,71b], L. Di Ciaccio[5], W. K. Di Clemente[133], C. Di Donato[67a,67b], A. Di Girolamo[35], B. Di Micco[72a,72b], R. Di Nardo[100], K. F. Di Petrillo[57], R. Di Sipio[164], D. Di Valentino[33], C. Diaconu[99], M. Diamond[164], F. A. Dias[39], T. Dias Do Vale[136a], M. A. Diaz[144a], J. Dickinson[18], E. B. Diehl[103], J. Dietrich[19], S. Díez Cornell[44], A. Dimitrievska[18], J. Dingfelder[24], F. Dittus[35], F. Djama[99], T. Djobava[156b], J. I. Djuvsland[59a], M. A. B. Do Vale[78c], D. Dobre[27b], D. Dodsworth[26], C. Doglioni[94], J. Dolejsi[139], Z. Dolezal[139], M. Donadelli[78d], J. Donini[37], A. D'onofrio[90], M. D'Onofrio[88], J. Dopke[141], A. Doria[67a], M. T. Dova[86], A. T. Doyle[55], E. Drechsler[51], E. Dreyer[149], T. Dreyer[51], Y. Du[58b], J. Duarte-Campderros[158], F. Dubinin[108], M. Dubovsky[28a], A. Dubreuil[52], E. Duchovni[177], G. Duckeck[112], A. Ducourthial[132], O. A. Ducu[107,w], D. Duda[113], A. Dudarev[35], A. C. Dudder[97], E. M. Duffield[18], L. Duflot[128], M. Dührssen[35], C. Dülsen[179], M. Dumancic[177], A. E. Dumitriu[27b,d], A. K. Duncan[55], M. Dunford[59a], A. Duperrin[99], H. Duran Yildiz[4a], M. Düren[54], A. Durglishvili[156b], D. Duschinger[46], B. Dutta[44], D. Duvnjak[1], M. Dyndal[44], S. Dysch[98], B. S. Dziedzic[82], C. Eckardt[44], K. M. Ecker[113], R. C. Edgar[103], T. Eifert[35], G. Eigen[17], K. Einsweiler[18], T. Ekelof[169], M. El Kacimi[34c], R. El Kosseifi[99], V. Ellajosyula[99], M. Ellert[169], F. Ellinghaus[179], A. A. Elliot[90], N. Ellis[35], J. Elmsheuser[29], M. Elsing[35], D. Emeliyanov[141], Y. Enari[160], J. S. Ennis[175], M. B. Epland[47], J. Erdmann[45], A. Ereditato[20], S. Errede[170], M. Escalier[128], C. Escobar[171], O. Estrada Pastor[171], A. I. Etienvre[142], E. Etzion[158], H. Evans[63], A. Ezhilov[134], M. Ezzi[34e], F. Fabbri[55], L. Fabbri[23a,23b], V. Fabiani[117],

G. Facini[92], R. M. Faisca Rodrigues Pereira[136a], R. M. Fakhrutdinov[140], S. Falciano[70a], P. J. Falke[5], S. Falke[5], J. Faltova[139], Y. Fang[15a], M. Fanti[66a,66b], A. Farbin[8], A. Farilla[72a], E. M. Farina[68a,68b], T. Farooque[104], S. Farrell[18], S. M. Farrington[175], P. Farthouat[35], F. Fassi[34e], P. Fassnacht[35], D. Fassouliotis[9], M. Faucci Giannelli[48], A. Favareto[53a,53b], W. J. Fawcett[52], L. Fayard[128], O. L. Fedin[134,o], W. Fedorko[172], M. Feickert[41], S. Feigl[130], L. Feligioni[99], C. Feng[58b], E. J. Feng[35], M. Feng[47], M. J. Fenton[55], A. B. Fenyuk[140], L. Feremenga[8], J. Ferrando[44], A. Ferrari[169], P. Ferrari[118], R. Ferrari[68a], D. E. Ferreira de Lima[59b], A. Ferrer[171], D. Ferrere[52], C. Ferretti[103], F. Fiedler[97], A. Filipčič[89], F. Filthaut[117], K. D. Finelli[25], M. C. N. Fiolhais[136a,136c,a], L. Fiorini[171], C. Fischer[14], W. C. Fisher[104], N. Flaschel[44], I. Fleck[148], P. Fleischmann[103], R. R. M. Fletcher[133], T. Flick[179], B. M. Flierl[112], L. M. Flores[133], L. R. Flores Castillo[61a], F. M. Follega[73a,73b], N. Fomin[17], G. T. Forcolin[98], A. Formica[142], F. A. Förster[14], A. C. Forti[98], A. G. Foster[21], D. Fournier[128], H. Fox[87], S. Fracchia[146], P. Francavilla[69a,69b], M. Franchini[23a,23b], S. Franchino[59a], D. Francis[35], L. Franconi[130], M. Franklin[57], M. Frate[168], M. Fraternali[68a,68b], D. Freeborn[92], S. M. Fressard-Batraneanu[35], B. Freund[107], W. S. Freund[78b], D. Froidevaux[35], J. A. Frost[131], C. Fukunaga[161], E. Fullana Torregrosa[171], T. Fusayasu[114], J. Fuster[171], O. Gabizon[157], A. Gabrielli[23a,23b], A. Gabrielli[18], G. P. Gach[81a], S. Gadatsch[52], P. Gadow[113], G. Gagliardi[53a,53b], L. G. Gagnon[107], C. Galea[27b], B. Galhardo[136a,136c], E. J. Gallas[131], B. J. Gallop[141], P. Gallus[138], G. Galster[39], R. Gamboa Goni[90], K. K. Gan[122], S. Ganguly[177], J. Gao[58a], Y. Gao[88], Y. S. Gao[150,l], C. García[171], J. E. García Navarro[171], J. A. García Pascual[15a], M. Garcia-Sciveres[18], R. W. Gardner[36], N. Garelli[150], V. Garonne[130], K. Gasnikova[44], A. Gaudiello[53a,53b], G. Gaudio[68a], I. L. Gavrilenko[108], A. Gavrilyuk[109], C. Gay[172], G. Gaycken[24], E. N. Gazis[10], C. N. P. Gee[141], J. Geisen[51], M. Geisen[97], M. P. Geisler[59a], K. Gellerstedt[43a,43b], C. Gemme[53b], M. H. Genest[56], C. Geng[103], S. Gentile[70a,70b], S. George[91], D. Gerbaudo[14], G. Gessner[45], S. Ghasemi[148], M. Ghasemi Bostanabad[173], M. Ghneimat[24], B. Giacobbe[23b], S. Giagu[70a,70b], N. Giangiacomi[23a,23b], P. Giannetti[69a], A. Giannini[67a,67b], S. M. Gibson[91], M. Gignac[143], D. Gillberg[33], G. Gilles[179], D. M. Gingrich[3,as], M. P. Giordani[64a,64c], F. M. Giorgi[23b], P. F. Giraud[142], P. Giromini[57], G. Giugliarelli[64a,64c], D. Giugni[66a], F. Giuli[131], M. Giulini[59b], S. Gkaitatzis[159], I. Gkialas[9,i], E. L. Gkougkousis[14], P. Gkountoumis[10], L. K. Gladilin[111], C. Glasman[96], J. Glatzer[14], P. C. F. Glaysher[44], A. Glazov[44], M. Goblirsch-Kolb[26], J. Godlewski[82], S. Goldfarb[102], T. Golling[52], D. Golubkov[140], A. Gomes[136a,136b,136d], R. Goncalves Gama[78a], R. Gonçalo[136a], G. Gonella[50], L. Gonella[21], A. Gongadze[77], F. Gonnella[21], J. L. Gonski[57], S. González de la Hoz[171], S. Gonzalez-Sevilla[52], L. Goossens[35], P. A. Gorbounov[109], H. A. Gordon[29], B. Gorini[35], E. Gorini[65a,65b], A. Gorišek[89], A. T. Goshaw[47], C. Gössling[45], M. I. Gostkin[77], C. A. Gottardo[24], C. R. Goudet[128], D. Goujdami[34c], A. G. Goussiou[145], N. Govender[32b,b], C. Goy[5], E. Gozani[157], I. Grabowska-Bold[81a], P. O. J. Gradin[169], E. C. Graham[88], J. Gramling[168], E. Gramstad[130], S. Grancagnolo[19], V. Gratchev[134], P. M. Gravila[27f], F. G. Gravili[65a,65b], C. Gray[55], H. M. Gray[18], Z. D. Greenwood[93,ai], C. Grefe[24], K. Gregersen[94], I. M. Gregor[44], P. Grenier[150], K. Grevtsov[44], J. Griffiths[8], A. A. Grillo[143], K. Grimm[150], S. Grinstein[14,y], Ph. Gris[37], J.-F. Grivaz[128], S. Groh[97], E. Gross[177], J. Grosse-Knetter[51], G. C. Grossi[93], Z. J. Grout[92], C. Grud[103], A. Grummer[116], L. Guan[103], W. Guan[178], J. Guenther[35], A. Guerguichon[128], F. Guescini[165a], D. Guest[168], R. Gugel[50], B. Gui[122], T. Guillemin[5], S. Guindon[35], U. Gul[55], C. Gumpert[35], J. Guo[58c], W. Guo[103], Y. Guo[58a,r], Z. Guo[99], R. Gupta[41], S. Gurbuz[12c], G. Gustavino[124], B. J. Gutelman[157], P. Gutierrez[124], C. Gutschow[92], C. Guyot[142], M. P. Guzik[81a], C. Gwenlan[131], C. B. Gwilliam[88], A. Haas[121], C. Haber[18], H. K. Hadavand[8], N. Haddad[34e], A. Hadef[58a], S. Hageböck[24], M. Hagihara[166], H. Hakobyan[181,*], M. Haleem[174], J. Haley[125], G. Halladjian[104], G. D. Hallewell[99], K. Hamacher[179], P. Hamal[126], K. Hamano[173], A. Hamilton[32a], G. N. Hamity[146], K. Han[58a,ah], L. Han[58a], S. Han[15d], K. Hanagaki[79,u], M. Hance[143], D. M. Handl[112], B. Haney[133], R. Hankache[132], P. Hanke[59a], E. Hansen[94], J. B. Hansen[39], J. D. Hansen[39], M. C. Hansen[24], P. H. Hansen[39], K. Hara[166], A. S. Hard[178], T. Harenberg[179], S. Harkusha[105], P. F. Harrison[175], N. M. Hartmann[112], Y. Hasegawa[147], A. Hasib[48], S. Hassani[142], S. Haug[20], R. Hauser[104], L. Hauswald[46], L. B. Havener[38], M. Havranek[138], C. M. Hawkes[21], R. J. Hawkings[35], D. Hayden[104], C. Hayes[152], C. P. Hays[131], J. M. Hays[90], H. S. Hayward[88], S. J. Haywood[141], M. P. Heath[48], V. Hedberg[94], L. Heelan[8], S. Heer[24], K. K. Heidegger[50], J. Heilman[33], S. Heim[44], T. Heim[18], B. Heinemann[44,an], J. J. Heinrich[112], L. Heinrich[121], C. Heinz[54], J. Hejbal[137], L. Helary[35], A. Held[172], S. Hellesund[130], S. Hellman[43a,43b], C. Helsens[35], R. C. W. Henderson[87], Y. Heng[178], S. Henkelmann[172], A. M. Henriques Correia[35], G. H. Herbert[19], H. Herde[26], V. Herget[174], Y. Hernández Jiménez[32c], H. Herr[97], M. G. Herrmann[112], G. Herten[50], R. Hertenberger[112], L. Hervas[35], T. C. Herwig[133], G. G. Hesketh[92], N. P. Hessey[165a], J. W. Hetherly[41], S. Higashino[79], E. Higón-Rodriguez[171], K. Hildebrand[36], E. Hill[173], J. C. Hill[31], K. K. Hill[29], K. H. Hiller[44], S. J. Hillier[21], M. Hils[46], I. Hinchliffe[18], M. Hirose[129], D. Hirschbuehl[179], B. Hiti[89], O. Hladik[137], D. R. Hlaluku[32c], X. Hoad[48], J. Hobbs[152], N. Hod[165a], M. C. Hodgkinson[146], A. Hoecker[35], M. R. Hoeferkamp[116], F. Hoenig[112], D. Hohn[24], D. Hohov[128], T. R. Holmes[36], M. Holzbock[112], M. Homann[45], S. Honda[166], T. Honda[79], T. M. Hong[135], A. Hönle[113], B. H. Hooberman[170], W. H. Hopkins[127], Y. Horii[115], P. Horn[46], A. J. Horton[149], L. A. Horyn[36], J.-Y. Hostachy[56], A. Hostiuc[145], S. Hou[155], A. Hoummada[34a], J. Howarth[98], J. Hoya[86], M. Hrabovsky[126], J. Hrdinka[35], I. Hristova[19], J. Hrivnac[128], A. Hrynevich[106], T. Hryn'ova[5], P. J. Hsu[62], S.-C. Hsu[145],

Q. Hu[29], S. Hu[58c], Y. Huang[15a], Z. Hubacek[138], F. Hubaut[99], M. Huebner[24], F. Huegging[24], T. B. Huffman[131], E. W. Hughes[38], M. Huhtinen[35], R. F. H. Hunter[33], P. Huo[152], A. M. Hupe[33], N. Huseynov[77,ae], J. Huston[104], J. Huth[57], R. Hyneman[103], G. Iacobucci[52], G. Iakovidis[29], I. Ibragimov[148], L. Iconomidou-Fayard[128], Z. Idrissi[34e], P. Iengo[35], R. Ignazzi[39], O. Igonkina[118,aa], R. Iguchi[160], T. Iizawa[52], Y. Ikegami[79], M. Ikeno[79], D. Iliadis[159], N. Ilic[150], F. Iltzsche[46], G. Introzzi[68a,68b], M. Iodice[72a], K. Iordanidou[38], V. Ippolito[70a,70b], M. F. Isacson[169], N. Ishijima[129], M. Ishino[160], M. Ishitsuka[162], W. Islam[125], C. Issever[131], S. Istin[12c,am], F. Ito[166], J. M. Iturbe Ponce[61a], R. Iuppa[73a,73b], A. Ivina[177], H. Iwasaki[79], J. M. Izen[42], V. Izzo[67a], P. Jacka[137], P. Jackson[1], R. M. Jacobs[24], V. Jain[2], G. Jäkel[179], K. B. Jakobi[97], K. Jakobs[50], S. Jakobsen[74], T. Jakoubek[137], D. O. Jamin[125], D. K. Jana[93], R. Jansky[52], J. Janssen[24], M. Janus[51], P. A. Janus[81a], G. Jarlskog[94], N. Javadov[77,ae], T. Javůrek[35], M. Javurkova[50], F. Jeanneau[142], L. Jeanty[18], J. Jejelava[156a,af], A. Jelinskas[175], P. Jenni[50,c], J. Jeong[44], S. Jézéquel[5], H. Ji[178], J. Jia[152], H. Jiang[76], Y. Jiang[58a], Z. Jiang[150,p], S. Jiggins[50], F. A. Jimenez Morales[37], J. Jimenez Pena[171], S. Jin[15c], A. Jinaru[27b], O. Jinnouchi[162], H. Jivan[32c], P. Johansson[146], K. A. Johns[7], C. A. Johnson[63], W. J. Johnson[145], K. Jon-And[43a,43b], R. W. L. Jones[87], S. D. Jones[153], S. Jones[7], T. J. Jones[88], J. Jongmanns[59a], P. M. Jorge[136a,136b], J. Jovicevic[165a], X. Ju[178], J. J. Junggeburth[113], A. Juste Rozas[14,y], A. Kaczmarska[82], M. Kado[128], H. Kagan[122], M. Kagan[150], T. Kaji[176], E. Kajomovitz[157], C. W. Kalderon[94], A. Kaluza[97], S. Kama[41], A. Kamenshchikov[140], L. Kanjir[89], Y. Kano[160], V. A. Kantserov[110], J. Kanzaki[79], B. Kaplan[121], L. S. Kaplan[178], D. Kar[32c], M. J. Kareem[165b], E. Karentzos[10], S. N. Karpov[77], Z. M. Karpova[77], V. Kartvelishvili[87], A. N. Karyukhin[140], L. Kashif[178], R. D. Kass[122], A. Kastanas[151], Y. Kataoka[160], C. Kato[58d,58c], J. Katzy[44], K. Kawade[80], K. Kawagoe[85], T. Kawamoto[160], G. Kawamura[51], E. F. Kay[88], V. F. Kazanin[120a,120b], R. Keeler[173], R. Kehoe[41], J. S. Keller[33], E. Kellermann[94], J. J. Kempster[21], J. Kendrick[21], O. Kepka[137], S. Kersten[179], B. P. Kerševan[89], R. A. Keyes[101], M. Khader[170], F. Khalil-Zada[13], A. Khanov[125], A. G. Kharlamov[120a,120b], T. Kharlamova[120a,120b], A. Khodinov[163], T. J. Khoo[52], E. Khramov[77], J. Khubua[156b], S. Kido[80], M. Kiehn[52], C. R. Kilby[91], Y. K. Kim[36], N. Kimura[64a,64c], O. M. Kind[19], B. T. King[88], D. Kirchmeier[46], J. Kirk[141], A. E. Kiryunin[113], T. Kishimoto[160], D. Kisielewska[81a], V. Kitali[44], O. Kivernyk[5], E. Kladiva[28b,*], T. Klapdor-Kleingrothaus[50], M. H. Klein[103], M. Klein[88], U. Klein[88], K. Kleinknecht[97], P. Klimek[119], A. Klimentov[29], R. Klingenberg[45,*], T. Klingl[24], T. Klioutchnikova[35], F. F. Klitzner[112], P. Kluit[118], S. Kluth[113], E. Kneringer[74], E. B. F. G. Knoops[99], A. Knue[50], A. Kobayashi[160], D. Kobayashi[85], T. Kobayashi[160], M. Kobel[46], M. Kocian[150], P. Kodys[139], T. Koffas[33], E. Koffeman[118], N. M. Köhler[113], T. Koi[150], M. Kolb[59b], I. Koletsou[5], T. Kondo[79], N. Kondrashova[58c], K. Köneke[50], A. C. König[117], T. Kono[79], R. Konoplich[121,aj], V. Konstantinides[92], N. Konstantinidis[92], B. Konya[94], R. Kopeliansky[63], S. Koperny[81a], K. Korcyl[82], K. Kordas[159], A. Korn[92], I. Korolkov[14], E. V. Korolkova[146], O. Kortner[113], S. Kortner[113], T. Kosek[139], V. V. Kostyukhin[24], A. Kotwal[47], A. Koulouris[10], A. Kourkoumeli-Charalampidi[68a,68b], C. Kourkoumelis[9], E. Kourlitis[146], V. Kouskoura[29], A. B. Kowalewska[82], R. Kowalewski[173], T. Z. Kowalski[81a], C. Kozakai[160], W. Kozanecki[142], A. S. Kozhin[140], V. A. Kramarenko[111], G. Kramberger[89], D. Krasnopevtsev[58a], M. W. Krasny[132], A. Krasznahorkay[35], D. Krauss[113], J. A. Kremer[81a], J. Kretzschmar[88], P. Krieger[164], K. Krizka[18], K. Kroeninger[45], H. Kroha[113], J. Kroll[137], J. Kroll[133], J. Krstic[16], U. Kruchonak[77], H. Krüger[24], N. Krumnack[76], M. C. Kruse[47], T. Kubota[102], S. Kuday[4b], J. T. Kuechler[179], S. Kuehn[35], A. Kugel[59a], F. Kuger[174], T. Kuhl[44], V. Kukhtin[77], R. Kukla[99], Y. Kulchitsky[105], S. Kuleshov[144b], Y. P. Kulinich[170], M. Kuna[56], T. Kunigo[83], A. Kupco[137], T. Kupfer[45], O. Kuprash[158], H. Kurashige[80], L. L. Kurchaninov[165a], Y. A. Kurochkin[105], M. G. Kurth[15d], E. S. Kuwertz[35], M. Kuze[162], J. Kvita[126], T. Kwan[101], A. La Rosa[113], J. L. La Rosa Navarro[78d], L. La Rotonda[40b,40a], F. La Ruffa[40b,40a], C. Lacasta[171], F. Lacava[70a,70b], J. Lacey[44], D. P. J. Lack[98], H. Lacker[19], D. Lacour[132], E. Ladygin[77], R. Lafaye[5], B. Laforge[132], T. Lagouri[32c], S. Lai[51], S. Lammers[63], W. Lampl[7], E. Lançon[29], U. Landgraf[50], M. P. J. Landon[90], M. C. Lanfermann[52], V. S. Lang[44], J. C. Lange[14], R. J. Langenberg[35], A. J. Lankford[168], F. Lanni[29], K. Lantzsch[24], A. Lanza[68a], A. Lapertosa[53a,53b], S. Laplace[132], J. F. Laporte[142], T. Lari[66a], F. Lasagni Manghi[23a,23b], M. Lassnig[35], T. S. Lau[61a], A. Laudrain[128], M. Lavorgna[67a,67b], A. T. Law[143], P. Laycock[88], M. Lazzaroni[66a,66b], B. Le[102], O. Le Dortz[132], E. Le Guirriec[99], E. P. Le Quilleuc[142], M. LeBlanc[7], T. LeCompte[6], F. Ledroit-Guillon[56], C. A. Lee[29], G. R. Lee[144a], L. Lee[57], S. C. Lee[155], B. Lefebvre[101], M. Lefebvre[173], F. Legger[112], C. Leggett[18], N. Lehmann[179], G. Lehmann Miotto[35], W. A. Leight[44], A. Leisos[159,v], M. A. L. Leite[78d], R. Leitner[139], D. Lellouch[177], B. Lemmer[51], K. J. C. Leney[92], T. Lenz[24], B. Lenzi[35], R. Leone[7], S. Leone[69a], C. Leonidopoulos[48], G. Lerner[153], C. Leroy[107], R. Les[164], A. A. J. Lesage[142], C. G. Lester[31], M. Levchenko[134], J. Levêque[5], D. Levin[103], L. J. Levinson[177], D. Lewis[90], B. Li[103], C.-Q. Li[58a], H. Li[58b], L. Li[58c], Q. Li[15d], Q. Y. Li[58a], S. Li[58d,58c], X. Li[58c], Y. Li[148], Z. Liang[15a], B. Liberti[71a], A. Liblong[164], K. Lie[61c], S. Liem[118], A. Limosani[154], C. Y. Lin[31], K. Lin[104], T. H. Lin[97], R. A. Linck[63], J. H. Lindon[21], B. E. Lindquist[152], A. L. Lionti[52], E. Lipeles[133], A. Lipniacka[17], M. Lisovyi[59b], T. M. Liss[170,ap], A. Lister[172], A. M. Litke[143], J. D. Little[8], B. Liu[76], B. L Liu[6], H. B. Liu[29], H. Liu[103], J. B. Liu[58a], J. K. K. Liu[131], K. Liu[132], M. Liu[58a], P. Liu[18], Y. Liu[15a], Y. L. Liu[58a], Y. W. Liu[58a], M. Livan[68a,68b], A. Lleres[56], J. Llorente Merino[15a], S. L. Lloyd[90], C. Y. Lo[61b], F. Lo Sterzo[41], E. M. Lobodzinska[44], P. Loch[7], A. Loesle[50],

T. Lohse[19], K. Lohwasser[146], M. Lokajicek[137], B. A. Long[25], J. D. Long[170], R. E. Long[87], L. Longo[65a,65b], K. A. Looper[122], J. A. Lopez[144b], I. Lopez Paz[14], A. Lopez Solis[146], J. Lorenz[112], N. Lorenzo Martinez[5], M. Losada[22], P. J. Lösel[112], X. Lou[44], X. Lou[15a], A. Lounis[128], J. Love[6], P. A. Love[87], J. J. Lozano Bahilo[171], H. Lu[61a], M. Lu[58a], N. Lu[103], Y. J. Lu[62], H. J. Lubatti[145], C. Luci[70a,70b], A. Lucotte[56], C. Luedtke[50], F. Luehring[63], I. Luise[132], L. Luminari[70a], B. Lund-Jensen[151], M. S. Lutz[100], P. M. Luzi[132], D. Lynn[29], R. Lysak[137], E. Lytken[94], F. Lyu[15a], V. Lyubushkin[77], H. Ma[29], L. L. Ma[58b], Y. Ma[58b], G. Maccarrone[49], A. Macchiolo[113], C. M. Macdonald[146], J. Machado Miguens[133,136b], D. Madaffari[171], R. Madar[37], W. F. Mader[46], A. Madsen[44], N. Madysa[46], J. Maeda[80], K. Maekawa[160], S. Maeland[17], T. Maeno[29], A. S. Maevskiy[111], V. Magerl[50], C. Maidantchik[78b], T. Maier[112], A. Maio[136a,136b,136d], O. Majersky[28a], S. Majewski[127], Y. Makida[79], N. Makovec[128], B. Malaescu[132], Pa. Malecki[82], V. P. Maleev[134], F. Malek[56], U. Mallik[75], D. Malon[6], C. Malone[31], S. Maltezos[10], S. Malyukov[35], J. Mamuzic[171], G. Mancini[49], I. Mandić[89], J. Maneira[136a], L. Manhaes de Andrade Filho[78a], J. Manjarres Ramos[46], K. H. Mankinen[94], A. Mann[112], A. Manousos[74], B. Mansoulie[142], J. D. Mansour[15a], M. Mantoani[51], S. Manzoni[66a,66b], G. Marceca[30], L. March[52], L. Marchese[131], G. Marchiori[132], M. Marcisovsky[137], C. A. Marin Tobon[35], M. Marjanovic[37], D. E. Marley[103], F. Marroquim[78b], Z. Marshall[18], M. U. F Martensson[169], S. Marti-Garcia[171], C. B. Martin[122], T. A. Martin[175], V. J. Martin[48], B. Martin dit Latour[17], M. Martinez[14,y], V. I. Martinez Outschoorn[100], S. Martin-Haugh[141], V. S. Martoiu[27b], A. C. Martyniuk[92], A. Marzin[35], L. Masetti[97], T. Mashimo[160], R. Mashinistov[108], J. Masik[98], A. L. Maslennikov[120a,120b], L. H. Mason[102], L. Massa[71a,71b], P. Massarotti[67a,67b], P. Mastrandrea[5], A. Mastroberardino[40a,40b], T. Masubuchi[160], P. Mättig[179], J. Maurer[27b], B. Maček[89], S. J. Maxfield[88], D. A. Maximov[120a,120b], R. Mazini[155], I. Maznas[159], S. M. Mazza[143], N. C. Mc Fadden[116], G. Mc Goldrick[164], S. P. Mc Kee[103], A. McCarn[103], T. G. McCarthy[113], L. I. McClymont[92], E. F. McDonald[102], J. A. Mcfayden[35], G. Mchedlidze[51], M. A. McKay[41], K. D. McLean[173], S. J. McMahon[141], P. C. McNamara[102], C. J. McNicol[175], R. A. McPherson[173,ac], J. E. Mdhluli[32c], Z. A. Meadows[100], S. Meehan[145], T. M. Megy[50], S. Mehlhase[112], A. Mehta[88], T. Meideck[56], B. Meirose[42], D. Melini[171,g], B. R. Mellado Garcia[32c], J. D. Mellenthin[51], M. Melo[28a], F. Meloni[44], A. Melzer[24], S. B. Menary[98], E. D. Mendes Gouveia[136a], L. Meng[88], X. T. Meng[103], A. Mengarelli[23a,23b], S. Menke[113], E. Meoni[40b,40a], S. Mergelmeyer[19], C. Merlassino[20], P. Mermod[52], L. Merola[67a,67b], C. Meroni[66a], F. S. Merritt[36], A. Messina[70a,70b], J. Metcalfe[6], A. S. Mete[168], C. Meyer[133], J. Meyer[157], J.-P. Meyer[142], H. Meyer Zu Theenhausen[59a], F. Miano[153], R. P. Middleton[141], L. Mijović[48], G. Mikenberg[177], M. Mikestikova[137], M. Mikuž[89], M. Milesi[102], A. Milic[164], D. A. Millar[90], D. W. Miller[36], A. Milov[177], D. A. Milstead[43a,43b], A. A. Minaenko[140], M. Miñano Moya[171], I. A. Minashvili[156b], A. I. Mincer[121], B. Mindur[81a], M. Mineev[77], Y. Minegishi[160], Y. Ming[178], L. M. Mir[14], A. Mirto[65a,65b], K. P. Mistry[133], T. Mitani[176], J. Mitrevski[112], V. A. Mitsou[171], A. Miucci[20], P. S. Miyagawa[146], A. Mizukami[79], J. U. Mjörnmark[94], T. Mkrtchyan[181], M. Mlynarikova[139], T. Moa[43a,43b], K. Mochizuki[107], P. Mogg[50], S. Mohapatra[38], S. Molander[43a,43b], R. Moles-Valls[24], M. C. Mondragon[104], K. Mönig[44], J. Monk[39], E. Monnier[99], A. Montalbano[149], J. Montejo Berlingen[35], F. Monticelli[86], S. Monzani[66a], N. Morange[128], D. Moreno[22], M. Moreno Llácer[35], P. Morettini[53b], M. Morgenstern[118], S. Morgenstern[46], D. Mori[149], M. Morii[57], M. Morinaga[176], V. Morisbak[130], A. K. Morley[35], G. Mornacchi[35], A. P. Morris[92], J. D. Morris[90], L. Morvaj[152], P. Moschovakos[10], M. Mosidze[156b], H. J. Moss[146], J. Moss[150,m], K. Motohashi[162], R. Mount[150], E. Mountricha[35], E. J. W. Moyse[100], S. Muanza[99], F. Mueller[113], J. Mueller[135], R. S. P. Mueller[112], D. Muenstermann[87], G. A. Mullier[20], F. J. Munoz Sanchez[98], P. Murin[28b], W. J. Murray[141,175], A. Murrone[66a,66b], M. Muškinja[89], C. Mwewa[32a], A. G. Myagkov[140,ak], J. Myers[127], M. Myska[138], B. P. Nachman[18], O. Nackenhorst[45], K. Nagai[131], K. Nagano[79], Y. Nagasaka[60], M. Nagel[50], E. Nagy[99], A. M. Nairz[35], Y. Nakahama[115], K. Nakamura[79], T. Nakamura[160], I. Nakano[123], H. Nanjo[129], F. Napolitano[59a], R. F. Naranjo Garcia[44], R. Narayan[11], D. I. Narrias Villar[59a], I. Naryshkin[134], T. Naumann[44], G. Navarro[22], R. Nayyar[7], H. A. Neal[103], P. Y. Nechaeva[108], T. J. Neep[142], A. Negri[68a,68b], M. Negrini[23b], S. Nektarijevic[117], C. Nellist[51], M. E. Nelson[131], S. Nemecek[137], P. Nemethy[121], M. Nessi[35,e], M. S. Neubauer[170], M. Neumann[179], P. R. Newman[21], T. Y. Ng[61c], Y. S. Ng[19], H. D. N. Nguyen[99], T. Nguyen Manh[107], E. Nibigira[37], R. B. Nickerson[131], R. Nicolaidou[142], J. Nielsen[143], N. Nikiforou[11], V. Nikolaenko[140,ak], I. Nikolic-Audit[132], K. Nikolopoulos[21], P. Nilsson[29], Y. Ninomiya[79], A. Nisati[70a], N. Nishu[58c], R. Nisius[113], I. Nitsche[45], T. Nitta[176], T. Nobe[160], Y. Noguchi[83], M. Nomachi[129], I. Nomidis[132], M. A. Nomura[29], T. Nooney[90], M. Nordberg[35], N. Norjoharuddeen[131], T. Novak[89], O. Novgorodova[46], R. Novotny[138], L. Nozka[126], K. Ntekas[168], E. Nurse[92], F. Nuti[102], F. G. Oakham[33,as], H. Oberlack[113], T. Obermann[24], J. Ocariz[132], A. Ochi[80], I. Ochoa[38], J. P. Ochoa-Ricoux[144a], K. O'Connor[26], S. Oda[85], S. Odaka[79], S. Oerdek[51], A. Oh[98], S. H. Oh[47], C. C. Ohm[151], H. Oide[53a,53b], M. L. Ojeda[164], H. Okawa[166], Y. Okazaki[83], Y. Okumura[160], T. Okuyama[79], A. Olariu[27b], L. F. Oleiro Seabra[136a], S. A. Olivares Pino[144a], D. Oliveira Damazio[29], J. L. Oliver[1], M. J. R. Olsson[36], A. Olszewski[82], J. Olszowska[82], D. C. O'Neil[149], A. Onofre[136a,136e], K. Onogi[115], P. U. E. Onyisi[11], H. Oppen[130], M. J. Oreglia[36], Y. Oren[158], D. Orestano[72a,72b], E. C. Orgill[98], N. Orlando[61b], A. A. O'Rourke[44], R. S. Orr[164], B. Osculati[53a,53b,*], V. O'Shea[55], R. Ospanov[58a], G. Otero y Garzon[30], H. Otono[85],

M. Ouchrif[34d], F. Ould-Saada[130], A. Ouraou[142], Q. Ouyang[15a], M. Owen[55], R. E. Owen[21], V. E. Ozcan[12c], N. Ozturk[8], J. Pacalt[126], H. A. Pacey[31], K. Pachal[149], A. Pacheco Pages[14], L. Pacheco Rodriguez[142], C. Padilla Aranda[14], S. Pagan Griso[18], M. Paganini[180], G. Palacino[63], S. Palazzo[40a,40b], S. Palestini[35], M. Palka[81b], D. Pallin[37], I. Panagoulias[10], C. E. Pandini[35], J. G. Panduro Vazquez[91], P. Pani[35], G. Panizzo[64a,64c], L. Paolozzi[52], T. D. Papadopoulou[10], K. Papageorgiou[9,i], A. Paramonov[6], D. Paredes Hernandez[61b], S. R. Paredes Saenz[131], B. Parida[58c], A. J. Parker[87], K. A. Parker[44], M. A. Parker[31], F. Parodi[53a,53b], J. A. Parsons[38], U. Parzefall[50], V. R. Pascuzzi[164], J. M. P. Pasner[143], E. Pasqualucci[70a], S. Passaggio[53b], F. Pastore[91], P. Pasuwan[43a,43b], S. Pataraia[97], J. R. Pater[98], A. Pathak[178,j], T. Pauly[35], B. Pearson[113], M. Pedersen[130], L. Pedraza Diaz[117], R. Pedro[136a,136b], S. V. Peleganchuk[120a,120b], O. Penc[137], C. Peng[15d], H. Peng[58a], B. S. Peralva[78a], M. M. Perego[142], A. P. Pereira Peixoto[136a], D. V. Perepelitsa[29], F. Peri[19], L. Perini[66a,66b], H. Pernegger[35], S. Perrella[67a,67b], V. D. Peshekhonov[77,*], K. Peters[44], R. F. Y. Peters[98], B. A. Petersen[35], T. C. Petersen[39], E. Petit[56], A. Petridis[1], C. Petridou[159], P. Petroff[128], M. Petrov[131], F. Petrucci[72a,72b], M. Pettee[180], N. E. Pettersson[100], A. Peyaud[142], R. Pezoa[144b], T. Pham[102], F. H. Phillips[104], P. W. Phillips[141], G. Piacquadio[152], E. Pianori[18], A. Picazio[100], M. A. Pickering[131], R. H. Pickles[98], R. Piegaia[30], J. E. Pilcher[36], A. D. Pilkington[98], M. Pinamonti[71a,71b], J. L. Pinfold[3], M. Pitt[177], M.-A. Pleier[29], V. Pleskot[139], E. Plotnikova[77], D. Pluth[76], P. Podberezko[120a,120b], R. Poettgen[94], R. Poggi[52], L. Poggioli[128], I. Pogrebnyak[104], D. Pohl[24], I. Pokharel[51], G. Polesello[68a], A. Poley[44], A. Policicchio[70a,70b], R. Polifka[35], A. Polini[23b], C. S. Pollard[44], V. Polychronakos[29], D. Ponomarenko[110], L. Pontecorvo[70a], G. A. Popeneciu[27d], D. M. Portillo Quintero[132], S. Pospisil[138], K. Potamianos[44], I. N. Potrap[77], C. J. Potter[31], H. Potti[11], T. Poulsen[94], J. Poveda[35], T. D. Powell[146], M. E. Pozo Astigarraga[35], P. Pralavorio[99], S. Prell[76], D. Price[98], M. Primavera[65a], S. Prince[101], N. Proklova[110], K. Prokofiev[61c], F. Prokoshin[144b], S. Protopopescu[29], J. Proudfoot[6], M. Przybycien[81a], A. Puri[170], P. Puzo[128], J. Qian[103], Y. Qin[98], A. Quadt[51], M. Queitsch-Maitland[44], A. Qureshi[1], P. Rados[102], F. Ragusa[66a,66b], G. Rahal[95], J. A. Raine[52], S. Rajagopalan[29], A. Ramirez Morales[90], T. Rashid[128], S. Raspopov[5], M. G. Ratti[66a,66b], D. M. Rauch[44], F. Rauscher[112], S. Rave[97], B. Ravina[146], I. Ravinovich[177], J. H. Rawling[98], M. Raymond[35], A. L. Read[130], N. P. Readioff[56], M. Reale[65a,65b], D. M. Rebuzzi[68a,68b], A. Redelbach[174], G. Redlinger[29], R. Reece[143], R. G. Reed[32c], K. Reeves[42], L. Rehnisch[19], J. Reichert[133], A. Reiss[97], C. Rembser[35], H. Ren[15d], M. Rescigno[70a], S. Resconi[66a], E. D. Resseguie[133], S. Rettie[172], E. Reynolds[21], O. L. Rezanova[120a,120b], P. Reznicek[139], E. Ricci[73a,73b], R. Richter[113], S. Richter[92], E. Richter-Was[81b], O. Ricken[24], M. Ridel[132], P. Rieck[113], C. J. Riegel[179], O. Rifki[44], M. Rijssenbeek[152], A. Rimoldi[68a,68b], M. Rimoldi[20], L. Rinaldi[23b], G. Ripellino[151], B. Ristić[87], E. Ritsch[35], I. Riu[14], J. C. Rivera Vergara[144a], F. Rizatdinova[125], E. Rizvi[90], C. Rizzi[14], R. T. Roberts[98], S. H. Robertson[101,ac], D. Robinson[31], J. E. M. Robinson[44], A. Robson[55], E. Rocco[97], C. Roda[69a,69b], Y. Rodina[99], S. Rodriguez Bosca[171], A. Rodriguez Perez[14], D. Rodriguez Rodriguez[171], A. M. Rodríguez Vera[165b], S. Roe[35], C. S. Rogan[57], O. Røhne[130], R. Röhrig[113], C. P. A. Roland[63], J. Roloff[57], A. Romaniouk[110], M. Romano[23a,23b], N. Rompotis[88], M. Ronzani[121], L. Roos[132], S. Rosati[70a], K. Rosbach[50], P. Rose[143], N.-A. Rosien[51], E. Rossi[44], E. Rossi[67a,67b], L. P. Rossi[53b], L. Rossini[66a,66b], J. H. N. Rosten[31], R. Rosten[14], M. Rotaru[27b], J. Rothberg[145], D. Rousseau[128], D. Roy[32c], A. Rozanov[99], Y. Rozen[157], X. Ruan[32c], F. Rubbo[150], F. Rühr[50], A. Ruiz-Martinez[171], Z. Rurikova[50], N. A. Rusakovich[77], H. L. Russell[101], J. P. Rutherfoord[7], E. M. Rüttinger[44,k], Y. F. Ryabov[134], M. Rybar[170], G. Rybkin[128], S. Ryu[6], A. Ryzhov[140], G. F. Rzehorz[51], P. Sabatini[51], G. Sabato[118], S. Sacerdoti[128], H. F.-W. Sadrozinski[143], R. Sadykov[77], F. Safai Tehrani[70a], P. Saha[119], M. Sahinsoy[59a], A. Sahu[179], M. Saimpert[44], M. Saito[160], T. Saito[160], H. Sakamoto[160], A. Sakharov[121,aj], D. Salamani[52], G. Salamanna[72a,72b], J. E. Salazar Loyola[144b], D. Salek[118], P. H. Sales De Bruin[169], D. Salihagic[113], A. Salnikov[150], J. Salt[171], D. Salvatore[40a,40b], F. Salvatore[153], A. Salvucci[61a,61b,61c], A. Salzburger[35], J. Samarati[35], D. Sammel[50], D. Sampsonidis[159], D. Sampsonidou[159], J. Sánchez[171], A. Sanchez Pineda[64a,64c], H. Sandaker[130], C. O. Sander[44], M. Sandhoff[179], C. Sandoval[22], D. P. C. Sankey[141], M. Sannino[53a,53b], Y. Sano[115], A. Sansoni[49], C. Santoni[37], H. Santos[136a], I. Santoyo Castillo[153], A. Santra[171], A. Sapronov[77], J. G. Saraiva[136a,136d], O. Sasaki[79], K. Sato[166], E. Sauvan[5], P. Savard[164,as], N. Savic[113], R. Sawada[160], C. Sawyer[141], L. Sawyer[93,ai], C. Sbarra[23b], A. Sbrizzi[23a,23b], T. Scanlon[92], J. Schaarschmidt[145], P. Schacht[113], B. M. Schachtner[112], D. Schaefer[36], L. Schaefer[133], J. Schaeffer[97], S. Schaepe[35], U. Schäfer[97], A. C. Schaffer[128], D. Schaile[112], R. D. Schamberger[152], N. Scharmberg[98], V. A. Schegelsky[134], D. Scheirich[139], F. Schenck[19], M. Schernau[168], C. Schiavi[53a,53b], S. Schier[143], L. K. Schildgen[24], Z. M. Schillaci[26], E. J. Schioppa[35], M. Schioppa[40a,40b], K. E. Schleicher[50], S. Schlenker[35], K. R. Schmidt-Sommerfeld[113], K. Schmieden[35], C. Schmitt[97], S. Schmitt[44], S. Schmitz[97], J. C. Schmoeckel[44], U. Schnoor[50], L. Schoeffel[142], A. Schoening[59b], E. Schopf[24], M. Schott[97], J. F. P. Schouwenberg[117], J. Schovancova[35], S. Schramm[52], A. Schulte[97], H.-C. Schultz-Coulon[59a], M. Schumacher[50], B. A. Schumm[143], Ph. Schune[142], A. Schwartzman[150], T. A. Schwarz[103], H. Schweiger[98], Ph. Schwemling[142], R. Schwienhorst[104], A. Sciandra[24], G. Sciolla[26], M. Scornajenghi[40a,40b], F. Scuri[69a], F. Scutti[102], L. M. Scyboz[113], J. Searcy[103], C. D. Sebastiani[70a,70b], P. Seema[24], S. C. Seidel[116], A. Seiden[143], T. Seiss[36], J. M. Seixas[78b], G. Sekhniaidze[67a], K. Sekhon[103], S. J. Sekula[41], N. Semprini-Cesari[23a,23b], S. Sen[47], S. Senkin[37],

C. Serfon[130], L. Serin[128], L. Serkin[64a,64b], M. Sessa[72a,72b], H. Severini[124], F. Sforza[167], A. Sfyrla[52], E. Shabalina[51], J. D. Shahinian[143], N. W. Shaikh[43a,43b], L. Y. Shan[15a], R. Shang[170], J. T. Shank[25], M. Shapiro[18], A. S. Sharma[1], A. Sharma[131], P. B. Shatalov[109], K. Shaw[153], S. M. Shaw[98], A. Shcherbakova[134], Y. Shen[124], N. Sherafati[33], A. D. Sherman[25], P. Sherwood[92], L. Shi[155,ao], S. Shimizu[79], C. O. Shimmin[180], M. Shimojima[114], I. P. J. Shipsey[131], S. Shirabe[85], M. Shiyakova[77], J. Shlomi[177], A. Shmeleva[108], D. Shoaleh Saadi[107], M. J. Shochet[36], S. Shojaii[102], D. R. Shope[124], S. Shrestha[122], E. Shulga[110], P. Sicho[137], A. M. Sickles[170], P. E. Sidebo[151], E. Sideras Haddad[32c], O. Sidiropoulou[35], A. Sidoti[23a,23b], F. Siegert[46], Dj. Sijacki[16], J. Silva[136a], M. Silva Jr.[178], M. V. Silva Oliveira[78a], S. B. Silverstein[43a], L. Simic[77], S. Simion[128], E. Simioni[97], M. Simon[97], R. Simoniello[97], P. Sinervo[164], N. B. Sinev[127], M. Sioli[23a,23b], G. Siragusa[174], I. Siral[103], S. Yu. Sivoklokov[111], J. Sjölin[43a,43b], P. Skubic[124], M. Slater[21], T. Slavicek[138], M. Slawinska[82], K. Sliwa[167], R. Slovak[139], V. Smakhtin[177], B. H. Smart[5], J. Smiesko[28a], N. Smirnov[110], S. Yu. Smirnov[110], Y. Smirnov[110], L. N. Smirnova[111], O. Smirnova[94], J. W. Smith[51], M. N. K. Smith[38], M. Smizanska[87], K. Smolek[138], A. Smykiewicz[82], A. A. Snesarev[108], I. M. Snyder[127], S. Snyder[29], R. Sobie[173,ac], A. M. Soffa[168], A. Soffer[158], A. Søgaard[48], D. A. Soh[155], G. Sokhrannyi[89], C. A. Solans Sanchez[35], M. Solar[138], E. Yu. Soldatov[110], U. Soldevila[171], A. A. Solodkov[140], A. Soloshenko[77], O. V. Solovyanov[140], V. Solovyev[134], P. Sommer[146], H. Son[167], W. Song[141], W. Y. Song[165b], A. Sopczak[138], F. Sopkova[28b], D. Sosa[59b], C. L. Sotiropoulou[69a,69b], S. Sottocornola[68a,68b], R. Soualah[64a,64c,h], A. M. Soukharev[120a,120b], D. South[44], B. C. Sowden[91], S. Spagnolo[65a,65b], M. Spalla[113], M. Spangenberg[175], F. Spanò[91], D. Sperlich[19], F. Spettel[113], T. M. Spieker[59a], R. Spighi[23b], G. Spigo[35], L. A. Spiller[102], D. P. Spiteri[55], M. Spousta[139], A. Stabile[66a,66b], R. Stamen[59a], S. Stamm[19], E. Stanecka[82], R. W. Stanek[6], C. Stanescu[72a], B. Stanislaus[131], M. M. Stanitzki[44], B. Stapf[118], S. Stapnes[130], E. A. Starchenko[140], G. H. Stark[36], J. Stark[56], S. H Stark[39], P. Staroba[137], P. Starovoitov[59a], S. Stärz[35], R. Staszewski[82], M. Stegler[44], P. Steinberg[29], B. Stelzer[149], H. J. Stelzer[35], O. Stelzer-Chilton[165a], H. Stenzel[54], T. J. Stevenson[90], G. A. Stewart[55], M. C. Stockton[127], G. Stoicea[27b], P. Stolte[51], S. Stonjek[113], A. Straessner[46], J. Strandberg[151], S. Strandberg[43a,43b], M. Strauss[124], P. Strizenec[28b], R. Ströhmer[174], D. M. Strom[127], R. Stroynowski[41], A. Strubig[48], S. A. Stucci[29], B. Stugu[17], J. Stupak[124], N. A. Styles[44], D. Su[150], J. Su[135], S. Suchek[59a], Y. Sugaya[129], M. Suk[138], V. V. Sulin[108], D. M. S. Sultan[52], S. Sultansoy[4c], T. Sumida[83], S. Sun[103], X. Sun[3], K. Suruliz[153], C. J. E. Suster[154], M. R. Sutton[153], S. Suzuki[79], M. Svatos[137], M. Swiatlowski[36], S. P. Swift[2], A. Sydorenko[97], I. Sykora[28a], T. Sykora[139], D. Ta[97], K. Tackmann[44,z], J. Taenzer[158], A. Taffard[168], R. Tafirout[165a], E. Tahirovic[90], N. Taiblum[158], H. Takai[29], R. Takashima[84], E. H. Takasugi[113], K. Takeda[80], T. Takeshita[147], Y. Takubo[79], M. Talby[99], A. A. Talyshev[120a,120b], J. Tanaka[160], M. Tanaka[162], R. Tanaka[128], B. B. Tannenwald[122], S. Tapia Araya[144b], S. Tapprogge[97], A. Tarek Abouelfadl Mohamed[132], S. Tarem[157], G. Tarna[27b,d], G. F. Tartarelli[66a], P. Tas[139], M. Tasevsky[137], T. Tashiro[83], E. Tassi[40b,40a], A. Tavares Delgado[136a,136b], Y. Tayalati[34e], A. C. Taylor[116], A. J. Taylor[48], G. N. Taylor[102], P. T. E. Taylor[102], W. Taylor[165b], A. S. Tee[87], P. Teixeira-Dias[91], H. Ten Kate[35], P. K. Teng[155], J. J. Teoh[118], F. Tepel[179], S. Terada[79], K. Terashi[160], J. Terron[96], S. Terzo[14], M. Testa[49], R. J. Teuscher[164,ac], S. J. Thais[180], T. Theveneaux-Pelzer[44], F. Thiele[39], D. W. Thomas[91], J. P. Thomas[21], A. S. Thompson[55], P. D. Thompson[21], L. A. Thomsen[180], E. Thomson[133], Y. Tian[38], R. E. Ticse Torres[51], V. O. Tikhomirov[108,al], Yu. A. Tikhonov[120a,120b], S. Timoshenko[110], P. Tipton[180], S. Tisserant[99], K. Todome[162], S. Todorova-Nova[5], S. Todt[46], J. Tojo[85], S. Tokár[28a], K. Tokushuku[79], E. Tolley[122], K. G. Tomiwa[32c], M. Tomoto[115], L. Tompkins[150,p], K. Toms[116], B. Tong[57], P. Tornambe[50], E. Torrence[127], H. Torres[46], E. Torró Pastor[145], C. Tosciri[131], J. Toth[99,ab], F. Touchard[99], D. R. Tovey[146], C. J. Treado[121], T. Trefzger[174], F. Tresoldi[153], A. Tricoli[29], I. M. Trigger[165a], S. Trincaz-Duvoid[132], M. F. Tripiana[14], W. Trischuk[164], B. Trocmé[56], A. Trofymov[128], C. Troncon[66a], M. Trovatelli[173], F. Trovato[153], L. Truong[32b], M. Trzebinski[82], A. Trzupek[82], F. Tsai[44], J. C.-L. Tseng[131], P. V. Tsiareshka[105], A. Tsirigotis[159], N. Tsirintanis[9], V. Tsiskaridze[152], E. G. Tskhadadze[156a], I. I. Tsukerman[109], V. Tsulaia[18], S. Tsuno[79], D. Tsybychev[152], Y. Tu[61b], A. Tudorache[27b], V. Tudorache[27b], T. T. Tulbure[27a], A. N. Tuna[57], S. Turchikhin[77], D. Turgeman[177], I. Turk Cakir[4b,t], R. Turra[66a], P. M. Tuts[38], E. Tzovara[97], G. Ucchielli[23a,23b], I. Ueda[79], M. Ughetto[43a,43b], F. Ukegawa[166], G. Unal[35], A. Undrus[29], G. Unel[168], F. C. Ungaro[102], Y. Unno[79], K. Uno[160], J. Urban[28b], P. Urquijo[102], P. Urrejola[97], G. Usai[8], J. Usui[79], L. Vacavant[99], V. Vacek[138], B. Vachon[101], K. O. H. Vadla[130], A. Vaidya[92], C. Valderanis[112], E. Valdes Santurio[43a,43b], M. Valente[52], S. Valentinetti[23a,23b], A. Valero[171], L. Valéry[44], R. A. Vallance[21], A. Vallier[5], J. A. Valls Ferrer[171], T. R. Van Daalen[14], W. Van Den Wollenberg[118], H. Van der Graaf[118], P. Van Gemmeren[6], J. Van Nieuwkoop[149], I. Van Vulpen[118], M. Vanadia[71a,71b], W. Vandelli[35], A. Vaniachine[163], P. Vankov[118], R. Vari[70a], E. W. Varnes[7], C. Varni[53a,53b], T. Varol[41], D. Varouchas[128], K. E. Varvell[154], G. A. Vasquez[144b], J. G. Vasquez[180], F. Vazeille[37], D. Vazquez Furelos[14], T. Vazquez Schroeder[101], J. Veatch[51], V. Vecchio[72a,72b], L. M. Veloce[164], F. Veloso[136a,136c], S. Veneziano[70a], A. Ventura[65a,65b], M. Venturi[173], N. Venturi[35], V. Vercesi[68a], M. Verducci[72a,72b], C. M. Vergel Infante[76], W. Verkerke[118], A. T. Vermeulen[118], J. C. Vermeulen[118], M. C. Vetterli[149,as], N. Viaux Maira[144b], M. Vicente Barreto Pinto[52], I. Vichou[170,*], T. Vickey[146], O. E. Vickey Boeriu[146], G. H. A. Viehhauser[131], S. Viel[18], L. Vigani[131], M. Villa[23a,23b], M. Villaplana Perez[66a,66b], E. Vilucchi[49], M. G. Vincter[33],

V. B. Vinogradov[77], A. Vishwakarma[44], C. Vittori[23a,23b], I. Vivarelli[153], S. Vlachos[10], M. Vogel[179], P. Vokac[138], G. Volpi[14], S. E. von Buddenbrock[32c], E. Von Toerne[24], V. Vorobel[139], K. Vorobev[110], M. Vos[171], J. H. Vossebeld[88], N. Vranjes[16], M. Vranjes Milosavljevic[16], V. Vrba[138], M. Vreeswijk[118], T. Šfiligoj[89], R. Vuillermet[35], I. Vukotic[36], T. Ženiš[28a], L. Živković[16], P. Wagner[24], W. Wagner[179], J. Wagner-Kuhr[112], H. Wahlberg[86], S. Wahrmund[46], K. Wakamiya[80], V. M. Walbrecht[113], J. Walder[87], R. Walker[112], S. D. Walker[91], W. Walkowiak[148], V. Wallangen[43a,43b], A. M. Wang[57], C. Wang[58b,d], F. Wang[178], H. Wang[18], H. Wang[3], J. Wang[154], J. Wang[59b], P. Wang[41], Q. Wang[124], R.-J. Wang[132], R. Wang[58a], R. Wang[6], S. M. Wang[155], W. T. Wang[58a], W. Wang[15c,ad], W. X. Wang[58a,ad], Y. Wang[58a], Z. Wang[58c], C. Wanotayaroj[44], A. Warburton[101], C. P. Ward[31], D. R. Wardrope[92], A. Washbrook[48], P. M. Watkins[21], A. T. Watson[21], M. F. Watson[21], G. Watts[145], S. Watts[98], B. M. Waugh[92], A. F. Webb[11], S. Webb[97], C. Weber[180], M. S. Weber[20], S. A. Weber[33], S. M. Weber[59a], A. R. Weidberg[131], B. Weinert[63], J. Weingarten[45], M. Weirich[97], C. Weiser[50], P. S. Wells[35], T. Wenaus[29], T. Wengler[35], S. Wenig[35], N. Wermes[24], M. D. Werner[76], P. Werner[35], M. Wessels[59a], T. D. Weston[20], K. Whalen[127], N. L. Whallon[145], A. M. Wharton[87], A. S. White[103], A. White[8], M. J. White[1], R. White[144b], D. Whiteson[168], B. W. Whitmore[87], F. J. Wickens[141], W. Wiedenmann[178], M. Wielers[141], C. Wiglesworth[39], L. A. M. Wiik-Fuchs[50], A. Wildauer[113], F. Wilk[98], H. G. Wilkens[35], L. J. Wilkins[91], H. H. Williams[133], S. Williams[31], C. Willis[104], S. Willocq[100], J. A. Wilson[21], I. Wingerter-Seez[5], E. Winkels[153], F. Winklmeier[127], O. J. Winston[153], B. T. Winter[24], M. Wittgen[150], M. Wobisch[93], A. Wolf[97], T. M. H. Wolf[118], R. Wolff[99], M. W. Wolter[82], H. Wolters[136a,136c], V. W. S. Wong[172], N. L. Woods[143], S. D. Worm[21], B. K. Wosiek[82], K. W. Woźniak[82], K. Wraight[55], M. Wu[36], S. L. Wu[178], X. Wu[52], Y. Wu[58a], T. R. Wyatt[98], B. M. Wynne[48], S. Xella[39], Z. Xi[103], L. Xia[175], D. Xu[15a], H. Xu[58a], L. Xu[29], T. Xu[142], W. Xu[103], B. Yabsley[154], S. Yacoob[32a], K. Yajima[129], D. P. Yallup[92], D. Yamaguchi[162], Y. Yamaguchi[162], A. Yamamoto[79], T. Yamanaka[160], F. Yamane[80], M. Yamatani[160], T. Yamazaki[160], Y. Yamazaki[80], Z. Yan[25], H. J. Yang[58c,58d], H. T. Yang[18], S. Yang[75], Y. Yang[160], Z. Yang[17], W.-M. Yao[18], Y. C. Yap[44], Y. Yasu[79], E. Yatsenko[58c,58d], J. Ye[41], S. Ye[29], I. Yeletskikh[77], E. Yigitbasi[25], E. Yildirim[97], K. Yorita[176], K. Yoshihara[133], C. J. S. Young[35], C. Young[150], J. Yu[8], J. Yu[76], X. Yue[59a], S. P. Y. Yuen[24], B. Zabinski[82], G. Zacharis[10], E. Zaffaroni[52], R. Zaidan[14], A. M. Zaitsev[140,ak], T. Zakareishvili[156b], N. Zakharchuk[44], J. Zalieckas[17], S. Zambito[57], D. Zanzi[35], D. R. Zaripovas[55], S. V. Zeißner[45], C. Zeitnitz[179], G. Zemaityte[131], J. C. Zeng[170], Q. Zeng[150], O. Zenin[140], D. Zerwas[128], M. Zgubič[131], D. F. Zhang[58b], D. Zhang[103], F. Zhang[178], G. Zhang[58a], H. Zhang[15c], J. Zhang[6], L. Zhang[15c], L. Zhang[58a], M. Zhang[170], P. Zhang[15c], R. Zhang[58a], R. Zhang[24], X. Zhang[58b], Y. Zhang[15d], Z. Zhang[128], P. Zhao[47], X. Zhao[41], Y. Zhao[58b,128,ah], Z. Zhao[58a], A. Zhemchugov[77], B. Zhou[103], C. Zhou[178], L. Zhou[41], M. S. Zhou[15d], M. Zhou[152], N. Zhou[58c], Y. Zhou[7], C. G. Zhu[58b], H. L. Zhu[58a], H. Zhu[15a], J. Zhu[103], Y. Zhu[58a], X. Zhuang[15a], K. Zhukov[108], V. Zhulanov[120a,120b], A. Zibell[174], D. Zieminska[63], N. I. Zimine[77], S. Zimmermann[50], Z. Zinonos[113], M. Zinser[97], M. Ziolkowski[148], G. Zobernig[178], A. Zoccoli[23a,23b], K. Zoch[51], T. G. Zorbas[146], R. Zou[36], M. Zur Nedden[19], L. Zwalinski[35]

1 Department of Physics, University of Adelaide, Adelaide, Australia

2 Physics Department, SUNY Albany, Albany, NY, USA

3 Department of Physics, University of Alberta, Edmonton, AB, Canada

4 (a)Department of Physics, Ankara University, Ankara, Turkey; (b)Istanbul Aydin University, Istanbul, Turkey; (c)Division of Physics, TOBB University of Economics and Technology, Ankara, Turkey

5 LAPP, Université Grenoble Alpes, Université Savoie Mont Blanc, CNRS/IN2P3, Annecy, France

6 High Energy Physics Division, Argonne National Laboratory, Argonne, IL, USA

7 Department of Physics, University of Arizona, Tucson, AZ, USA

8 Department of Physics, University of Texas at Arlington, Arlington, TX, USA

9 Physics Department, National and Kapodistrian University of Athens, Athens, Greece

10 Physics Department, National Technical University of Athens, Zografou, Greece

11 Department of Physics, University of Texas at Austin, Austin, TX, USA

12 (a)Faculty of Engineering and Natural Sciences, Bahcesehir University, Istanbul, Turkey; (b)Faculty of Engineering and Natural Sciences, Istanbul Bilgi University, Istanbul, Turkey; (c)Department of Physics, Bogazici University, Istanbul, Turkey; (d)Department of Physics Engineering, Gaziantep University, Gaziantep, Turkey

13 Institute of Physics, Azerbaijan Academy of Sciences, Baku, Azerbaijan

14 Institut de Física d'Altes Energies (IFAE), Barcelona Institute of Science and Technology, Barcelona, Spain

15 (a)Institute of High Energy Physics, Chinese Academy of Sciences, Beijing, China; (b)Physics Department, Tsinghua University, Beijing, China; (c)Department of Physics, Nanjing University, Nanjing, China; (d)University of Chinese Academy of Science (UCAS), Beijing, China

16 Institute of Physics, University of Belgrade, Belgrade, Serbia

[17] Department for Physics and Technology, University of Bergen, Bergen, Norway

[18] Physics Division, Lawrence Berkeley National Laboratory and University of California, Berkeley, CA, USA

[19] Institut für Physik, Humboldt Universität zu Berlin, Berlin, Germany

[20] Albert Einstein Center for Fundamental Physics and Laboratory for High Energy Physics, University of Bern, Bern, Switzerland

[21] School of Physics and Astronomy, University of Birmingham, Birmingham, UK

[22] Centro de Investigaciónes, Universidad Antonio Nariño, Bogotá, Colombia

[23] [a]Dipartimento di Fisica e Astronomia, Università di Bologna, Bologna, Italy; [b]INFN Sezione di Bologna, Bologna, Italy

[24] Physikalisches Institut, Universität Bonn, Bonn, Germany

[25] Department of Physics, Boston University, Boston, MA, USA

[26] Department of Physics, Brandeis University, Waltham, MA, USA

[27] [a]Transilvania University of Brasov, Brasov, Romania; [b]Horia Hulubei National Institute of Physics and Nuclear Engineering, Bucharest, Romania; [c]Department of Physics, Alexandru Ioan Cuza University of Iasi, Iasi, Romania; [d]Physics Department, National Institute for Research and Development of Isotopic and Molecular Technologies, Cluj-Napoca, Romania; [e]University Politehnica Bucharest, Bucharest, Romania; [f]West University in Timisoara, Timisoara, Romania

[28] [a]Faculty of Mathematics, Physics and Informatics, Comenius University, Bratislava, Slovakia; [b]Department of Subnuclear Physics, Institute of Experimental Physics of the Slovak Academy of Sciences, Kosice, Slovak Republic

[29] Physics Department, Brookhaven National Laboratory, Upton, NY, USA

[30] Departamento de Física, Universidad de Buenos Aires, Buenos Aires, Argentina

[31] Cavendish Laboratory, University of Cambridge, Cambridge, UK

[32] [a]Department of Physics, University of Cape Town, Cape Town, South Africa; [b]Department of Mechanical Engineering Science, University of Johannesburg, Johannesburg, South Africa; [c]School of Physics, University of the Witwatersrand, Johannesburg, South Africa

[33] Department of Physics, Carleton University, Ottawa, ON, Canada

[34] [a]Faculté des Sciences Ain Chock, Réseau Universitaire de Physique des Hautes Energies-Université Hassan II, Casablanca, Morocco; [b]Centre National de l'Energie des Sciences Techniques Nucleaires (CNESTEN), Rabat, Morocco; [c]Faculté des Sciences Semlalia, Université Cadi Ayyad, LPHEA-Marrakech, Marrakech, Morocco; [d]Faculté des Sciences, Université Mohamed Premier and LPTPM, Oujda, Morocco; [e]Faculté des sciences, Université Mohammed V, Rabat, Morocco

[35] CERN, Geneva, Switzerland

[36] Enrico Fermi Institute, University of Chicago, Chicago, IL, USA

[37] LPC, Université Clermont Auvergne, CNRS/IN2P3, Clermont-Ferrand, France

[38] Nevis Laboratory, Columbia University, Irvington, NY, USA

[39] Niels Bohr Institute, University of Copenhagen, Copenhagen, Denmark

[40] [a]Dipartimento di Fisica, Università della Calabria, Rende, Italy; [b]INFN Gruppo Collegato di Cosenza, Laboratori Nazionali di Frascati, Frascati, Italy

[41] Physics Department, Southern Methodist University, Dallas, TX, USA

[42] Physics Department, University of Texas at Dallas, Richardson, TX, USA

[43] [a]Department of Physics, Stockholm University, Stockholm, Sweden; [b]Oskar Klein Centre, Stockholm, Sweden

[44] Deutsches Elektronen-Synchrotron DESY, Hamburg and Zeuthen, Germany

[45] Lehrstuhl für Experimentelle Physik IV, Technische Universität Dortmund, Dortmund, Germany

[46] Institut für Kern- und Teilchenphysik, Technische Universität Dresden, Dresden, Germany

[47] Department of Physics, Duke University, Durham, NC, USA

[48] SUPA-School of Physics and Astronomy, University of Edinburgh, Edinburgh, UK

[49] INFN e Laboratori Nazionali di Frascati, Frascati, Italy

[50] Physikalisches Institut, Albert-Ludwigs-Universität Freiburg, Freiburg, Germany

[51] II. Physikalisches Institut, Georg-August-Universität Göttingen, Göttingen, Germany

[52] Département de Physique Nucléaire et Corpusculaire, Université de Genève, Geneva, Switzerland

[53] [a]Dipartimento di Fisica, Università di Genova, Genoa, Italy; [b]INFN Sezione di Genova, Genoa, Italy

[54] II. Physikalisches Institut, Justus-Liebig-Universität Giessen, Giessen, Germany

[55] SUPA-School of Physics and Astronomy, University of Glasgow, Glasgow, UK

56 LPSC, Université Grenoble Alpes, CNRS/IN2P3, Grenoble INP, Grenoble, France

57 Laboratory for Particle Physics and Cosmology, Harvard University, Cambridge, MA, USA

58 (a)Department of Modern Physics and State Key Laboratory of Particle Detection and Electronics, University of Science and Technology of China, Hefei, China; (b)Institute of Frontier and Interdisciplinary Science and Key Laboratory of Particle Physics and Particle Irradiation (MOE), Shandong University, Qingdao, China; (c)School of Physics and Astronomy, Shanghai Jiao Tong University, KLPPAC-MoE, SKLPPC, Shanghai, China; (d)Tsung-Dao Lee Institute, Shanghai, China

59 (a)Kirchhoff-Institut für Physik, Ruprecht-Karls-Universität Heidelberg, Heidelberg, Germany; (b)Physikalisches Institut, Ruprecht-Karls-Universität Heidelberg, Heidelberg, Germany

60 Faculty of Applied Information Science, Hiroshima Institute of Technology, Hiroshima, Japan

61 (a)Department of Physics, Chinese University of Hong Kong, Shatin, NT, Hong Kong; (b)Department of Physics, University of Hong Kong, Hong Kong, China; (c)Department of Physics and Institute for Advanced Study, Hong Kong University of Science and Technology, Clear Water Bay, Kowloon, Hong Kong, China

62 Department of Physics, National Tsing Hua University, Hsinchu, Taiwan

63 Department of Physics, Indiana University, Bloomington, IN, USA

64 (a)INFN Gruppo Collegato di Udine, Sezione di Trieste, Udine, Italy; (b)ICTP, Trieste, Italy; (c)Dipartimento di Chimica, Fisica e Ambiente, Università di Udine, Udine, Italy

65 (a)INFN Sezione di Lecce, Lecce, Italy; (b)Dipartimento di Matematica e Fisica, Università del Salento, Lecce, Italy

66 (a)INFN Sezione di Milano, Milan, Italy; (b)Dipartimento di Fisica, Università di Milano, Milan, Italy

67 (a)INFN Sezione di Napoli, Naples, Italy; (b)Dipartimento di Fisica, Università di Napoli, Naples, Italy

68 (a)INFN Sezione di Pavia, Pavia, Italy; (b)Dipartimento di Fisica, Università di Pavia, Pavia, Italy

69 (a)INFN Sezione di Pisa, Pisa, Italy; (b)Dipartimento di Fisica E. Fermi, Università di Pisa, Pisa, Italy

70 (a)INFN Sezione di Roma, Rome, Italy; (b)Dipartimento di Fisica, Sapienza Università di Roma, Rome, Italy

71 (a)INFN Sezione di Roma Tor Vergata, Rome, Italy; (b)Dipartimento di Fisica, Università di Roma Tor Vergata, Rome, Italy

72 (a)INFN Sezione di Roma Tre, Rome, Italy; (b)Dipartimento di Matematica e Fisica, Università Roma Tre, Rome, Italy

73 (a)INFN-TIFPA, Povo, Italy; (b)Università degli Studi di Trento, Trento, Italy

74 Institut für Astro- und Teilchenphysik, Leopold-Franzens-Universität, Innsbruck, Austria

75 University of Iowa, Iowa City, IA, USA

76 Department of Physics and Astronomy, Iowa State University, Ames, IA, USA

77 Joint Institute for Nuclear Research, Dubna, Russia

78 (a)Departamento de Engenharia Elétrica, Universidade Federal de Juiz de Fora (UFJF), Juiz de Fora, Brazil; (b)Universidade Federal do Rio De Janeiro COPPE/EE/IF, Rio de Janeiro, Brazil; (c)Universidade Federal de São João del Rei (UFSJ), São João del Rei, Brazil; (d)Instituto de Física, Universidade de São Paulo, São Paulo, Brazil

79 KEK, High Energy Accelerator Research Organization, Tsukuba, Japan

80 Graduate School of Science, Kobe University, Kobe, Japan

81 (a)Faculty of Physics and Applied Computer Science, AGH University of Science and Technology, Kraków, Poland; (b)Marian Smoluchowski Institute of Physics, Jagiellonian University, Kraków, Poland

82 Institute of Nuclear Physics Polish Academy of Sciences, Kraków, Poland

83 Faculty of Science, Kyoto University, Kyoto, Japan

84 Kyoto University of Education, Kyoto, Japan

85 Research Center for Advanced Particle Physics and Department of Physics, Kyushu University, Fukuoka, Japan

86 Instituto de Física La Plata, Universidad Nacional de La Plata and CONICET, La Plata, Argentina

87 Physics Department, Lancaster University, Lancaster, UK

88 Oliver Lodge Laboratory, University of Liverpool, Liverpool, UK

89 Department of Experimental Particle Physics, Jožef Stefan Institute and Department of Physics, University of Ljubljana, Ljubljana, Slovenia

90 School of Physics and Astronomy, Queen Mary University of London, London, UK

91 Department of Physics, Royal Holloway University of London, Egham, UK

92 Department of Physics and Astronomy, University College London, London, UK

93 Louisiana Tech University, Ruston, LA, USA

94 Fysiska institutionen, Lunds universitet, Lund, Sweden

[95] Centre de Calcul de l'Institut National de Physique Nucléaire et de Physique des Particules (IN2P3), Villeurbanne, France

[96] Departamento de Física Teorica C-15 and CIAFF, Universidad Autónoma de Madrid, Madrid, Spain

[97] Institut für Physik, Universität Mainz, Mainz, Germany

[98] School of Physics and Astronomy, University of Manchester, Manchester, UK

[99] CPPM, Aix-Marseille Université, CNRS/IN2P3, Marseille, France

[100] Department of Physics, University of Massachusetts, Amherst, MA, USA

[101] Department of Physics, McGill University, Montreal, QC, Canada

[102] School of Physics, University of Melbourne, Parkville, VIC, Australia

[103] Department of Physics, University of Michigan, Ann Arbor, MI, USA

[104] Department of Physics and Astronomy, Michigan State University, East Lansing, MI, USA

[105] B.I. Stepanov Institute of Physics, National Academy of Sciences of Belarus, Minsk, Belarus

[106] Research Institute for Nuclear Problems of Byelorussian State University, Minsk, Belarus

[107] Group of Particle Physics, University of Montreal, Montreal, QC, Canada

[108] P.N. Lebedev Physical Institute of the Russian Academy of Sciences, Moscow, Russia

[109] Institute for Theoretical and Experimental Physics (ITEP), Moscow, Russia

[110] National Research Nuclear University MEPhI, Moscow, Russia

[111] D.V. Skobeltsyn Institute of Nuclear Physics, M.V. Lomonosov Moscow State University, Moscow, Russia

[112] Fakultät für Physik, Ludwig-Maximilians-Universität München, Munich, Germany

[113] Max-Planck-Institut für Physik (Werner-Heisenberg-Institut), Munich, Germany

[114] Nagasaki Institute of Applied Science, Nagasaki, Japan

[115] Graduate School of Science and Kobayashi-Maskawa Institute, Nagoya University, Nagoya, Japan

[116] Department of Physics and Astronomy, University of New Mexico, Albuquerque, NM, USA

[117] Institute for Mathematics, Astrophysics and Particle Physics, Radboud University Nijmegen/Nikhef, Nijmegen, The Netherlands

[118] Nikhef National Institute for Subatomic Physics, University of Amsterdam, Amsterdam, The Netherlands

[119] Department of Physics, Northern Illinois University, De Kalb, IL, USA

[120] (a)Budker Institute of Nuclear Physics, SB RAS, Novosibirsk, Russia; (b)Novosibirsk State University, Novosibirsk, Russia

[121] Department of Physics, New York University, New York, NY, USA

[122] Ohio State University, Columbus, OH, USA

[123] Faculty of Science, Okayama University, Okayama, Japan

[124] Homer L. Dodge Department of Physics and Astronomy, University of Oklahoma, Norman, OK, USA

[125] Department of Physics, Oklahoma State University, Stillwater, OK, USA

[126] Palacký University, RCPTM, Joint Laboratory of Optics, Olomouc, Czech Republic

[127] Center for High Energy Physics, University of Oregon, Eugene, OR, USA

[128] LAL, Université Paris-Sud, CNRS/IN2P3, Université Paris-Saclay, Orsay, France

[129] Graduate School of Science, Osaka University, Osaka, Japan

[130] Department of Physics, University of Oslo, Oslo, Norway

[131] Department of Physics, Oxford University, Oxford, UK

[132] LPNHE, Sorbonne Université, Paris Diderot Sorbonne Paris Cité, CNRS/IN2P3, Paris, France

[133] Department of Physics, University of Pennsylvania, Philadelphia, PA, USA

[134] Konstantinov Nuclear Physics Institute of National Research Centre "Kurchatov Institute", PNPI, St. Petersburg, Russia

[135] Department of Physics and Astronomy, University of Pittsburgh, Pittsburgh, PA, USA

[136] (a)Laboratório de Instrumentação e Física Experimental de Partículas-LIP, Lisbon, Portugal; (b)Departamento de Física, Faculdade de Ciências, Universidade de Lisboa, Lisbon, Portugal; (c)Departamento de Física, Universidade de Coimbra, Coimbra, Portugal; (d)Centro de Física Nuclear da Universidade de Lisboa, Lisbon, Portugal; (e)Departamento de Física, Universidade do Minho, Braga, Portugal; (f)Departamento de Física Teorica y del Cosmos, Universidad de Granada, Granada, Spain; (g)Dep Física and CEFITEC of Faculdade de Ciências e Tecnologia, Universidade Nova de Lisboa, Caparica, Portugal

[137] Institute of Physics, Academy of Sciences of the Czech Republic, Prague, Czech Republic

[138] Czech Technical University in Prague, Prague, Czech Republic

[139] Faculty of Mathematics and Physics, Charles University, Prague, Czech Republic

140 State Research Center Institute for High Energy Physics, NRC KI, Protvino, Russia

141 Particle Physics Department, Rutherford Appleton Laboratory, Didcot, UK

142 IRFU, CEA, Université Paris-Saclay, Gif-sur-Yvette, France

143 Santa Cruz Institute for Particle Physics, University of California Santa Cruz, Santa Cruz, CA, USA

144 (a)Departamento de Física, Pontificia Universidad Católica de Chile, Santiago, Chile; (b)Departamento de Física, Universidad Técnica Federico Santa María, Valparaíso, Chile

145 Department of Physics, University of Washington, Seattle, WA, USA

146 Department of Physics and Astronomy, University of Sheffield, Sheffield, UK

147 Department of Physics, Shinshu University, Nagano, Japan

148 Department Physik, Universität Siegen, Siegen, Germany

149 Department of Physics, Simon Fraser University, Burnaby, BC, Canada

150 SLAC National Accelerator Laboratory, Stanford, CA, USA

151 Physics Department, Royal Institute of Technology, Stockholm, Sweden

152 Departments of Physics and Astronomy, Stony Brook University, Stony Brook, NY, USA

153 Department of Physics and Astronomy, University of Sussex, Brighton, UK

154 School of Physics, University of Sydney, Sydney, Australia

155 Institute of Physics, Academia Sinica, Taipei, Taiwan

156 (a)E. Andronikashvili Institute of Physics, Iv. Javakhishvili Tbilisi State University, Tbilisi, Georgia; (b)High Energy Physics Institute, Tbilisi State University, Tbilisi, Georgia

157 Department of Physics, Technion, Israel Institute of Technology, Haifa, Israel

158 Raymond and Beverly Sackler School of Physics and Astronomy, Tel Aviv University, Tel Aviv, Israel

159 Department of Physics, Aristotle University of Thessaloniki, Thessaloniki, Greece

160 International Center for Elementary Particle Physics and Department of Physics, University of Tokyo, Tokyo, Japan

161 Graduate School of Science and Technology, Tokyo Metropolitan University, Tokyo, Japan

162 Department of Physics, Tokyo Institute of Technology, Tokyo, Japan

163 Tomsk State University, Tomsk, Russia

164 Department of Physics, University of Toronto, Toronto, ON, Canada

165 (a)TRIUMF, Vancouver, BC, Canada; (b)Department of Physics and Astronomy, York University, Toronto, ON, Canada

166 Division of Physics and Tomonaga Center for the History of the Universe, Faculty of Pure and Applied Sciences, University of Tsukuba, Tsukuba, Japan

167 Department of Physics and Astronomy, Tufts University, Medford, MA, USA

168 Department of Physics and Astronomy, University of California Irvine, Irvine, CA, USA

169 Department of Physics and Astronomy, University of Uppsala, Uppsala, Sweden

170 Department of Physics, University of Illinois, Urbana, IL, USA

171 Instituto de Física Corpuscular (IFIC), Centro Mixto Universidad de Valencia - CSIC, Valencia, Spain

172 Department of Physics, University of British Columbia, Vancouver, BC, Canada

173 Department of Physics and Astronomy, University of Victoria, Victoria, BC, Canada

174 Fakultät für Physik und Astronomie, Julius-Maximilians-Universität Würzburg, Würzburg, Germany

175 Department of Physics, University of Warwick, Coventry, UK

176 Waseda University, Tokyo, Japan

177 Department of Particle Physics, Weizmann Institute of Science, Rehovot, Israel

178 Department of Physics, University of Wisconsin, Madison, WI, USA

179 Fakultät für Mathematik und Naturwissenschaften, Fachgruppe Physik, Bergische Universität Wuppertal, Wuppertal, Germany

180 Department of Physics, Yale University, New Haven, CT, USA

181 Yerevan Physics Institute, Yerevan, Armenia

a Also at Borough of Manhattan Community College, City University of New York, NY, USA

b Also at Centre for High Performance Computing, CSIR Campus, Rosebank, Cape Town, South Africa

c Also at CERN, Geneva, Switzerland

d Also at CPPM, Aix-Marseille Université, CNRS/IN2P3, Marseille, France

e Also at Département de Physique Nucléaire et Corpusculaire, Université de Genève, Genève, Switzerland

f Also at Departament de Fisica de la Universitat Autonoma de Barcelona, Barcelona, Spain

[g] Also at Departamento de Física Teorica y del Cosmos, Universidad de Granada, Granada (Spain), Spain

[h] Also at Department of Applied Physics and Astronomy, University of Sharjah, Sharjah, United Arab Emirates

[i] Also at Department of Financial and Management Engineering, University of the Aegean, Chios, Greece

[j] Also at Department of Physics and Astronomy, University of Louisville, Louisville, KY, USA

[k] Also at Department of Physics and Astronomy, University of Sheffield, Sheffield, UK

[l] Also at Department of Physics, California State University, Fresno, CA, USA

[m] Also at Department of Physics, California State University, Sacramento, CA, USA

[n] Also at Department of Physics, King's College London, London, UK

[o] Also at Department of Physics, St. Petersburg State Polytechnical University, St. Petersburg, Russia

[p] Also at Department of Physics, Stanford University, USA

[q] Also at Department of Physics, University of Fribourg, Fribourg, Switzerland

[r] Also at Department of Physics, University of Michigan, Ann Arbor, MI, USA

[s] Also at Dipartimento di Fisica E. Fermi, Università di Pisa, Pisa, Italy

[t] Also at Giresun University, Faculty of Engineering, Giresun, Turkey

[u] Also at Graduate School of Science, Osaka University, Osaka, Japan

[v] Also at Hellenic Open University, Patras, Greece

[w] Also at Horia Hulubei National Institute of Physics and Nuclear Engineering, Bucharest, Romania

[x] Also at II Physikalisches Institut, Georg-August-Universität Göttingen, Göttingen, Germany

[y] Also at Institucio Catalana de Recerca i Estudis Avancats, ICREA, Barcelona, Spain

[z] Also at Institut für Experimentalphysik, Universität Hamburg, Hamburg, Germany

[aa] Also at Institute for Mathematics, Astrophysics and Particle Physics, Radboud University Nijmegen/Nikhef, Nijmegen, The Netherlands.

[ab] Also at Institute for Particle and Nuclear Physics, Wigner Research Centre for Physics, Budapest, Hungary

[ac] Also at Institute of Particle Physics (IPP), Canada

[ad] Also at Institute of Physics, Academia Sinica, Taipei, Taiwan

[ae] Also at Institute of Physics, Azerbaijan Academy of Sciences, Baku, Azerbaijan

[af] Also at Institute of Theoretical Physics, Ilia State University, Tbilisi, Georgia

[ag] Also at Istanbul University, Department of Physics, Istanbul, Turkey

[ah] Also at LAL, Université Paris-Sud, CNRS/IN2P3, Université Paris-Saclay, Orsay, France

[ai] Also at Louisiana Tech University, Ruston, LA, USA

[aj] Also at Manhattan College, New York, NY, USA

[ak] Also at Moscow Institute of Physics and Technology State University, Dolgoprudny, Russia

[al] Also at National Research Nuclear University MEPhI, Moscow, Russia

[am] Also at Near East University, Nicosia, North Cyprus, Mersin, Turkey

[an] Also at Physikalisches Institut, Albert-Ludwigs-Universität Freiburg, Freiburg, Germany

[ao] Also at School of Physics, Sun Yat-sen University, Guangzhou, China

[ap] Also at The City College of New York, New York, NY, USA

[aq] Also at The Collaborative Innovation Center of Quantum Matter (CICQM), Beijing, China

[ar] Also at Tomsk State University, Tomsk, and Moscow Institute of Physics and Technology State University, Dolgoprudny, Russia

[as] Also at TRIUMF, Vancouver, BC, Canada

[at] Also at Universita di Napoli Parthenope, Naples, Italy

[*] Deceased